Title:
Vitamin B_{12} modulates Parkinson's disease LRRK2 kinase activity through allosteric regulation and confers neuroprotection

(Short title: Vitamin B_{12} modulates LRRK2 activity and toxicity)

Adam Schaffner[1,2], Xianting Li[1], Yacob Gomez-Llorente[2,] Emmanouela Leandrou[3], Anna Memou[3,] Nicolina Clemente[4], Chen Yao[5], Farinaz Afsari[6], Lianteng Zhi[7], Nina Pan[1], Keita Morohashi[2], Xiaoluan Hua[1,2], Ming-Ming Zhou[2], Chunyu Wang[4], Hui Zhang[7], Shu G. Chen[5], Christopher J. Elliott[6], Hardy Rideout[3], Iban Ubarretxena-Belandia[2,8], and Zhenyu Yue[1]

These authors contributed equally: Adam Schaffner, Xianting Li
Correspondence: Zhenyu Yue (zhenyu.yue@mssm.edu)

Affiliation
[1]Department of Neurology and Neuroscience, Friedman Brain Institute, Icahn School of Medicine at Mount Sinai, New York, NY 10029
[2]Department of Pharmacological Sciences, Icahn School of Medicine at Mount Sinai, New York, NY 10029
[3]Division of Basic Neurosciences, Biomedical Research Foundation of the Academy of Athens, Athens, Greece
[4]Department of Biological Sciences, Center for Biotechnology and Interdisciplinary Studies, Rensselaer Polytechnic Institute, Troy, New York 12180, USA
[5]Department of Pathology, Case Western Reserve University, Cleveland, OH 44106, USA
[6]Department of Biology, University of York, York, YO1 5DD, UK
[7]Department of Neuroscience, Thomas Jefferson University, Philadelphia, PA 19107, USA
[8]Biofisika Institute (CSIC, UPV/EHU), University of the Basque Country, Leioa, Spain

Classification: Biological Sciences

Abstract

Missense mutations in *Leucine-Rich Repeat Kinase 2* (LRRK2) cause the majority of familial and some sporadic forms of Parkinson's disease (PD). The hyperactivity of LRRK2 kinase induced by the pathogenic mutations underlies neurotoxicity, promoting the development of LRRK2 kinase inhibitors as therapeutics. Many potent and specific small molecule LRRK2 inhibitors have been reported with promise. However, nearly all inhibitors are ATP competitive – some with unwanted side effects and unclear clinical outcome - alternative types of LRRK2 inhibitors are lacking. Herein we find 5'-deoxyadenosylcobalamin (AdoCbl), a physiological form of the essential micronutrient vitamin B_{12} as a mixed-type allosteric inhibitor of LRRK2 kinase activity. Multiple assays show that AdoCbl directly binds LRRK2, leading to the alterations of protein conformation and ATP binding in LRRK2. STD-NMR analysis of a LRRK2 homologous kinase reveals the contact sites in AdoCbl that interface with the kinase domain. Furthermore, we provide evidence that AdoCbl modulates LRRK2 activity through disruption of LRRK2 dimerization. Treatment with AdoCbl inhibits LRRK2 kinase activity in cultured cells and brain tissue, and importantly prevents neurotoxicity in primary rodent cultures as well as in transgenic *C. elegans* and *D. melanogaster* expressing LRRK2 disease variants. Finally, AdoCbl alleviates deficits in dopamine release sustainability caused by *LRRK2* disease variants in mouse models. Our study uncovers vitamin B_{12} as a novel class of LRRK2 kinase modulator with a distinct mechanism, which can be harnessed to develop new LRRK2-based PD therapeutics in the future.

Key words: Vitamin B_{12}, LRRK2, Parkinson's disease, kinase

Introduction

Parkinson's disease (PD) is the most common chronic neurodegenerative movement disorder affecting 1% of the world population over the age of sixty. The pathological hallmarks of PD include the age-dependent loss of dopaminergic neurons in the substantia nigra and the progressive spatiotemporal distribution of Lewy bodies and Lewy neurites[1]. There is currently no cure or disease-modifying therapy for PD, and available treatments target only the symptoms of the disease but not its progression[2]. In addition, the pathogenesis of PD remains poorly understood. Discovered over a decade ago, Leucine-Rich Repeat Kinase 2 (LRRK2) has now emerged as a major target not only for understanding the molecular basis of PD pathogenesis but also for therapeutic intervention[3].

Missense mutations in the *PARK8*/*LRRK2* gene represent the prevalent cause for autosomal-dominant PD[4,5]. In addition, *LRRK2* mutations have been implicated in a significant number of sporadic PD cases[6-9]. PD-linked *LRRK2* variants associate with neuropathologies and clinical symptoms indistinguishable from idiopathic PD cases[10,11], suggesting that both inherited and sporadic forms of the disease share a similar pathogenic mechanism. *LRRK2* encodes a 286kDa protein containing catalytic GTPase and kinase domains, as well as Armadillo, Ankyrin, LRR and WD40 protein-protein interaction accessory domains (**Fig. 1a**). LRRK2 adopts a highly compact dimer structure with extensive intramolecular interactions[12], and dimerization has been proposed to correlate with LRRK2 kinase activity in vitro[13]. Of the six reported pathogenic mutations, the G2019S variant has the highest prevalence[14], accounting for 1% of sporadic and 5% of hereditary PD cases worldwide[10], and up to 30–40% of all PD cases among North Africans and Ashkenazi Jews[15]. Located in a conserved region of the kinase activation loop, the G2019S variant has been consistently associated with increased LRRK2 kinase activity *in*

vitro[13,16-18] and *in vivo*[19-22]. In addition, the G2019S variant also increases the phosphorylation of a subset of Rab GTPases, recently identified as promising physiological LRRK2 substrates[23,24].

Multiple lines of evidence demonstrate that LRRK2 kinase hyperactivity caused by PD pathogenic mutations, including G2019S, is causal to neurotoxicity or neuronal dysfunctions. LRRK2 kinase inhibitors attenuate the cell toxicity caused by the G2019S mutation in primary cortical neurons[25] and normalize G2019S-mediated postsynaptic abnormal activity in brain slice cultures[26]. In addition, LRRK2 kinase activity inhibitors prevent G2019S-potentiated α-synuclein accumulation in dopaminergic neurons[27,28], and their administration suppressed neurodegeneration in *C. elegans*, *D. melanogaster* and mouse PD models[25,29-31]. Consequently, extensive effort has been devoted to the development of ATP-competitive small molecule LRRK2 kinase inhibitors. Early generation kinase inhibitors displayed high potency against LRRK2, but lacked the specificity required to be considered for therapeutics[25,32-34]. Among the next generation, several inhibitors were highly potent and specific, but did not possess the pharmacokinetic properties for effective brain penetration[35,36], while others elicited dose toxicity and abnormal lung phenotypes in nonhuman primates[37]. The current generation of ATP-competitive inhibitors show promise, but will require further modification[38] and preclinical testing[39] before their therapeutic potential can be fully assessed. Remarkably, LRRK2 kinase activity inhibitors displaying alternative mechanisms of inhibition to these ATP-competitive inhibitors have yet to be reported.

Here we discovered that the FDA-approved natural compound 5'-deoxyadenosylcobalamin (AdoCbl), one of two physiological forms of the essential human micronutrient vitamin B_{12}, is a unique mixed-type allosteric modulator of LRRK2 kinase activity. AdoCbl is capable of disturbing LRRK2 protein conformation and dimerization. In

addition, we explore the ability of AdoCbl to prevent mutant *LRRK2* induced neurotoxicity and Parkinson-like phenotypes in PD animal models. We conclude that vitamin B_{12} is a novel type of LRRK2 kinase modulator, which is distinguished from other ATP competitive inhibitors. Future experiment should investigate the structural basis for LRRK2- vitamin B_{12} interaction that can be harnessed to develop new therapeutics for LRRK2-based PD.

Results

Identification of vitamin B_{12} as a LRRK2 kinase activity inhibitor

AdoCbl (Supplimentary information, **Fig. S1a**) was identified as a kinase activity inhibitor of FLAG-tagged wild type (WT) LRRK2 purified from BAC transgenic mouse brain[19] (Supplimentary information, **Fig. S1b**) from a high-throughput screen (HTS) of a small library of 2,080 FDA-approved compounds (Supplimentary information, **Table S1**). To assay LRRK2 kinase activity we measured the time-resolved fluorescence resonance energy transfer (TR-FRET) between phosphorylated Fluorescein-LRRKtide peptide and Terbidium-labeled anti-pLRRKtide antibody[40]. In this screen AdoCbl displayed a half-maximal inhibitory concentration (IC_{50}) of 1.2 μM (**Fig. 1b**). Vitamin B_{12} consists of a central cobalt ion that is equatorially chelated by a tetradentate corrin macrocycle and up to two axially coordinating ligands (Supplimentary information, **Fig. S1a**). The 'lower' (α)-coordinating ligand is usually a dimethylbenzimidazole (DMZ) base that connects to the f-side chain of the chelator by an α-ribazole containing backbone[41].

Vitamin B_{12} has additional forms in addition to AdoCbl, including cyanocobalamin (CNCbl), hydroxycobalamin (HOCbl), and methylcobalamin (MeCbl), which are distinguished by their (β)-coordinating ligand[42] (Supplimentary information, **Fig. S1a**). Only MeCbl and

AdoCbl are physiologically active in cells, as coenzymes of MeCbl-dependent methionine synthase and AdoCbl-dependent methylmalonyl coenzyme A mutase[42]. In humans, these enzymatic reactions play a key role in the metabolism of amino acids, nucleotides, and fatty acids, in addition to the normal functioning of the nervous system, and the formation of red blood cells[43].

Similar to AdoCbl, these other forms of vitamin B_{12} inhibited the LRRK2 catalyzed phosphorylation of the LRRKtide peptide with an IC_{50} of ~1 μM (**Fig. 1b**), suggesting that the nature of the (β)-coordinating ligand was not essential for the inhibition. Next, we validated the LRRK2 kinase inhibition by the various forms of vitamin B_{12} using highly pure strep-tagged LRRK2-WT expressed in HEK293 cells (Supplimentary information, **Fig. S1c**). To this end, we assayed LRRK2 autophosphorylation (**Fig. 1c**) and phosphorylation of the generic substrate myelin basic protein (MBP) (**Fig. 1d**) by measuring the incorporation of radioactive ^{32}P. In both cases, we determined IC_{50}s in the ~10 μM range for each form of vitamin B_{12}. We note that AdoCbl inhibited LRRK2-G2019S catalyzed phosphorylation of the recently identified LRRK2 physiological substrate Rab10[23,24] also with a ~10 μM IC_{50} (**Fig. 1e**).

Next, we derived Mouse Embryonic Fibroblast (MEF) cells from our LRRK2-G2019S BAC transgenic mice[19], and incubated them with AdoCbl, CNCbl, HOCbl, or MeCbl to measure their effect on LRRK2 autophosphorylation. As a readout we measured autophosphorylation using anti-LRRK2 pS935[44] and pS1292[20] antibodies. In this system both antibodies reported decreased LRRK2 autophosphorylation levels upon treatment with the established LRRK2 GNE-1023[20] inhibitor (Supplimentary information, **Figs. S2a-b**). These MEFs constitutively overexpress the pathogenic LRRK2-G2019S variant, which in accordance with literature displayed kinase hyperactivity compared to LRRK2-WT[19-22] (Supplimentary information, **Fig.**

153 **S2c**). Interestingly, we found that only AdoCbl, but not the other forms of vitamin B_{12}, exhibited
154 inhibition of LRRK2-G2019S autophosphorylation in MEF cells with an IC_{50} of ~10 μM, similar
155 to that measured in vitro (**Figs. 1f-g**). We observed a similar inhibition profile for the different
156 forms of vitamin B_{12} in macrophages derived from the LRRK2-G2019S transgenic mice
157 (Supplimentary information, **Fig. S2d**). The lack of inhibition displayed by CNCbl, HOCbl, or
158 MeCbl is not understood at present, but one possibility is that differences in cellular uptake,
159 localization and metabolism in the cells affect their efficacy compared to AdoCbl. Because
160 AdoCbl showed the greatest potential for LRRK2 inhibition in cultured cells we focused our
161 research efforts on this physiological form of vitamin B_{12}.
162
163 **AdoCbl binds directly to LRRK2**
164 We next tested if AdoCbl binds directly to human LRRK2. We first used agarose functionalized
165 with AdoCbl to pull-down purified LRRK2, which could be eluted as a function of AdoCbl
166 concentration (**Fig. 2a** and **Supplimentary information, Fig. S3**). In thermal shift assays
167 (TSA)[45] the melting temperature of LRRK2 increased substantially from 50 to 54°C in the
168 presence of AdoCbl (**Fig. 2b**). This thermostabilization by AdoCbl was comparable to that
169 measured in the presence of the established LRRK2 kinase inhibitor PF-06447475[38].
170 Furthermore, we applied microscale thermophoresis (MST)[46] to measure the binding affinity of
171 AdoCbl for LRRK2 and determined an apparent dissociation equilibrium constant (K_D) of 12.0
172 and 4.1 μM for purified LRRK2-WT and LRRK2-G2019S, respectively (**Fig. 2c**), in agreement
173 with our IC_{50} values. As a validation of the MST assay, under the same conditions LRRK2-
174 G2019S binds PF-06447475 with a K_D of 70 nM (**Fig. 2d**), in line with the reported IC_{50} of 11
175 nM for this inhibitor[38].

We next sought to identify the functional groups in AdoCbl responsible for interacting with LRRK2 by using an extension of the saturation transfer difference (STD) NMR method termed ATP-STD NMR[47]. This method was developed to screen protein kinase inhibitors by recording STD signals in the presence of competing ATP[48]. Due to an unstable and aggregation prone human LRRK2 kinase domain, which makes it intractable for biophysical/structural analysis, we decided to use the humanized kinase domain of the Roco4 protein from *Dictyostelium discoideum*[49]. The kinase domain of Roco4 (amino acids 1018–1292) has a 47% similarity with the kinase domain of human LRRK2 (amino acids 1879–2138), and its humanized variant, where amino acid residues F1107 and F1161 are substituted for Leucine to mimic the residues L1949 and L2001 in LRRK2, is considered a valuable model for the structural characterization of LRRK2 kinase inhibitors[47,49]. We first verified that AdoCbl inhibited autophosphorylation of the humanized Roco4 kinase (**Fig. 2e**) with an IC_{50} of 73.6 μM (**Fig. 2f**). In agreement with published data[47], we obtained a clear STD signal for ATP binding to Roco4 kinase (**Fig. 2g, orange spectrum**). Addition of AdoCbl to the ATP/Roco4 sample in a 1:1 AdoCbl:ATP ratio resulted in the emergence of additional STD signals corresponding to AdoCbl protons, confirming a direct binding of AdoCbl to Roco4. At a 10:1 AdoCbl:ATP ratio, the STD peaks corresponding to AdoCbl became much stronger while ATP peaks weakened, demonstrating that AdoCbl diminished ATP binding to Roco4 kinase. Stronger STD signals likely correspond to AdoCbl protons in the vicinity or at the protein binding interface. These protons are distributed around one side of the molecule and are contributed by the adenine, corrin, and DMZ moieties (**Fig. 2h**).

AdoCbl is a mixed-type allosteric LRRK2 kinase inhibitor

The current collection of commercially available LRRK2 kinase inhibitors, including the latest generation PF-06447475[38] and MLi-2[39], are considered to be ATP-competitive, with the exception of FX2149 that is GTP-competitive[50]. To determine the mode of inhibition of vitamin B_{12} we measured V_{max} and K_m as a function of ATP and in the presence of an increasing concentration of AdoCbl. For our *in vitro* inhibition kinetics assays we used purified full-length LRRK2-WT and LRRK2-G2019S to measure relative velocity based on the quantification of LRRK2 autophosphorylation pS1292 signal (Supplimentary information, **Fig. S4**). Consistent with literature[13,16-18], the relative velocity of LRRK2-G2019S was two-fold higher than LRRK2-WT (Supplimentary information, **Table S2**). Titration of AdoCbl caused a decrease in apparent V_{max} and an increase in apparent K_m (**Figs. 3a-c**), suggesting mixed-type inhibition, as confirmed by reciprocal Lineweaver-Burk plots of the data (**Figs. 3b-d and Supplementary information, Table S2**). Mixed-type inhibitors generally bind to an allosteric site and can affect an enzyme's ability to catalyze a reaction and to bind its substrate[51]. To further characterize the mode of AdoCbl inhibition of LRRK2 we measured the competition with AMP-PNP using MST (**Fig. 3e**). Under our assay conditions AMP-PNP displayed a K_D of 0.9 μM against LRRK2 (**Fig. 3f**). In further support of the mixed-inhibition mode of action, increasing concentrations of AMP-PNP reduced but did not overcome the binding of AdoCbl to LRRK2 (**Fig. 3e**).

We further compared AdoCbl with the reported ATP-competitive LRRK2 inhibitor IN-1 (LRRK2-IN-1) for its ability to inhibit the human LRRK2 A2016T variant. The A2016T substitution in the ATP-site of LRRK2 results in a normally active enzyme, which is, however, significantly less sensitive to the ATP-competitive inhibitors H-1152 and sunitinib[52], and up to 400-fold less sensitive against LRRK2-IN-1 compared to the WT protein[35]. Using the G2019S mutation as a background we confirmed that the A2016T substitution confers resistance to

LRRK2-IN-1 (Supplimentary information, **Figs. S5a-b**). In contrast, this variant displayed a similar level of inhibition by AdoCbl as the G2019S protein alone. Similarly WT Roco4 from *D. discoideum*[47,49], which has a 241-fold lower affinity for LRRK2-IN-1 than humanized Roco4[47], was inhibited by the same degree as the humanized version (Supplimentary information, **Figs. S5c-d**). The data suggests distinct mechanisms of LRRK2 binding between LRRK2-IN-1 and AdoCbl.

AdoCbl induces conformational changes and disrupts dimerization of LRRK2

Allosteric inhibitor binding normally induces a conformational change in the enzyme that results in reduced affinity for the substrate[53]. To test the possibility of an AdoCbl-induced conformational change in LRRK2 we conducted limited proteolysis assays in the presence of AdoCbl. The addition of AdoCbl markedly increased the susceptibility of LRRK2 to proteolysis by both trypsin and chymotrypsin (**Fig. 4a**). At a 90-min. interval, we showed that the presence of AdoCbl significantly increases the sensitivity of trypsin degradation of LRRK2 protein in a dose dependent manner (**Fig. 4b**). This observation does not result from an enhancement of the intrinsic activity of these proteases, as demonstrated by the fact that AdoCbl did not affect the proteolysis rate of a control kinase TBK1 (Supplimentary information, **Fig. S6a**). Of note, the well-known ATP-competitive LRRK2 kinase inhibitors GSK2578215A[36], GNE-1023[20] and PF-06447475[38], produced the opposite effect as AdoCbl, i.e. they protected LRRK2 from proteolytic digestion (**Fig. 4b**), whereas AMP-PNP had no effect (**Supplimentary information, Fig. S6b**). For more evidence in support of conformational changes in LRRK2 upon binding to AdoCbl we measured the intrinsic fluorescence of LRRK2 as a function of AdoCbl. With 27 tryptophan amino acid residues, the fluorescence emission spectra of LRRK2 at an excitation wavelength of 295 nm displayed an AdoCbl dose-dependent decrease in fluorescence intensity (**Fig. 4c**). Note

246 that AdoCbl absorbs light at 295 nm and 340-360 nm, thus it was necessary to correct for the
247 inner-filter effect (**Supplimentary information, Figs. S6c-d**). Such a decrease in fluorescence
248 intensity is consistent with conformational changes in LRRK2 where initially buried tryptophan
249 residues become exposed to the solvent as a function of AdoCbl.

250 We hypothesize that the effect of AdoCbl binding in LRRK2 conformation alters
251 oligomeric state of LRRK2. Ample evidence now supports dimeric LRRK2 as the main
252 oligomeric species of the enzyme *in vitro*[12], and available data indicates that LRRK2
253 dimerization correlates with kinase activity[13]. We quantified cellular LRRK2 dimers using a
254 novel adaptation of the proximity biotinylation approach. We expressed recombinant LRRK2
255 protein fusion to BirA (biotin ligase) or to AP (acceptor peptide) in HEK293T cells in the
256 presence of vehicle or AdoCbl. As a negative control BirA- and AP-LRRK2 expressing cells
257 were lysed without having been given the biotin pulse; and in such samples, the number of
258 labeled LRRK2 dimers purified on streptavidin plates is negligible (**Fig. 4d**). Expression levels
259 of both forms of LRRK2 are comparable as determined by ELISA or Western immunoblot. Cells
260 co-expressing BirA-LRRK2/AP-LRRK2 contain robust levels of biotinylated LRRK2 dimers,
261 normalized to total expression of LRRK2. However, in cells treated with AdoCbl, we detected a
262 dose-dependent reduction in the levels of LRRK2 dimers, both in cells expressing WT LRRK2,
263 as well as in cells expressing the LRRK2-G2019S or LRRK2-I2020T variant proteins (**Fig. 4e**).
264 In contrast to other LRRK2 kinase inhibitors[54-56], we did not observe a significant decrease in
265 LRRK2 expression following treatment with AdoCbl (**Figs. 4d-f**), indicating that this compound
266 disrupts LRRK2 dimers without affecting expression.
267

AdoCbl protects dopaminergic neurons from *LRRK2-G2019S* induced neurotoxicity in C. elegans

The degeneration of dopaminergic (DAergic) neurons is the pathological hallmark of PD[2]. However, recapitulating this phenotype in mammalian models of LRRK2-linked PD has been a challenge, nearly all reported genetic models (either transgenic overexpression or knock-in) failed to display clear neurodegeneration[19,57-59]. In contrast, invertebrate PD models of LRRK2 show a robust degeneration of DAergic neurons[60-63]. The DAergic pathway in *C. elegans* is important for the basal slowing response, a behavior by which worms slow their locomotive movement when encountering food[64]. Transgenic *LRRK2-G2019S* nematodes exhibit progressive impairment of the basal slowing response, but this locomotive behavioral deficit can be restored by treatment with the LRRK2 kinase inhibitors LRRK2-IN-1 and TTT-3002[30]. In this *C. elegans* model of LRRK2 PD, these two inhibitors targeted specifically LRRK2, as they were ineffective against the neurodegenerative phenotype displayed in transgenic *LRRK2-A2016T/G2019S* worms carrying the inhibitor-resistant LRRK2 A2016T mutation[30]. Therefore, we selected the established human *LRRK2-G2019S C. elegans* model to ask if AdoCbl protects against DAergic neuron degeneration. *LRRK2-G2019S* transgenic worms that were fed up to 1.25 μM AdoCbl during their larval stage resisted the locomotive behavioral deficit on adult day 3 in a dose-dependent manner with a half-maximal effective concentration (EC_{50}) value of 0.53 μM (**Fig. 5a**). Consistent with the lack of an effect of the LRRK2 A2016T mutation on the inhibition by AdoCbl in vitro (**Supplimentary information, Figs. S5a-b**), treating transgenic *LRRK2-A2016T/G2019S* worms with AdoCbl resulted in a rescued neurodegenerative phenotype (Supplimentary information, **Fig. S7a**). The data also supports the distinct mechanism of AdoCbl in blocking LRRK2 activity and LRRK2 associated neurodegeneration from IN-1. Additionally,

the AdoCbl-induced rescue was observed in transgenic *LRRK2-R1441C* worms as well, which also display an impaired basal slowing response (Supplimentary information, **Fig. S7b**). *C. elegans* possess eight DAergic neurons that can be readily visualized by coupling GFP to a DA-neuron-specific promoter. Four GFP-tagged DAergic neurons of cephalic sensilla (CEP neurons) in the head were examined using fluorescence microscopy. Overexpression of *LRRK2-G2019S* causes age-dependent degeneration of these DAergic neurons, where less than 60% remain on adult day 9, compared to 75% in control worms expressing *GFP* alone. When fed 1.25 μM AdoCbl during their larval stage, age-synchronized adult *LRRK2-G2019S* worms displayed a robust increase in DAergic neuron survival, nearly back to the levels of the GFP-control worms (**Figs. 5b-c**). As in the case of TTT-3002 and LRRK2-IN-1[30], treatment of WT worms expressing GFP marker alone with AdoCbl did not result in any significant changes in basal slowing response or DAergic neuron survival, suggesting that the effect of AdoCbl was specific to the transgenic *LRRK2-G2019S* worms.

AdoCbl prevents *LRRK2-G2019S* induced neurotoxicity in *D. melanogaster* model of PD

Signal regulation in the human retina depends largely on dopamine[65], and this process can be affected by the loss of DA that is characteristic in PD patients[66]. In *D. melanogaster*, vision is also regulated by comparable DAergic circuits[67,68]. Transgenic overexpression of the human *LRRK2-G2019S* gene in *D. melanogaster* has been shown to elicit DA-dependent retinal degeneration and loss of visual response due to an abnormal increase in contrast sensitivity, which can be rescued using LRRK2 kinase activity inhibitors[31,69]. After feeding *Drosophila* larvae with AdoCbl at concentrations up to 2.5 μM, we recorded the visual response to flickering blue light in 1-day-old flies. Our Fast Fourier Transform (FFT) algorithm separates this visual

response according to the first three stages of the fly visual system: photoreceptors, lamina neurons, and medulla neurons (**Fig. 6a**). Increasing the contrast of the flickering light resulted in a greater retinal response of the fly, revealing characteristic Contrast Response Functions (CRFs) that are dependent on the combination of genotype and AdoCbl treatment (**Fig. 6b**). In the photoreceptors and lamina neurons, the physiological response increased and plateaued at 70% applied contrast, while the medulla neurons generated a complex response, as indicated by the peak response at 40% applied contrast. In each case, flies with dopaminergic expression of *LRRK2-G2019S* have a much greater response compared to those expressing *LRRK-WT*. Notably, feeding flies with 2.5 μM AdoCbl throughout larval life rescued the *LRRK2-G2019S* phenotype completely, with the photoreceptor, lamina neurons and medulla neurons all showing a CRF close to that of WT flies (**Fig. 6b**). Furthermore, titration of AdoCbl revealed an EC_{50} between 250 and 500 nM in all three stages of the visual pathway (**Fig. 6c, and Supplimentary information, Fig. S8**). To determine the specificity of AdoCbl toward LRRK2 kinase activity, we tested a 2.5 μM concentration against flies with a kinase-dead background (*LRRK2-G2019S-K1906M*) and found no significant change in any of the three measured regions (**Fig. 6d**). In contrast to the results from *C. elegans*, treating wild-type *drosophila* with a 2.5 μM concentration of AdoCbl significantly rescues the visual response (**Fig. 6e**). Finally, we tested for off-target effects by feeding 2.5 μM of AdoCbl to flies with little expression of the LRRK2 homolog (*dLRRK*$^{-}$) and found no statistically significant difference between any of the photoreceptor, lamina and medulla neurons (**Fig. 6f**).

AdoCbl prevents *LRRK2-G2019S* induced neurotoxicity and rescues deficits in dopamine transmission in LRRK2-PD mouse models

Previous studies have demonstrated that transient overexpression of *LRRK2-G2019S*, but not *LRRK2-WT*, leads to toxicity in primary cortical neuron cultures[70,71]. We employed the same approach and found that transfection of *LRRK2-G2019S* indeed caused neurotoxicity in dissociated cortical neurons, as evidenced by apoptotic nuclear features. Treatment of the transfected neurons with AdoCbl, however, suppressed the frequency of apoptotic neurons in a dose-dependent manner **(Fig. 7a)**. As a positive control in this assay, the most recent generation LRRK2 inhibitor MLi-2[39] showed potent protection at a 10 nM concentration.

The lack of frank neurodegeneration in nearly all LRRK2 transgenic mouse models prevents us from testing AdoCbl neuroprotection *in vivo*. However, a common pathological feature for reported LRRK2 models is the deficit in DA transmission[19,72]. To investigate if AdoCbl prevents such a defect, we first tested the inhibition of neuronal LRRK2 by AdoCbl using striatal brain slices from *LRRK2-G2019S* BAC transgenic mice under *ex vivo* conditions. Striatal slices were incubated in oxygenated artificial cerebrospinal fluid (ACSF) for two hours in the presence of LRRK2 inhibitor or vehicle. Administration of AdoCbl in the ACSF caused dose-dependent inhibition of LRRK2 autophosphorylation in slice lysates (**Fig. 7b**). Similarly, GNE-1023 exhibited dose dependent inhibition of LRRK2 under the same conditions (***SI*** Supplimentary information, **Figs. S9a-b**). Compared to WT controls, *LRRK2-G2019S* BAC transgenic mice were reported to have decreased sustainability of evoked DA release at the age of 12 months old[19]. Therefore, we measured single-pulse evoked DA release sustainability in striatal slices from *LRRK2-G2019S* BAC transgenic mice and WT littermates at the age of 12-15 months using Fast Scan Cyclic Voltammetry (FSCV)[73](**Figs. 7c-d**). A bipolar stimulating electrode was placed in the dorsal striatum ~150 μm from the recording microelectrode and depolarizing currents were applied at 2-minute intervals for 20 minutes. In control slices, the

amplitude of DA release at a given site evoked by single pulses decreased with the first few stimulations and declined by 20% by the end of the 20-minute period. Consistent with a previous report[19], this decline was much more profound in the brain slices of the G2019S mice. Remarkably, AdoCbl alleviated this deficit and restored the sustainability to the level of WT control slices.

In addition, we examined the effects of AdoCbl using striatal slices from another preclinical *LRRK2-R1441G* BAC transgenic mouse model. The declined DA release evoked by 2-minute intervals during a 20-minute period was robust in slices from LRRK2-R1441G mice compared to WT controls, and again, AdoCbl alleviated this deficit, restoring the sustainability to the level of WT control slices (**Figs. 7e-f**). Taken together, our data demonstrates that AdoCbl is capable of rescuing the impairment of DAergic neurons in evoked DA release caused by multiple LRRK2 PD mutants.

Discussion

LRRK2 has emerged as a most promising drug target for the treatment of PD. Although extensive research has yielded potent and selective LRRK2 kinase inhibitors, they are ATP competitors, some of which are associated with unwanted side effect and unclear clinical outcome[37]. Thus, an alternative class of inhibitors should be considered. Herein, we present evidence that AdoCbl, one of two physiologically active forms of vitamin B_{12}, inhibits LRRK2 kinase activity with a distinct mechanism. Despite the less potent nature in LRRK2 inhibition compared to many industrially produced compounds, AdoCbl displays a unique feature of LRRK2 binding and kinase activity modulation mechanism by disturbing LRRK2 protein conformation or dimerization, which may serve as a base for the development of novel allosteric inhibitors of LRRK2. Moreover, AdoCbl prevents neurotoxicity and dopamine deficits in animal

383 models carrying LRRK2 disease variants. Therefore, our study identifies a novel class of LRRK2
384 kinase modulator that can be used to probe LRRK2 structure and function relationship and
385 develop new allosteric LRRK2 inhibitors in the future.

386 Our studies demonstrated the ability of AdoCbl to bind directly human LRRK2 through
387 multiple methods including kinetics, TSA, MST and intrinsic fluorescence (**Figs. 1-3**). Our data
388 indicates that AdoCbl acts as a mixed-type allosteric inhibitor capable of affecting ATP binding
389 to LRRK2. To date, the majority of reported LRRK2 kinase inhibitors has been known as ATP-
390 competitors. Although the structure details of the binding between LRRK2 kinase domain and
391 the inhibitors are unavailable, insight based on Roco4 kinase studies suggests they are type I and
392 II inhibitors[47,49]. These types of inhibitors target the kinase active site; but while Type I bind to
393 the active conformation, type II bind to the inactive conformation[74]. Vitamin B_{12} was shown to
394 suppress the activity of nitric oxide synthase[75] and HIV-1 integrase[76], while the ability of B_{12} to
395 inhibit kinase activity has never been documented. Indeed, the structure of Vitamin B_{12} does not
396 resemble any known kinase inhibitor and no Vitamin B_{12} mediated kinase inhibition has ever
397 been reported. In the absence of detailed structural information, our STD-NMR analysis revealed
398 extensive contacts between vitamin B_{12} and the Roco4 kinase domain involving the adenosyl
399 moiety, the bulky corrin ring of cobalamin, and the DMZ base (**Fig. 2h**). Although ATP and
400 AdoCbl share an adenosyl moiety, the fact that HOCbl, MeCbl and CNCbl could inhibit LRRK2
401 kinase activity *in vitro* with comparable IC_{50}s (**Fig. 1**) suggests that the (β)-coordinating ligand
402 in vitamin B_{12} is not essential for binding to LRRK2. In addition, the ATP-site LRRK2 variant
403 A2016T, which displays resistance against several ATP-competitive inhibitors such as LRRK2-
404 IN-1 did not have an effect on AdoCbl inhibition in vitro, or in the rescuing by AdoCbl of
405 behavioral abnormality and DA neuron degeneration in *C. elegans* expressing LRRK2-

406 A2016T/G2019S. Thus, our study suggests that vitamin B_{12} modulates LRRK2 activity by
407 binding at distinct sites in kinase domain than those for other known LRRK2 inhibitors.

408 Mechanistically AdoCbl distinguishes itself from other LRRK2 inhibitors by being
409 capable of altering LRRK2 protein conformation and disturbing LRRK2 dimer status. Several
410 groups including ours have previously demonstrated that LRRK2 can form dimers[12,17,18], which
411 is thought to represent the kinase active form of LRRK2 in detriment of LRRK2 monomers[13].
412 Since AdoCbl did not affect total LRRK2 levels in cells, it is likely that AdoCbl inhibits LRRK2
413 kinase activity by shifting the equilibrium from LRRK2 dimers to the kinase inactive monomeric
414 form (**Fig. 4**). This hypothesis is consistent with our observation that in contrast to ATP-
415 competitive inhibitors, AdoCbl renders LRRK2 susceptible to proteolysis, as the monomeric
416 species might be structurally more accessible to proteases than the dimer. Our study also raises a
417 possibility that AdoCbl prefers dimeric to monomeric LRRK2[12] for binding. While this idea is
418 under investigation, our data suggests that the ability of AdoCbl to disrupt dimerization might
419 offer advantages over known ATP-competitive inhibitors as an allosteric inhibitor to modulate
420 LRRK2 kinase function. A better understanding of the mode of LRRK2 - vitamin B_{12} interaction
421 underlying the mechanism of inhibition of LRRK2 activity will depend on future efforts to solve
422 the structures of LRRK2-vitamin B_{12} complexes.

423 Compared to the nM inhibition efficacy displayed by the second generation ATP-
424 competitive LRRK2 kinase inhibitors PF-06447475[38] and MLi-2[39], vitamin B_{12} showed a modest
425 μM inhibition *in vitro*. However, it is surprising that the efficacy of AdoCbl in animal models
426 (**Figs. 5-6**) was comparable to those high-affinity inhibitors[25,30,31]. While the unusual increase in
427 efficacy of AdoCbl inside the cells relative to *in vitro* condition is surprising and not understood
428 at present, we speculate that a couple of factors may contribute to the unexpected efficacy of

AdoCbl in the cells. First, vitamin B_{12} enters the cells through active transport mediated by specific proteins transcobalamin and its receptor (CD320), which ubiquitously located on the cell surface, rather than diffusion (e.g. small compounds)[77,78]. This mechanism may enhance intracellular AdoCbl bioavailability, especially in the mitochondria where AdoCbl is normally located. Second, a potential cell non-autonomous mechanism, where a variety of cells (including glial cells) produce and secret transcobalamin that could facilitate the uptake of cobalamins in neurons, may help explain the observation[79]. Third, vitamin B_{12} may provide benefits through acting on additional targets. Thus, the increased efficacy could result from a combination of multiple target effects including LRRK2 inhibition. Vitamin B_{12} is capable of crossing the blood brain barrier (BBB), and it plays a key role in the regulation of excitotoxic homocysteine levels in the brain[80], as well as in the synthesis of fatty acids incorporated into neuronal lipids and myelin sheaths[81]. Indeed, vitamin B_{12} deficiency in humans is known to contribute to a variety of neurological conditions[80,81]. Low vitamin B_{12} levels have been described in patients with idiopathic PD[82-84], and there is also evidence that chronic L-3,4-Dihydroxyphenylalanine (L-dopa) intake decreases vitamin B_{12} plasma levels[85]. A recent study showed that low levels of vitamin B_{12} predicts worse motor symptom in early PD[86], however, the mechanism is unknown. It is likely that vitamin B_{12} supplement provides some benefit in PD [84,88], but the lack of knowledge of bioavailability of specific forms of vitamin B_{12} (particularly in CNS) due to the limitation of measurements hinders the understanding of the beneficial effect of vitamin B_{12} in human tissues.

Although it is challenging to understand the benefit or therapeutic potential of vitamin B_{12} in PD due to above obstacles, our study implies inhibition of LRRK2 through vitamin B_{12} as a potential mechanism. Our observation raises a possibility that tissue levels of AdoCbl

(including CNS and peripheral tissues) might modulate disease penetrance or progression of LRRK2 variants in light of current reports showing the involvement of peripheral tissue/cells in LRRK2 related pathogenesis[87-90]. Related epidemiologic studies should be performed in the near future to address the possible association[91]. Indeed, future studies should investigate biochemical and structural basis underlying the modulation of LRRK2 activity by vitamin B_{12} as well as vitamin B_{12} efficacy and bioavailability in tissues in order to understand the therapeutic potential of vitamin B_{12} in PD. Nonetheless, AdoCbl represents a starting point for the development of a new class of LRRK2 activity modulators (e.g. allosteric inhibitor) for the much-needed treatment of LRRK2-linked pathological conditions such as PD and inflammatory bowel disease (IBD)[92].

Materials and Methods

Chemicals

The FDA-approved chemical library used for the primary screen at the Mount Sinai Integrated Screening Core was purchased from Microsource Discovery (Gaylordsville, CT, USA) and contained 2,080 bioactive compounds approved for use in humans or animals. Trypsin, ATP, AMP-PNP, and all forms of cobalamin were purchased from Sigma Aldrich (St. Louis, MO, USA). All experiments involving AdoCbl were performed under light-protected conditions to reduce photolability. GNE-1023 was kindly gifted to us by Genentech (South San Francisco, CA,

USA). The inhibitors GSK2578215A, PF-06447475, and MLi-2 were purchased from Tocris (Bristol, UK). Bovine purified myelin basic protein was obtained from EMD Millipore (Darmstadt, Germany) and purified Rab10 was purchased from Origene (Rockville, MD, USA). Purified full-length flag-tagged LRRK2 was purchased from Invitrogen (Carlsbad, CA, USA).

Antibodies

Anti-LRRK2 N241A/34 NeuroMab clone was obtained from the Michael J. Fox Foundation, anti-pS935[44] LRRK2 (ab133450) was from Abcam, and anti-pS1292[20] was kindly gifted by Genentech. Anti-Rab10 (8127) was purchased from Cell Signaling and anti-pRab10 pT73 was obtained from the University of Dundee, UK.

Protein Purification

BAC-transgenic mouse brain overexpressing flag-tagged LRRK2 was homogenized in homogenization buffer (20 mM HEPES at pH 7.4, 0.32 M Sucrose, 1 mM NaHCO3, 0.25 mM CaCl2, 1 mM MgCl2, 1 mM PMSF, and complete protease inhibitor cocktail), then Triton X-100 was added to a final concentration of 1% and incubated at 4°C on a rotator for 30 min. Homogenized brain was clarified at 12,000 x g for 10 min at 4°C and the FLAG-LRRK2 protein were purified using Anti-FLAG Affinity Gel (Sigma, A220) with extensive wash before elution. The protein was eluted using 150 ng/µL FLAG-peptide (Sigma, F4799) and stored at 80°C until use.

The human *LRRK2* pDEST-NSF-tandem affinity plasmid was kindly gifted by Dr. Christian Johannes Gloeckner (University of Tubingen, Germany). Strep-tagged LRRK2 was expressed in

HEK293T cells through transient transfection for 48 hours, as described previously[12]. Cells were harvested and incubated in lysis buffer (50 mM Tris pH 7.5, 100 mM NaCl, 2 mM DTT, 5 mM $MgCl_2$, 0.5 mM EGTA, 1% Triton X-100, 10% Glycerol, Roche protease inhibitors (11836170001)) for 30 minutes at 4°C. Lysate was centrifuged at 13,000 x g for 15 minutes. Supernatant was mixed with Strep-Tactin Sepharose (2-1206-002) from Iba Life Sciences for 2 hours and washed extensively with buffer above, substituting 0.02% Triton X-100 for 1%. Strep-Flag LRRK2 was eluted using 10mM desthiobiotin and stored at 80°C until use.

The 6xHis-GST-tagged *Roco4 kinase* domain plasmid, kindly gifted by Dr. Andy West (University of Alabama Birmingham, AL, USA), was transformed into BL21 (DE3) cells (Agilent Technologies, 230132) and grown at 37°C in 2xYT broth until reaching an OD600 of 0.6. Overexpression was induced for 16 hours at 18°C with 300 µM IPTG. Cells were pelleted and resuspended in 50 mM Tris pH 7.5, 150 mM NaCl, 1 mM TCEP, 0.02% Reduced TX100, 1 mM PMSF, 25 µg/mL lysozyme, 4 ug/mL DNase. Protein was bound to Ni-NTA resin and washed and eluted with increasing concentrations of imidazole. Protein was concentrated and treated with TEV protease to cleave the 6xHis-GST tag, while dialyzing in buffer overnight to remove imidazole. 6xHis-GST tag was separated using Ni-NTA resin and pure Roco4 kinase domain was collected in the flow through.

The pGEX-6p-1 construct was expressed as above using BL21 (DE3) cells. Crude lysate was bound to Glutathione Sepharose 4B (17-0618-01, GE Healthcare) for 1 hour before beads were washed 3x with PBS. GST protein was eluted with reduced glutathione.

Compound Screen and TR-FRET Kinase Assay

Compounds from the FDA-Approved library were tested against flag-tagged LRRK2 purified from BAC transgenic mouse brain. LRRK2 kinase activity was monitored by measuring time resolved fluorescence resonance energy transfer (TR-FRET) emission ratio upon the phosphorylation of Fluorescein-LRRKtide (PV4901, Invitrogen) and subsequent binding of Terbidium-pLRRKtide antibody (PV4898, Invitrogen). This TR-FRET-based assay was used in a high-throughput screen (HTS) of small molecule chemical compounds for LRRK2 using the TECAN (Mannedorf, Switzerland) Freedom EVO 200 liquid handling system, and relative fluorescence was measured using the TECAN Safire 2 fluorescence spectrometer. To determine the TR-FRET ratio between Fluorescein-LRRKtide and Terbidium-pLRRKtide antibody, fluorescent intensity was measured at wavelengths 515 nm and 485 nm.

Prior to the HTS, each compound was prepared at 4x final concentration (1.6 or 4% residual DMSO volume) in Kinase Buffer S, containing 50 mM Tris pH 8.5, 10 mM $MgCl_2$, 0.01% Brij-35, 1 mM EGTA in 96-well polypropylene non-treated plates (Thermo Scientific, #12-565-436). The kinase reaction was performed in 10 µl total volume in a low-volume white 384-well plate (Corning, #3673), with 20 nM LRRK2, 400 nM Fluorescein-ERM (LRRKtide), and small molecules in Kinase Buffer S supplemented with 2 mM DTT on the day of the experiment. Small molecules were screened at 3.3 or 4 µM with 0.4 or 1% residual DMSO in duplicate. The assay plates were prepared by adding 2.5 µl of 4x compound solutions, 2.5 µl of 4x LRRK2, and 5 µl of 2x LRRKtide and ATP mixture. After incubation at room temperature for 4 hours, the kinase reaction was terminated by the addition of 10 µl of 2x EDTA and 2x Tb-anti-pERM antibody in the detection buffer, containing 20 mM Tris-HCl, 0.01% NP40. EDTA was mixed with the antibody right before the addition of the mixture to wells, as the antibody was stable in EDTA only for several hours. The final concentration of EDTA and Tb-anti-pERM

were 5 mM and 2.5 nM, respectively. After 1-hour incubation at room temperature, TR-FRET measurements were obtained according to the parameters described in instrument settings. During the incubation, 384-well plates were covered by aluminum sealing tapes (Corning, #6570) to reduce evaporation and exposure to light. All the liquid handling was carried out using fixed 8-tip LiHa arms on TECAN EVO200 workstation. HTS was performed with 0.4 or 1% DMSO as negative control and no LRRK2 as positive control. Hit compounds were selected based on the normalized percent inhibition by first computing emission ratio (emission intensity of acceptor divided by donor) and then computing percent inhibition of kinase activity relative to the DMSO treated control as 0% inhibition and the control in the absence of LRRK2 as 100% inhibition. Compounds in wells showing greater than 30% inhibition in either of the duplicates were selected as hits.

In Vitro Kinase Assays

Kinase reactions were performed in 30 uL kinase buffer (20 mM Tris pH 7.5, 1 mM DTT, 15 mM $MnCl_2$, 20 mM β-glycerophosphate) at 37°C for 30 minutes in the presence of [γ-^{32}P] ATP (3000 Ci/mmol; BLU502H250UC, PerkinElmer Life Sciences) and 50 μM cold ATP. Beforehand, LRRK2 or Roco4 Kinase was loaded with inhibitor and/or substrate, followed by 30 min incubation on ice. Reactions were stopped by addition of Laemmli buffer and boiling at 95°C for 10 minutes. Samples were resolved on 4-12% SDS-PAGE pre-cast gels (NP0323BOX, Invitrogen). Radioactive signal was captured onto a phosphor-screen (S0230, GE Lifesciences) and was digitally collected using a Typhoon scanner. ImageQuant densitometry was used to quantify the phosphor-signal.

GTP Hydrolysis Assay

GTPase activity of strep-tagged LRRK2 was measured in 30 uL GTPase buffer (20 mM Tris pH 7.5, 150 mM NaCl, 1 mM DTT, 5 mM $MgCl_2$, 1 mM EDTA) at 30°C for 90 minutes. LRRK2 was incubated with inhibitor for 30 min on ice before reactions were initiated with the addition of 50 μM cold GTP and [α-^{32}P] GTP (3000Ci/mmol; BLU006H250UC, PerkinElmer Life Sciences). Reactions were terminated with the addition of 0.5 M EDTA. 2 uL of the reaction mixture were dotted onto TLC plates (M1055790001, EMD Millipore). GDP and GTP were separated by TLC using 0.5 M KH_2PO_4 pH 3.5 for 60 minutes. The TLC plate was dried for 15 minutes and radioactive signal was captured and using a phosphor-screen and a Typhoon scanner. ImageQuant densitometry was used to quantify the phosphor-signal.

B12-Agarose Binding Assay

500 μL of 40 nM strep-tagged LRRK2 or 500 uL of 100 nM GST, pre-loaded with AdoCbl or buffer for 30 min on ice, were incubated with 50 uL B12-Agarose (V3254, Sigma Aldrich). B12-Agarose was washed 3x with buffer (50 mM Tris-HCl pH 7.5, 150 mM NaCl, 1 mM TCEP, 0.02% Triton X-100, 1% Ficoll 400) and bound protein was eluted with Laemmli buffer and boiling at 95°C. Bound LRRK2 or GST was analyzed by western blot.

Thermal Shift Assay

300 nM strep-tagged LRRK2 was incubated with Sypro Orange and inhibitor or buffer to a final volume of 30 uL. Using a Stratagene Mx3000 Real-time PCR machine, samples were heated to 95°C and fluorescence intensity of Sypro Orange was measured at every 0.5°C increment. For each experiment, data was normalized to the maximum fluorescent intensity.

590

591 ***Microscale Thermophoresis***

592 Microscale Thermophoresis (MST) measurements were obtained using a Monolith NT.115
593 (NanoTemper Technologies). Purified strep-tagged LRRK2 was labeled with NT-647 dye
594 (NanoTemper Technologies) and experiments were performed using a 2 nM final concentration.
595 A 12-point dilution series of AdoCbl, ranging from 200 nM to 100 μM, was added to labeled
596 LRRK2. After 30 min incubation on ice, the binding reaction was loaded onto Standard
597 capillaries (NanoTemper Technologies) and measurements were taken using 30% LED power
598 and 50% MST power. Laser on-time was set to 30 seconds and laser off-time was set to 5
599 seconds. Data was processed using GraphPad Prism 6.0 and a K_D was derived from three
600 independent thermophoresis experiments by fitting a curve based on the law of mass action.
601 Quality of each MST run was assessed by performing a capillary scan before and after each data
602 collection to check that the fluorescence between samples stays within ± 10%. Furthermore, each
603 time-trace showed a smooth decrease in normalized fluorescence, suggesting that no
604 precipitation occurred during the experiments.

605

606 ***STD-NMR***

607 Saturation Transfer Difference (STD) NMR was carried out with 1024 scans on a Bruker
608 800MHz NMR spectrometer equipped with a cryogenic probe at 277 K according to Mayer et
609 al[93]. Saturation on and off frequencies were set to -1 and -20 ppm, respectively, with saturation
610 achieved using a 2 s train of 50 ms Gaussian pulses at 86 Hz. 1024 scans were used. STD-NMR
611 samples contained 50 mM Tris, 150 mM NaCl, 1 mM TCEP and 2 mM MgCl2 at a pH of 7.5,

612 20-30 μM Roco4 protein, with vitamin B_{12} at 100-fold excess over Roco4 in concentration.
613 Vitamin B_{12} resonances were assigned in D2O according to Summers et al[94].
614
615 ***Intrinsic Fluorescence***
616 Strep-tagged LRRK2 at a concentration of 150 nM was incubated with AdoCbl or buffer in a
617 total volume of 80uL. Samples were loaded onto a 96-well black-walled plate and fluorescence
618 was measured using a Tecan Safire microplate reader. For these experiments, a correction
619 equation must be applied to the fluorescent measurements to compensate for the inner filter
620 effect. AdoCbl absorbs light at 295 nm, which affects the excitation strength of the incident light,
621 and from 340-360 nm, which affects the amount of light reaching the detector after tryptophan
622 emission. Therefore, we calculated a corrected fluorescence value (**Supplementary**
623 **information, Figs. S5c-d**) for each sample by measuring the absorbance at the excitation and
624 emission wavelengths and multiplying by the original fluorescence value [95].
625
626 ***Limited Proteolysis Assays***
627 Strep-tagged LRRK2 or TBK1 was subjected to limited proteolysis by trypsin or chymotrypsin
628 with a 10:1 molar ratio of LRRK2 to protease at 37°C. LRRK2 was loaded with inhibitor for 30
629 min on ice before protease was added. Reactions were stopped with the addition of Laemmli
630 buffer and boiling at 95°C.
631
632 ***In situ labeling and detection of LRRK2 dimers.***

For the biochemical detection and purification of biotinylated LRRK2 dimers, we used an adaptation of the proximity biotinylation approach[96]. A manuscript describing the full characterization of this assay is currently under review (Leandrou et al.; submitted to Biochem J). HEK293T cells, maintained throughout the duration of the experiment in biotin-depleted media, were co-transfected with plasmids encoding WT LRRK2, fused to biotin ligase (BirA) or an acceptor peptide (AP). The following day, the growth media was replaced and the indicated concentrations of AdoCbl, diluted in media, were added, and the cultures maintained for an additional 48h. Prior to cell lysis, the cells were washed in pre-warmed PBS and given a brief (5 min) pulse with 50 μM biotin, followed extensive washing with PBS. Cytoplasmic extracts were prepared in lysis buffer (20mM HEPES, pH 7.4; 150 mM NaCl; 0.5% NP-40; 2mM EGTA; 2 mM $MgCl_2$; 10% glycerol; pH 7.2). Following lysis, 5 μg of total clarified cell extract was bound to streptavidin-coated ELISA plates for 1h at 37ºC under constant agitation. The supernatant was removed and retained, and the wells were washed, and the amount of biotinylated LRRK2 present in each sample was quantified using HRP-conjugated (in house) anti-LRRK2 (75-253, NeuroMab/Antibodies Incorporated; clone N241A/B34). Duplicate samples were incubated in the parallel ELISA plates pre-coated with anti-LRRK2 (ab195024, Abcam) in order to quantify the total amount of LRRK2 present in each sample. In each experiment, control samples were prepared from cells co-expressing AP-LRRK2 together with Flag-LRRK2 (without the BirA biotin ligase). To visualize expression of both LRRK2 constructs, parallel extracts were separated by SDS-PAGE (6%), and membranes probed with anti-LRRK2 (clone N241A/B34).

Generation of Mouse Embryonic Fibroblasts (MEFs)

LRRK2-G2019S and wild type control MEFs were isolated from mouse embryos at day E13.5 resulting from crosses between heterozygous LRRK2-G2019S and wild type C57/BL/6J mice. All the MEFs were cultured for at least 30 passages to immortalize the cells. All cells were cultured in DMEM containing 10% FBS, 2mM L-glutamine and 100 units/ml Penicillin-Streptomycin, and were maintained at 37°C with 5% CO_2. All cells lines were confirmed by PCR genotyping and western blot, but were not tested for mycoplasma contamination. To test inhibition, cells were treated with inhibitor or DMSO for 24 hours in DMEM with 3% FBS before being lysed and subject to western blot for analysis.

Treatment of C. elegans with AdoCbl

C. elegans strains were cultured on standard nematode growth medium (NGM) agar plates seeded with *E. coli* OP50 as a food source. Mixed stage animals were maintained as bulk culture on NGM agar at room temperature (22^{o}C). Prior to each experiment, animals were age-synchronized by standard bleaching and washing protocol to obtain embryos, from which developmental stages were followed. The following transgenic *C. elegans* lines expressing green fluorescent protein (GFP) either alone (SGC730: Pdat-1::GFP) or together with human *LRRK2-G2019S* (SGC856: Pdat-1::LRRK2-G2019S; Pdat-1::GFP) or human *LRRK2-R1441C* (SGC851: Pdat-1::LRRK2-R1441C Pdat-1::GFP) in dopaminergic neurons were used[63].

Treatment with AdoCbl was done in liquid culture to ensure adequate drug exposure using the published protocol as described[30]. Briefly, worms were age-synchronized to generate L1 larva in M9 buffer [For 1 liter: KH2PO4, 3 g; Na2HPO4, 6 g; NaCl, 5 g; MgSO4 (1 M), 1 ml], which

were distributed into a 12-well microtiter plate seeded with *E. coli* OP50 with roughly 50 L1 worms in a total volume of 900 ml. AdoCbl stock made in water was added to achieve the desired concentrations. The 12-well plate was covered in aluminum foil to protect from light, maintained in a humidified chamber at room temperature and shaken at 100 rpm. Worms were monitored every day and placed onto agar plates with OP50 when most of them reached L4 larval stage (about 3 days). L4 worms were grown on NGM agar plates seeded with *E. coli* OP50 for 3 days for behavioral assay or 9 days for neuronal assessment as described below.

C. elegans Basal Slowing Assay

Well-fed worms with intact dopaminergic neural circuitry move slower in the presence of bacterial food than in its absence[64]. This basal slowing response was assayed as described previously[63,64]. Briefly, a set of NGM assay plates were seeded with bacterial food, *E. coli* OP50, in a ring shape, and another set of NGM assay plates were uncoated. Age-synchronized worms (about 10 worms of each strain) were washed twice in S basal buffer (100 mM NaCl, 10 mg/ml cholesterol, 50 mM potassium phosphate, pH 6.0). Worms were then transferred to the center of the NGM plates coated with or without *E. coli* OP50 as described above, settled for 5 min, and their locomotion were recorded with a digital camera in 20 s intervals. Body bends were examined using an unbiased machine-vision analysis system (WormLab, MBF Bioscience, Williston, VT). Basal slowing was calculated as the percent slowing in body bends per 20 s in the presence vs. the absence of bacterial lawn.

Assessment of Dopaminergic Neuron Survival in C. elegans

699 Dopaminergic neurons in live *C. elegans* were examined essentially as described[63]. Briefly,
700 worms were immobilized in the presence of 3 mM levamisole and were mounted on glass slides.
701 The dopaminergic neurons in the head regions [four cephalic neurons (CEPs)] were visualized
702 for GFP fluorescence under a Zeiss Axiovert 200M microscope. The total numbers of CEPs with
703 the intact cell body (survived) as well as those missing most of the cell body and neurites
704 (degenerated) were counted. For each strain, about 30 worms were analyzed in at least three
705 independent experiments. The percent of dopaminergic neuron survival was calculated as the
706 number of intact CEPs observed in all animals divided by total number of CEPs expected if no
707 degeneration occurred (four in each animal times the number of animals tested), times 100.
708 Fluorescent images of DA neurons in the head region of worms were taken with a Zeiss Axiovert
709 200M microscope using 1 s exposure time at 20× magnification.
710
711 Sample size was determined according to the Statistical Solutions LLC calculator
712 (http://www.statisticalsolutions.net/pssTtest_calc.php). Assuming alpha value of 0.05, to detect
713 difference of 10% between 100% mean for the control group and 90% mean for an experimental
714 group, 5% expected standard deviation (two-sided t-test), and a power of 0.8, a sample site of 4
715 animals is obtained. In Fig. 4, more than 20 worms were used for each group. All live and age-
716 synchronized worms were included in the experiments. Only dead worms, if any, were excluded.
717 The number of worms available for experiments was in general five times more than the number
718 of worms being assayed (e.g., 20 worms were randomly picked for from a culture of 100
719 worms). For these experiments, the investigator was not blinded to group allocations. Data is
720 normally distributed, and the variance was similar between the groups that are being statistically
721 compared.

722

723 ***Treatment of Drosophila with AdoCbl***

724 Flies were used and raised as described recently[31]. Briefly, the *TH* (*tyrosine hydroxylase*) GAL4
725 was crossed with either UAS-*hLRRK2-wildtype,* UAS-*hLRRK2-G2019S* or the kinase-dead
726 UAS-*hLRRK2-G2019S-K1906M* line to produce progeny dopaminergic expression of the
727 transgene (*DA → hLRRK2, DA → G2019S, DA → KD*). The crosses were allowed to lay eggs
728 onto instant fly food (Carolina) or onto instant food supplemented with AdoCbl. The final
729 concentration of AdoCbl in the fly food ranged from 100 to 2500 nM. Females were collected on
730 the day of emergence and transferred to new vials (no AdoCbl) for 24 hours. In control
731 experiments, low expression dLRRK flies ($dLRRK^{e03680}$) were fed instant fly food or food
732 supplemented with AdoCbl.

733

734 **Physiological recordings**: 18-24 hour old females were aspirated in a pipette tip, restrained with
735 nail polish, and allowed to recover for >20 minutes. A recording electrode was placed in the
736 center of the eye, and a reference electrode in the mouthparts. After 2 minutes in the dark, the fly
737 was illuminated with light from a blue flickering LED and the resulting electroretinogram signal
738 amplified and stored for off-line analysis. The response was analyzed by the Fast Fourier
739 Transform (FFT), generating components corresponding to the photoreceptors, second order
740 lamina neurons, and third/fourth order medulla neurons. Stimulus generation, recording and
741 analysis were accomplished in Matlab, as described recently[31]; Matlab code available at
742 https://github.com/wadelab/flyCode). The number of flies used was sufficient according to
743 previously published data[31]. All data from tested flies were included. Male and female flies of
744 the required genotype were placed in randomly chosen vials (+/- drug) and allowed to mate and

lay eggs. Offspring were harvested daily and flies were sampled at random. The investigators were blinded to the genotype while the experiments were in progress. For statistical analysis, estimates of variation were made and are similar between groups being compared.

Determination of Survival of Primary Cortical Neurons

Primary rat embryonic cortical neurons were prepared and cultured as described[70,97]. Briefly, embryonic day 17 rat cortices were dissociated and plated on poly-d-lysine coated 12mm diameter glass coverslips in Neurobasal medium (12348017, Invitrogen-ThermoScientific) with B-27 serum free supplements (17504044, Invitrogen-ThermoScientific) at a density of 125,000 neurons per cm^2. On day four following plating, neurons were transiently co-transfected with LRRK2-WT or LRRK2-G2019S and pcms-EGFP at a ratio of 4:1 using Lipofectamine 2000 according to the manufacturer's instructions. The indicated concentrations of AdoCbl or MLi-2 in Neurobasal/B-27 medium was added to the neurons on the morning following transfection and supplemented one additional time at the mid-point (36 h) of the total duration of the experiment. Following a period of 72 h of expression, the coverslips were fixed in 4% formaldehyde and stained with anti-GFP antibodies (ab13970, Abcam) and DAPI. We had determined in parallel neurons double stained with GFP and anti-LRRK2 antibodies (ab133474, Abcam) that the percentage of GFP-positive neurons over-expressing LRRK2 was approximately 90% (not shown). To simplify quantification of apoptotic degenerating neurons, GFP-positive neurons were visualized and determine to be apoptotic or viable. For quantification, apoptotic neurons were defined as those having condensed fragmented chromatin comprised of two or more apoptotic bodies. More than 100 neurons per coverslip were assessed in triplicate coverslips in a

767 blinded fashion, from two to three independent cultures. The data are presented as the percentage
768 of GFP-positive neurons containing apoptotic nuclear features.

769

770 ***Animals and Brain Slice Preparation***

771 The use of the animals followed the National Institutes of Health guidelines and was approved
772 by the Institutional Animal Care and Use Committee at Thomas Jefferson University. All efforts
773 were made to minimize the number of animals used. BAC LRRK2(hR1441G) transgenic (TG)
774 mice were obtained from Chenjian Li's laboratory at Weill Medical College of Cornell
775 University and maintained on Taconic FVB/N background and BAC LRRK2(G2019S) TG mice
776 previously described[19] maintained on C57/NJ background.

777 Three- to 5-month-old male transgenic LRRK2-G2019S mice and their non-transgenic
778 littermates were used for LRRK2 kinase inhibition in striatal brain slices. For preparing striatal
779 slices, mice were decapitated without anesthesia after cervical dislocation and brains were
780 immediately dissected out. Coronal striatal brain slices at 250 μm were prepared on a vibratome
781 (VT1200, Leica, Solms, Germany). The striatal slices were allowed to recover for 0.5 to 1 hour
782 at 36°C in a holding chamber containing oxygenated artificial CSF (ASCF: 125 mM NaCl, 2.5
783 mM KCl, 26 mM $NaHCO_3$, 2.4 mM $CaCl_2$, 1.3 mM $MgSO_4$, 0.3 mM KH_2PO_4, and 10 mM
784 glucose, pH 7.3-7.4). To examine the effects of the LRRK2 inhibitors, slices were incubated for
785 2 h in oxygenated ACSF containing LRRK2 inhibitors. For the incubation treatment, striatal
786 slices were bisected, and one striatum was exposed to LRRK2 inhibitor (2 h) while the other was
787 exposed to vehicle (DMSO or water). After treatment, the slices were collected and rapidly
788 frozen in dry ice and stored in -80°C until assayed.

789

790 ***Slice Preparation for Evoked DA Transmission***

791 Twelve- to 15-month-old male LRRK2-G2019S as well as 6- to 14-month-old male
792 LRRK2-R1441G BAC transgenic mice and their age-matched non-transgenic littermates were
793 used. For preparing striatal slices, mice were decapitated without anesthesia after cervical
794 dislocation and brains were immediately dissected out. Coronal striatal brain slices at 250 μm
795 were prepared on a vibratome (VT1200, Leica, Solms, Germany) for electrophysiological
796 recording. The striatal slices were allowed to recover for at least 1 hour at 36°C in a holding
797 chamber containing oxygenated artificial CSF (ASCF) and then placed in a recording chamber
798 superfused (1.5 ml/min) with ACSF at 36°C. The pH of all ACSF solutions were adjusted to 7.3–
799 7.4 with concentrated hydrochloric acid and ACSF solutions were saturated with carbogen (95%
800 O_2/5% CO_2) prior to use to ensure stable pH buffering and adequate oxygenation.

801 Striatal slices were bisected, and one striatum was incubated for 2 hours in ACSF at 36°C
802 containing 300 μM AdoCbl while the other was exposed to vehicle (water) as the control. Slices
803 were washed with ACSF for 20 min after treatment before fast scan cyclic voltammetry (FSCV)
804 recording.

805

806 ***Fast scan cyclic voltammetry recording (FSCV)***

807 FSCV was used to measure evoked DA release in the dorsal striatum (dSTR). Electrochemical
808 recordings and electrical stimulation were performed as previously described[73]. Briefly, freshly
809 cut carbon fiber electrodes ~5 μm in diameter were inserted ~50 μm into the dSTR slice. For
810 FSCV, a triangular voltage wave (-400 to 900 mV at 280 V/sec versus Ag/AgCl) was applied to
811 the electrode every 100 msec. Current was recorded with an Axopatch 200B amplifier (Axon
812 Instruments, Foster City, CA), with a low-pass Bessel filter set at 10 kHz, digitized at 25 kHz
813 (ITC-18 board; InstruTech, Great Neck, NY). Triangular wave generation and data acquisition

were controlled by a personal computer running a locally written (Dr. E. Mosharov, Columbia University, New York, NY) IGOR program (WaveMetrics, Lake Oswego, OR). Striatal slices were electrically stimulated (400 μA x 1 ms pulse duration) by an Iso-Flex stimulus isolator triggered by a Master-8 pulse generator (AMPI, Jerusalem, Israel) using a bipolar stimulating electrode placed at a distance of ~150 μm from the recording electrode. The slices were stimulated every 2 min. Background-subtracted cyclic voltammograms served for electrode calibration and to identify the released substance. DA oxidation current was converted to concentration based upon a calibration of 5 μM DA in ACSF after the experiment. For each experimental condition, at least three slices from at least three different mice were examined unless specified otherwise. The number of the recording sites was determined according to previously published experiments[19] and SSD sample size power analysis. No randomization and no blinding were used for experimental groupings. All recorded data was included. Statistical tests were justified as appropriate, as data meets test assumptions, with a similar estimated variance between groups that are statistically compared.

Acknowledgements

This work was supported in part by awards from the Michael J. Fox Foundation to MMZ, IU-B ZY, HJR. ZY was also supported by NIH R01NS060809. ZY and IU-B were supported by NIH R01GM115844. HZ was supported by NIH R01NS097530. SGC was supported by NIH R21NS073170. CE was supported by an award from The Welcome Trust [ref: 097829] through the Centre for Chronic Diseases and Disorders (C2D2) at the University of York. We thank Dr. Insup Choi, Dr. Kerry Purtell, and Yuanxi Zhang from Yue's lab for technical support.

Author contributions: X.L., N.P., K.M., M-M.Z, and Z.Y. performed the HTS and identified vitamin B_{12} as a LRRK2 inhibitor. X.L. and Z.Y. performed brain LRRK2 purification. A.S., X.H., Y.G.-Ll. and I.U.-B. performed HEK293T LRRK2, Roco4 kinase, and GST purifications. A.S., Z.Y., and I.U.-B. performed in vitro kinase and GTP hydrolysis assays. A.S. and I.U.-B. performed B12-agarose binding, Microscale Thermophoresis, Thermal Shift Assays, Intrinsic Fluorescence, and Limited proteolysis assays. X.L. and Z.Y. performed Michaelis-Menten kinetics assays. N.C. and C.W. performed STD-NMR. X.L. and Z.Y. generated LRRK2 MEFs. A.S., X.L. and Z.Y. performed cellular inhibition assays. L.Z. and H.Z. prepared mouse brain slices, inhibitor incubation, and performed FSCV recording experiments. E.L., A.M., and H.R. performed apoptotic analysis of primary cortical neurons. C.Y. and S.C. performed all *C. elegans* experiments. F.A. and C.E. performed all *D. melanogaster* experiments. A.S. and I.U.-B. wrote manuscript drafts. A.S., I.U.-B., and Z.Y. edited the manuscript. I.U.-B. and Z.Y. designed the research.

Glossary of Terms

ACSF: artificial cerebrospinal fluid
AdoCbl: 5'-deoxyadenosylcobalamin, or adenosylcobalamin
AP: acceptor peptide
a.u.: arbitrary unit
BirA: biotin ligase
BAC: bacterial artificial chromosome
CEP: cephalic neurons
CNCbl: cyanocobalamin
CRF: contrast response function
DAergic: dopaminergic
DMZ: dimethylbenzimidazole
FFT: fast Fourier transform

FSCV: fast scan cyclic voltammetry

HOCbl: hydroxycobalamin
HTS: High-throughput Screen
LRRK2: Leucine-Riche Repeat Kinase 2
MBP: myelin basic protein
MeCbl: methylcobalamin
MEF: mouse embryonic fibroblast
MST: microscale thermophoresis
PD: Parkinson's Disease
STD-NMR: saturation transfer difference nuclear magnetic resonance
TR-FRET: time-resolved fluorescence resonance energy transfer
TSA: thermal stability assay
WT: wild-type

References

1 Dickson, D. W. *et al.* Neuropathology of non-motor features of Parkinson disease. *Parkinsonism & Related Disorders* **15, Supplement 3**, S1-S5, doi:http://dx.doi.org/10.1016/S1353-8020(09)70769-2 (2009).

2 Lees, A. J., Hardy, J. & Revesz, T. Parkinson's disease. *The Lancet* **373**, 2055-2066, doi:10.1016/S0140-6736(09)60492-X (2009).

3 Funayama, M. *et al.* A new locus for Parkinson's disease (PARK8) maps to chromosome 12p11.2-q13.1. *Ann Neurol* **51**, 296-301, doi:10.1002/ana.10113 [pii] (2002).

4 Paisán-Ruíz, C. *et al.* Cloning of the gene containing mutations that cause PARK8-linked Parkinson's disease. *Neuron* **44**, 595-600, doi:10.1016/j.neuron.2004.10.023 (2004).

5 Zimprich, A. *et al.* Mutations in LRRK2 cause autosomal-dominant parkinsonism with pleomorphic pathology. *Neuron* **44**, 601-607, doi:S0896627304007202 [pii]
10.1016/j.neuron.2004.11.005 (2004).

6 Satake, W. *et al.* Genome-wide association study identifies common variants at four loci as genetic risk factors for Parkinson's disease. *Nature Genet.* **41**, 1303-U1361, doi:10.1038/ng.485 (2009).

7 Simon-Sanchez, J. *et al.* Genome-wide association study reveals genetic risk underlying Parkinson's disease. *Nature Genet.* **41**, 1308-U1368, doi:10.1038/ng.487 (2009).

8 Do, C. B. *et al.* Web-based genome-wide association study identifies two novel loci and a substantial genetic component for Parkinson's disease. *PLoS genetics* **7**, e1002141, doi:10.1371/journal.pgen.1002141 (2011).

9 Lill, C. M. *et al.* Comprehensive research synopsis and systematic meta-analyses in Parkinson's disease genetics: The PDGene database. *PLoS genetics* **8**, e1002548, doi:10.1371/journal.pgen.1002548 (2012).

10 Healy, D. G. *et al.* Phenotype, genotype, and worldwide genetic penetrance of LRRK2-associated Parkinson's disease: a case-control study. *The Lancet Neurology* **7**, 583-590, doi:10.1016/S1474-4422(08)70117-0 (2008).

11 Tomiyama, H. *et al.* Clinicogenetic study of mutations in LRRK2 exon 41 in Parkinsons's disease patients from 18 countries. *Movement Disorders* **21**, 1102-1108, doi:10.1002/mds.20886 (2006).

12 Guaitoli, G. *et al.* Structural model of the dimeric Parkinson's protein LRRK2 reveals a compact architecture involving distant interdomain contacts. *Proceedings of the National Academy of Sciences of the United States of America*, 201523708-201523708, doi:10.1073/pnas.1523708113 (2016).

13 Sen, S., Webber, P. J. & West, A. B. Dependence of leucine-rich repeat kinase 2 (LRRK2) kinase activity on dimerization. *Journal of Biological Chemistry* **284**, 36346-36356, doi:10.1074/jbc.M109.025437 (2009).

14 Bardien, S., Lesage, S., Brice, A. & Carr, J. Genetic characteristics of leucine-rich repeat kinase 2 (LRRK2) associated Parkinson's disease. *Parkinsonism and Related Disorders* **17**, 501-508, doi:10.1016/j.parkreldis.2010.11.008 (2011).

15 Benamer, H. T. S. & De Silva, R. LRRK2 G2019S in the North African population: A review. *European Neurology* **63**, 321-325, doi:10.1159/000279653 (2010).

16 West, A. B. *et al.* Parkinson's disease-associated mutations in leucine-rich repeat kinase 2 augment kinase activity. *Proceedings of the National Academy of Sciences of the United States of America* **102**, 16842-16847, doi:10.1073/pnas.0507360102 (2005).

17 Greggio, E. *et al.* The Parkinson disease-associated leucine-rich repeat kinase 2 (LRRK2) is a dimer that undergoes intramolecular autophosphorylation. *Journal of Biological Chemistry* **283**, 16906-16914, doi:10.1074/jbc.M708718200 (2008).

18 Berger, Z., Smith, K. A. & Lavoie, M. J. Membrane localization of LRRK2 is associated with increased formation of the highly active lrrk2 dimer and changes in its phosphorylation. *Biochemistry* **49**, 5511-5523, doi:10.1021/bi100157u (2010).
19 Li, X. *et al.* Enhanced striatal dopamine transmission and motor performance with LRRK2 overexpression in mice is eliminated by familial Parkinson's disease mutation G2019S. *The Journal of Neuroscience: The Official Journal of the Society for Neuroscience* **30**, 1788-1797, doi:10.1523/JNEUROSCI.5604-09.2010 (2010).
20 Sheng, Z. *et al.* Ser1292 autophosphorylation is an indicator of LRRK2 kinase activity and contributes to the cellular effects of PD mutations. *Science translational medicine* **4**, 164ra161-164ra161, doi:10.1126/scitranslmed.3004485 (2012).
21 Yue, M. *et al.* Progressive dopaminergic alterations and mitochondrial abnormalities in LRRK2 G2019S knock-in mice. *Neurobiology of Disease* **78**, 172-195, doi:http://dx.doi.org/10.1016/j.nbd.2015.02.031 (2015).
22 Fraser, K. B., Moehle, M. S., Alcalay, R. N. & West, A. B. Urinary LRRK2 phosphorylation predicts parkinsonian phenotypes in G2019S LRRK2 carriers. *Neurology* **86**, 994-999, doi:10.1212/wnl.0000000000002436 (2016).
23 Steger, M. *et al.* Phosphoproteomics reveals that Parkinson's disease kinase LRRK2 regulates a subset of Rab GTPases. *eLife* **5**, doi:10.7554/eLife.12813.001 (2016).
24 Ito, G. *et al.* Phos-tag analysis of Rab10 phosphorylation by LRRK2: a powerful assay for assessing kinase function and inhibitors. *Biochemical Journal* **473**, 2671 (2016).
25 Lee, B. D. *et al.* Inhibitors of leucine-rich repeat kinase-2 protect against models of Parkinson's disease. *Nature medicine* **16**, 998-1000, doi:10.1038/nm.2199 (2010).
26 Sweet, E. S., Saunier-Rebori, B., Yue, Z. & Blitzer, R. D. The Parkinson's Disease-Associated Mutation LRRK2-G2019S Impairs Synaptic Plasticity in Mouse Hippocampus. *The Journal of Neuroscience* **35**, 11190 (2015).
27 Daher, J. P. L. *et al.* Leucine-rich Repeat Kinase 2 (LRRK2) Pharmacological Inhibition Abates α-Synuclein Gene-induced Neurodegeneration. *Journal of Biological Chemistry* **290**, 19433-19444 (2015).
28 Volpicelli-Daley, L. A. *et al.* G2019S-LRRK2 Expression Augments α-Synuclein Sequestration into Inclusions in Neurons. *The Journal of Neuroscience* **36**, 7415 (2016).
29 Liu, Z. *et al.* Inhibitors of LRRK2 kinase attenuate neurodegeneration and Parkinson-like phenotypes in Caenorhabditis elegans and Drosophila Parkinson's disease models. *Human Molecular Genetics* **20**, 3933-3942, doi:10.1093/hmg/ddr312 (2011).
30 Yao, C. *et al.* Kinase inhibitors arrest neurodegeneration in cell and C. elegans models of LRRK2 toxicity. *Human Molecular Genetics* **22**, 328-344, doi:10.1093/hmg/dds431 (2013).
31 Afsari, F. *et al.* Abnormal visual gain control in a Parkinson's disease model. *Human Molecular Genetics* **23**, 4465-4478, doi:10.1093/hmg/ddu159 (2014).
32 Dzamko, N. *et al.* Inhibition of LRRK2 kinase activity leads to dephosphorylation of Ser(910)/Ser(935), disruption of 14-3-3 binding and altered cytoplasmic localization. *The Biochemical journal* **430**, 405-413, doi:10.1042/BJ20100784 (2010).
33 Ramsden, N. *et al.* Chemoproteomics-based design of potent LRRK2-selective lead compounds that attenuate Parkinson's disease-related toxicity in human neurons. *ACS Chemical Biology* **6**, 1021-1028, doi:10.1021/cb2002413 (2011).
34 Zhang, J., Deng, X., Geun, H., Alessi, D. R. & Gray, N. S. Characterization of TAE684 as a potent LRRK2 kinase inhibitor. *Bioorganic & Medicinal Chemistry Letters* **22**, 1864-1869, doi:10.1016/j.bmcl.2012.01.084 (2012).
35 Deng, X. *et al.* Characterization of a selective inhibitor of the Parkinson's disease kinase LRRK2. *Nature chemical biology* **7**, 203-205, doi:10.1038/nchembio.538 (2011).

36 Reith, A. D. *et al.* GSK2578215A ; A potent and highly selective 2-arylmethyloxy-5-substitutent- N -arylbenzamide LRRK2 kinase inhibitor. *Bioorganic & Medicinal Chemistry Letters* **22**, 5625-5629, doi:10.1016/j.bmcl.2012.06.104 (2012).

37 Fuji, R. N. *et al.* Effect of selective LRRK2 kinase inhibition on nonhuman primate lung. *Science translational medicine* **7**, 273ra215-273ra215, doi:10.1126/scitranslmed.aaa3634 (2015).

38 Henderson, J. L. *et al.* Discovery and preclinical profiling of 3-[4-(morpholin-4-yl)-7H-pyrrolo[2,3-d]pyrimidin-5-yl]benzonitrile (PF-06447475), a highly potent, selective, brain penetrant, and in vivo active LRRK2 kinase inhibitor. *Journal of Medicinal Chemistry* **58**, 419-432, doi:10.1021/jm5014055 (2015).

39 Fell, M. J. *et al.* MLi-2, a Potent, Selective, and Centrally Active Compound for Exploring the Therapeutic Potential and Safety of LRRK2 Kinase Inhibition. *The Journal of pharmacology and experimental therapeutics* **355**, 397-409, doi:10.1124/jpet.115.227587 (2015).

40 Anand, V. S. *et al.* Investigation of leucine-rich repeat kinase 2: Enzymological properties and novel assays. *FEBS Journal* **276**, 466-478, doi:10.1111/j.1742-4658.2008.06789.x (2009).

41 Randaccio, L., Geremia, S., Demitri, N. & Wuerges, J. Vol. 15 3228-3259 (2010).

42 Banerjee, R., Gherasim, C. & Padovani, D. The tinker , tailor , soldier in intracellular B 12 trafficking. *Current Opinion in Chemical Biology* **13**, 484-491, doi:10.1016/j.cbpa.2009.07.007 (2009).

43 Green, R. *et al.* Vitamin B12 deficiency. *Nature Reviews Disease Primers* **3**, 17040, doi:10.1038/nrdp.2017.40 (2017).

44 Li, X. *et al.* Phosphorylation-dependent 14-3-3 binding to LRRK2 is impaired by common mutations of familial parkinson's disease. *PLoS ONE* **6**, 1-13, doi:10.1371/journal.pone.0017153 (2011).

45 Semisotnov, G. V. *et al.* Study of the "molten globule" intermediate state in protein folding by a hydrophobic fluorescent probe. *Biopolymers* **31**, 119-128, doi:10.1002/bip.360310111 (1991).

46 Wienken, C. J., Baaske, P., Rothbauer, U., Braun, D. & Duhr, S. Protein-binding assays in biological liquids using microscale thermophoresis. *Nature Communications* **1**, 1-7, doi:10.1038/ncomms1093 (2010).

47 Gilsbach, B. K. *et al.* Structural characterization of LRRK2 inhibitors. *Journal of Medicinal Chemistry* **58**, 3751-3756, doi:10.1021/jm5018779 (2015).

48 McCoy, M. A., Senior, M. M. & Wyss, D. F. Screening of Protein Kinases by ATP-STD NMR Spectroscopy. *Journal of the American Chemical Society* **127**, 7978-7979, doi:10.1021/ja0425942 (2005).

49 Gilsbach, B. K. *et al.* Roco kinase structures give insights into the mechanism of Parkinson disease-related leucine-rich-repeat kinase 2 mutations. *Proceedings of the National Academy of Sciences of the United States of America* **109**, 10322-10327, doi:10.1073/pnas.1203223109 (2012).

50 Li, T. *et al.* A novel GTP-binding inhibitor, FX2149, attenuates LRRK2 toxicity in Parkinson's disease models. *PLoS ONE* **10**, 1-15, doi:10.1371/journal.pone.0122461 (2015).

51 Copeland, R. A. in *Evaluation of Enzyme Inhibitors in Drug Discovery* 57-121 (John Wiley & Sons, Inc., 2013).

52 Nichols, R. J. *et al.* Substrate specificity and inhibitors of LRRK2, a protein kinase mutated in Parkinson's disease. *The Biochemical journal* **424**, 47-60, doi:10.1042/BJ20091035 (2009).

53 Copeland, R. A., Harpel, M. R. & Tummino, P. J. Targeting enzyme inhibitors in drug discovery. *Expert Opinion on Therapeutic Targets* **11**, 967-978, doi:10.1517/14728222.11.7.967 (2007).

54 Lobbestael, E. *et al.* Pharmacological LRRK2 kinase inhibition induces LRRK2 protein destabilization and proteasomal degradation. *Scientific Reports* **6**, 33897, doi:10.1038/srep33897 (2016).

55 Zhao, J., Molitor, T. P., Langston, J. W. & Nichols, R. J. LRRK2 dephosphorylation increases its ubiquitination. *Biochemical Journal* **469**, 107-120 (2015).
56 Skibinski, G., Nakamura, K., Cookson, M. R. & Finkbeiner, S. Mutant LRRK2 toxicity in neurons depends on LRRK2 levels and synuclein but not kinase activity or inclusion bodies. *Journal of Neuroscience* **34**, 418-433 (2014).
57 Li, X. *et al.* Leucine-rich repeat kinase 2 (LRRK2)/PARK8 possesses GTPase activity that is altered in familial Parkinson's disease R1441C/G mutants. *Journal of Neurochemistry* **103**, 238-247, doi:10.1111/j.1471-4159.2007.04743.x (2007).
58 Melrose, H. L. *et al.* Impaired dopaminergic neurotransmission and microtubule-associated protein tau alterations in human LRRK2 transgenic mice. *Neurobiology of Disease* **40**, 503-517, doi:10.1016/j.nbd.2010.07.010 (2010).
59 Tong, Y. *et al.* R1441C mutation in LRRK2 impairs dopaminergic neurotransmission in mice. *Proceedings of the National Academy of Sciences of the United States of America* **106**, 14622-14627, doi:10.1073/pnas.0906334106 (2009).
60 Imai, Y. *et al.* Phosphorylation of 4E-BP by LRRK2 affects the maintenance of dopaminergic neurons in Drosophila. *The EMBO journal* **27**, 2432-2443, doi:10.1038/emboj.2008.163 (2008).
61 Liu, Z. *et al.* A Drosophila model for LRRK2-linked parkinsonism. *Proceedings of the National Academy of Sciences of the United States of America* **105**, 2693-2698, doi:10.1073/pnas.0708452105 (2008).
62 Saha, S. *et al.* LRRK2 modulates vulnerability to mitochondrial dysfunction in Caenorhabditis elegans. *The Journal of neuroscience : the official journal of the Society for Neuroscience* **29**, 9210-9218, doi:10.1523/JNEUROSCI.2281-09.2009 (2009).
63 Yao, C. *et al.* LRRK2-mediated neurodegeneration and dysfunction of dopaminergic neurons in a Caenorhabditis elegans model of Parkinson ' s disease. *Neurobiology of Disease* **40**, 73-81, doi:10.1016/j.nbd.2010.04.002 (2010).
64 Sawin, E. R., Ranganathan, R. & Horvitz, H. R. C. elegans Locomotory Rate Is Modulated by the Environment through a Dopaminergic Pathway and by Experience through a Serotonergic Pathway. *Neuron* **26**, 619-631, doi:10.1016/S0896-6273(00)81199-X (2000).
65 Jackson, C. R. *et al.* Retinal Dopamine Mediates Multiple Dimensions of Light-Adapted Vision. *Journal of Neuroscience* **32**, 9359-9368, doi:10.1523/JNEUROSCI.0711-12.2012 (2012).
66 Harnois, C. & Di Paolo, T. Decreased dopamine in the retinas of patients with Parkinson's disease. *Investigative Ophthalmology and Visual Science* **31**, 2473-2475 (1990).
67 Hindle, S. *et al.* Dopaminergic expression of the Parkinsonian gene LRRK2-G2019S leads to non-autonomous visual neurodegeneration, accelerated by increased neural demands for energy. *Human Molecular Genetics* **22**, 2129-2140, doi:10.1093/hmg/ddt061 (2013).
68 Chyb, S. *et al.* Modulation of the light response by cAMP in Drosophila photoreceptors. *The Journal of neuroscience : the official journal of the Society for Neuroscience* **19**, 8799-8807 (1999).
69 West, R. J. H., Furmston, R., Williams, C. A. C. & Elliott, C. J. H. Neurophysiology of Drosophila Models of Parkinson's Disease. *Parkinson's Disease* **2015**, 11, doi:10.1155/2015/381281 (2015).
70 Ho, C. C.-Y., Rideout, H. J., Ribe, E., Troy, C. M. & Dauer, W. T. The Parkinson disease protein leucine-rich repeat kinase 2 transduces death signals via Fas-associated protein with death domain and caspase-8 in a cellular model of neurodegeneration. *The Journal of neuroscience : the official journal of the Society for Neuroscience* **29**, 1011-1016, doi:10.1523/JNEUROSCI.5175-08.2009 (2009).
71 Xiong, Y., Yuan, C., Chen, R., Dawson, T. M. & Dawson, V. L. ArfGAP1 is a GTPase activating protein for LRRK2: reciprocal regulation of ArfGAP1 by LRRK2. *The Journal of neuroscience : the*

official journal of the Society for Neuroscience **32**, 3877-3886, doi:10.1523/JNEUROSCI.4566-11.2012 (2012).

72 Li, Y. *et al.* Mutant LRRK2(R1441G) BAC transgenic mice recapitulate cardinal features of Parkinson's disease. *Nature neuroscience* **12**, 826-828, doi:10.1038/nn.2349 (2009).

73 Zhang, H. & Sulzer, D. Glutamate Spillover in the Striatum Depresses Dopaminergic Transmission by Activating Group I Metabotropic Glutamate Receptors. *The Journal of Neuroscience* **23**, 10585 (2003).

74 Dar, A. C. & Shokat, K. M. The Evolution of Protein Kinase Inhibitors from Antagonists to Agonists of Cellular Signaling. *Annual Review of Biochemistry* **80**, 769-795, doi:10.1146/annurev-biochem-090308-173656 (2011).

75 Weinberg, J. B. *et al.* Free Radical Biology & Medicine Inhibition of nitric oxide synthase by cobalamins and cobinamides. *Free Radical Biology and Medicine* **46**, 1626-1632, doi:10.1016/j.freeradbiomed.2009.03.017 (2009).

76 Weinberg, J. B., Shugars, D. C., Sherman, P. A., Sauls, D. L. & Fyfe, J. A. Cobalamin Inhibition of HIV-1 Integrase and Integration of HIV-1 DNA into Cellular DNA. *BIOCHEMICAL AND BIOPHYSICAL RESEARCH COMMUNICATIONS* **397**, 393-397, doi:10.1006/bbrc.1998.8629 (1998).

77 Carkeet, C. *et al.* Human vitamin B(12) absorption measurement by accelerator mass spectrometry using specifically labeled (14)C-cobalamin. *Proceedings of the National Academy of Sciences of the United States of America* **103**, 5694-5699, doi:10.1073/pnas.0601251103 (2006).

78 Wuerges, J. *et al.* Structural basis for mammalian vitamin B12 transport by transcobalamin. *Proceedings of the National Academy of Sciences of the United States of America* **103**, 4386-4391, doi:10.1073/pnas.0509099103 (2006).

79 Pezacka, E. H., Jacobsen, D. W., Luce, K. & Green, R. Glial cells as a model for the role of cobalamin in the nervous system: Impaired synthesis of cobalamin coenzymes in cultured human astrocytes following short-term cobalamin-deprivation. *Biochemical and Biophysical Research Communications* **184**, 832-839, doi:https://doi.org/10.1016/0006-291X(92)90665-8 (1992).

80 Bhatia, P. & Singh, N. Homocysteine excess: Delineating the possible mechanism of neurotoxicity and depression. *Fundamental and Clinical Pharmacology* **29**, 522-528, doi:10.1111/fcp.12145 (2015).

81 Miller, A., Korem, M., Almog, R. & Galboiz, Y. Vitamin B12, demyelination, remyelination and repair in multiple sclerosis. *Journal of the Neurological Sciences* **233**, 93-97, doi:10.1016/j.jns.2005.03.009 (2005).

82 Shen, L. Associations between B vitamins and Parkinson's disease. *Nutrients* **7**, 7197-7208, doi:10.3390/nu7095333 (2015).

83 Triantafyllou, N. I. *et al.* Folate and vitamin B12 levels in levodopa-treated Parkinson's disease patients: Their relationship to clinical manifestations, mood and cognition. *Parkinsonism & Related Disorders* **14**, 321-325, doi:http://dx.doi.org/10.1016/j.parkreldis.2007.10.002 (2008).

84 Toth, C. *et al.* Levodopa, methylmalonic acid, and neuropathy in idiopathic Parkinson disease. *Annals of Neurology* **68**, 28-36, doi:10.1002/ana.22021 (2010).

85 Muller, T., Renger, K. & Kuhn, W. Levodopa-associated increase of homocysteine levels and sural axonal neurodegeneration. *Archives of neurology* **61**, 657-660, doi:10.1001/archneur.61.5.657 (2004).

86 Christine, C. A., Peggy; Joslin, Amelia; Yelpaala, Yuora; Green, Ralph. Vitamin B12 and Homocysteine Levels Predict Different Outcomes in Early Parkinson's Disease. *Movement Disorders* **33**, 762-770, doi:10.1002/mds.27301 (2018).

87 Baptista, M. A. S. *et al.* Loss of Leucine-Rich Repeat Kinase 2 (LRRK2) in Rats Leads to Progressive Abnormal Phenotypes in Peripheral Organs. *PLOS ONE* **8**, e80705, doi:10.1371/journal.pone.0080705 (2013).
88 Perera, G., Ranola, M., Rowe, D. B., Halliday, G. M. & Dzamko, N. Inhibitor treatment of peripheral mononuclear cells from Parkinson's disease patients further validates LRRK2 dephosphorylation as a pharmacodynamic biomarker. *Scientific Reports* **6**, 31391, doi:10.1038/srep31391
https://www.nature.com/articles/srep31391 - supplementary-information (2016).
89 Fan, Y. *et al.* Interrogating Parkinson's disease LRRK2 kinase pathway activity by assessing Rab10 phosphorylation in human neutrophils. *Biochemical Journal* **475**, 23 (2018).
90 Fraser, K. R., Ashlee; Clark, Rachel; Alcalay, Roy, Standaert, David; Liu, Nianjun; West, Andrew. Ser(P)-1292 LRRK2 in urinary exosomes is elevated in idiopathic Parkinson's disease. *Movement Disorders* **31**, 1543-1550, doi:10.1002/mds.26686 (2016).
91 Santos-garcía, D. *et al.* COPPADIS-2015 (COhort of Patients with PArkinson ' s DIsease in Spain , 2015), a global – clinical evaluations , serum biomarkers , genetic studies and neuroimaging – prospective , multicenter , non-interventional , long-term study on Parkinson ' s dise. *BMC Neurology* **2015**, 1-14, doi:10.1186/s12883-016-0548-9 (2016).
92 Hui, K. Y. *et al.* Functional variants in the LRRK2 gene confer shared effects on risk for Crohn's disease and Parkinson's disease. *Science Translational Medicine* **10** (2018).
93 Mayer, M. & Meyer, B. Group Epitope Mapping by Saturation Transfer Difference NMR To Identify Segments of a Ligand in Direct Contact with a Protein Receptor. *Journal of the American Chemical Society* **123**, 6108-6117, doi:10.1021/ja0100120 (2001).
94 Summers, M. F., Marzilli, L. G. & Bax, A. Complete proton and carbon-13 assignments of coenzyme B12 through the use of new two-dimensional NMR experiments. *Journal of the American Chemical Society* **108**, 4285-4294, doi:10.1021/ja00275a008 (1986).
95 Zhang, J., Tian, Z., Liang, L., Subirade, M. & Chen, L. Binding interactions of beta-conglycinin and glycinin with vitamin B12. *J Phys Chem B* **117**, 14018-14028, doi:10.1021/jp408578m (2013).
96 Fernández-Suárez, M., Chen, T. S. & Ting, A. Y. Protein−Protein Interaction Detection in Vitro and in Cells by Proximity Biotinylation. *Journal of the American Chemical Society* **130**, 9251-9253, doi:10.1021/ja801445p (2008).
97 Melachroinou, K. *et al.* Activation of FADD-Dependent Neuronal Death Pathways as a Predictor of Pathogenicity for LRRK2 Mutations. *PLOS ONE* **11**, e0166053, doi:10.1371/journal.pone.0166053 (2016).

Supplementary information is available at *Cell Research*'s website

Fig. 1. **AdoCbl inhibits LRRK2 kinase activity.** (**a**) Domain structure of LRRK2. (**b**) Dose-response curves of brain-purified flag-tagged LRRK2 kinase as a function of different forms of

cobalamin. Phosphorylation is quantified by measuring TR-FRET emission ratios of fluorescein-LRRKtide and a Terbidium-labeled pLRRKtide antibody. (**c**) Dose-response curves of strep-tagged LRRK2 autophosphorylation or (**d**) phosphorylation of myelin basic protein as a function of different forms of cobalamin. (**e**) Dose-response curve of strep-tagged LRRK2-G2019S phosphorylation of purified Rab10 as a function of AdoCbl. (**f**) Dose-response curves of pS935/Total LRRK2 and (**g**) pS1292/Total LRRK2 after treatment with different forms of cobalamin in MEF cells derived from LRRK2-G2019S BAC transgenic mice. Data from each replicate was normalized to LRRK2 phosphorylation without cobalamin treatment. All data points represent the mean (± s.d.) of three biological replicates.

Fig. 2. **Direct binding of AdoCbl to LRRK2 protein.** (a) Binding of strep-tagged LRRK2 to AdoCbl-agarose in the presence of AdoCbl. Input represents the amount of protein that was

added to beads, while pull-down denotes the amount of protein left on the beads after washes. Significance was calculated by one-way ANOVA using the mean (± s.d.) of three biological replicates. * $p \leq 0.05$, ** $p \leq 0.005$ (b) Thermal shift assays showing melting temperatures of strep-LRRK2 in the presence of AdoCbl or PF-06447475. (c) Microscale thermophoretic analysis of the interaction between AdoCbl or (d) PF-06447475 with strep-tagged LRRK2. (e) Coomassie stained SDS-PAGE of the Roco4 kinase domain purified from E. coli. (f) Dose-response curve of Roco4 kinase activity as a function of AdoCbl. (g) ATP STD-NMR shows direct binding of AdoCbl to the Roco4 kinase domain and competition with ATP. From top to bottom, the spectra are as follows: 1D 1H NMR of ATP (blue), AdoCbl (red), STD negative control with ATP + AdoCbl only (green), STD positive control with ATP and Roco4 kinase domain (orange), STD of AdoCbl and Roco4 kinase domain with 1:1 ratio of AdoCbl to ATP (purple), and STD of AdoCbl and Roco4 kinase domain with 10:1 ratio of AdoCbl to ATP (yellow). AdoCbl protons showing strong STD signals are labeled with assignment. All experiments were collected at 4°C on a Bruker 800MHz spectrometer equipped with a cryoprobe. (h) Protons with strong STD signals (highlighted in red) mapped onto the structure of AdoCbl. The NMR assignment and nomenclature of vitamin B12 is from Summers et al.[94] Data points in (a,c,d,f) represent the mean (± s.d.) of three biological replicates.

Fig. 3. **AdoCbl exhibits a mixed-mode of inhibition**. (**a**) Michaelis-Menten kinetics curves of full-length Invitrogen flag-tagged LRRK2-WT and (**c**) LRRK2-G2019S as a function of AdoCbl.

Relative velocity represents the value of pS1292/Total LRRK2 after 20 minutes of reaction time at 30°C (during the linear reaction rate), as detected by western blot and quantified by densitometry. (**b**) Lineweaver-Burk plots of LRRK2-WT and (**d**) LRRK2-G2019S kinetics data. (**e**) Microscale thermophoretic analysis of the interaction between AdoCbl and strep-tagged LRRK2 in the presence of increasing concentrations of AMP-PNP. Fluorescently-labeled strep-tagged LRRK2 was pre-incubated with AMP-PNP before binding between LRRK2 and AdoCbl was measured by MST. (**f**) Microscale thermophoretic analysis of the interaction between AMP-PNP and LRRK2, showing a K_D of 0.9 μM. Data points represent the mean (± s.d.) of three biological replicates.

Fig. 4. AdoCbl causes a LRRK2 conformational change and destabilizes LRRK2 dimers. (**a**) Coomassie stained SDS-PAGE showing limited proteolysis analysis using a 10:1 molar ratio

of LRRK2: Trypsin (left panel) and LRRK2: Chymotrypsin (right panel). Proteolysis was performed at 30°C with or without 50 μM AdoCbl and reactions were quenched at the indicated times by the addition of sample loading buffer. The observed data was consistent across three biological replicates. (**b**) Limited proteolysis of LRRK2-WT by trypsin in the presence of increasing concentrations of AdoCbl, or 1 μM LRRK2 kinase inhibitor. Proteolysis was performed for 90 minutes at 30°C. Shown is a representative SDS-PAGE of full-length LRRK2, in which bands were quantified and values were normalized to LRRK2 proteolysis without AdoCbl. (**c**) The peak intrinsic fluorescence of LRRK2 (339 nm) was measured as a function of AdoCbl. Strep-tagged LRRK2 was incubated with indicated concentrations of AdoCbl for 30 minutes prior to fluorescence measurements. Significance was measured by one-way ANOVA. * $p \leq 0.05$, ** $p \leq 0.005$. (**d**) HEK293T cells co-expressing BirA-WT (biotin ligase) and AP-WT LRRK2 (acceptor peptide) were lysed following a biotin pulse to label dimeric LRRK2, and extracts bound to streptavidin-coated ELISA plates. LRRK2 was detected using anti-LRRK2 conjugated to HRP (clone N241A/B34) and expressed as a ratio of total LRRK2 levels detected by ELISA in parallel plates coated with total LRRK2 antibodies (clone c41-2). In the plot, "WT/WT NP" refers to cells expressing WT LRRK2 dimers that were harvested without receiving a biotin pulse ("no pulse"). AdoCbl significantly reduced levels of dimeric WT-LRRK2. Sub-panel shows representative immunoblot of parallel extracts detected with anti-LRRK2 (clone N241A/B34). BirA-LRRK2 represents the top band, and AP-LRRK2 the bottom band. (**e**) HEK293T cells expressing BirA- G2019S or I2020T mutant LRRK2 together with AP-G2019S or I2020T LRRK2, and dimeric LRRK2 quantified by ELISA. Treatment with AdoCbl significantly reduces dimeric mutant LRRK2. * $p < 0.05$ compared to WT/WT-LRRK2; *** $p < 0.001$ compared to G2019S-LRRK2 dimers or I2020T-LRRK2 dimers alone. (**f**) Representative

immunoblot of parallel extracts detected with anti-LRRK2 (clone N241A/B34). BirA-LRRK2 represents the top band, and AP-LRRK2 the bottom band.

Fig. 5. AdoCbl rescues mutant human LRRK2-induced behavioral defects and dopaminergic neurodegeneration in *C. elegans*. (**a**) AdoCbl dose dependently rescues the loss

of basal slowing response in transgenic *hLRRK2-G2019S C. elegans*. Age-synchronized nematodes expressing GFP marker only or additionally *hLRRK2-G2019S* in dopaminergic neurons were treated with either vehicle or AdoCbl in liquid culture during the larval stage L1 to L4 (3 days), followed by growth on NGM plates for 3 days prior to behavior assay. Basal slowing response was assayed on NGM plates using an unbiased machine-vision analysis system (WormLab) as the percent slowing in body bends per 20 s in the presence vs. the absence of bacterial lawn. Data represent the mean (± s.d.) of three biological replicates, each with 20-25 worms per treatment condition. (**b**) AdoCbl treatment attenuated the loss of dopaminergic neurons induced by *hLRRK2-G2019S* in *C. elegans*. Representative fluorescence images of dopaminergic neurons (CEP neurons within the outlined head region) in transgenic *C. elegans* expressing GFP marker only or additionally *hLRRK2-G2019S* following treatment with either vehicle or 1.25 μM AdoCbl. Age-synchronized nematodes were treated with either vehicle or AdoCbl in liquid culture during the larval stage L1 to L4 (3 days), followed by growth on NGM plates for 9 days. GFP-tagged dopaminergic neurons in live animals were counted under a fluorescence microscope. (**c**) Quantification of percent dopaminergic neurons survived. Data are presented as the mean (± s.d.) of three biological replicates, each with approximately 30-50 worms per treatment condition. $P < 0.01$, Student's t-test. n.s., not statistically significant.

Fig. 6. AdoCbl rescues deficits in *Drosophila* visual physiology induced by the dopaminergic expression of human *LRRK2-G2019S*. (**a**) Outline of the retinal neural network of *Drosophila*, with three main neuronal layers: photoreceptors, lamina neurons and medulla

neurons (Modified after Afsari et al[31]). (**b**) Contrast response functions (CRFs) for the photoreceptors, lamina neurons and medulla neurons show that the dopaminergic expression of *hLRRK2-G2019S* (*DA → G2019S*) flies have a much bigger response than either the *DA → hLRRK2* or the *DA → G2019S* which have been fed 2.5 µM AdoCbl. (**c**) Dose-response curve for the effect of AdoCbl on the *DA → G2019S* flies, shows a 50% reduction in phenotypes by 250-500 nM AdoCbl, with almost complete rescue by 2.5 µM AdoCbl. (**d**) There is no effect of 2.5 µM AdoCbl on flies with dopaminergic expression of kinase-dead *hLRRK2-G2019S-K1906M* (*DA → KD*). (**e**) The visual response of flies with wild-type *dLRRK2* is reduced by 2.5µM AdoCbl. (**f**) Applying 2.5 µM AdoCbl to *dLRRK*$^{-/-}$ transheterozygote flies (in which the *drosophila* LRRK2 homolog has been knocked out) has no statistically significant effect. Data represents the mean (± s.d.) and the numbers in brackets are the number of flies tested. In (**c**), statistical analysis from Tukey Post-hoc tests on the first principal component of a PCA, which accounted for 88% of the variance (Supplementary information, **Fig. S9**). (**d-f**), analysis by MANOVA. n.s. not significant; ***$p < 0.001$). Boxes correspond to the median +/- quartiles. Dots indicate data from individual flies. *dLRRK*$^{-}$ genotype: *dLRRK^e03680/dLRRK^ex1*; *wild type* genotype: *w^a/w^1118*.

Fig. 7. AdoCbl prevents LRRK2-G2019S induced neurotoxicity and rescues deficits in dopamine transmission in LRRK2-PD mouse models. (**a**) Quantification of percent apoptotic

neurons after LRRK2 overexpression and treatment with MLi-2 or AdoCbl. Cortical neurons were co-transfected with LRRK2 and a GFP reporter. Transfected neurons displaying apoptotic nuclear morphology were counted 48 h after transfection using DAPI. Apoptotic neurons were defined as those having condensed fragmented chromatin comprised of two or more apoptotic bodies. Data represents the mean (± s.d.) from n = 3 biological replicates of triplicate coverslips. Significance was measured by one-way ANOVA. (**b**) Quantification of pS1292/Total LRRK2 after brain slice tissue from LRRK2-G2019S BAC-transgenic mice were treated with AdoCbl. One mouse brain provided enough slices to test each treatment condition one time. Three mouse brains were used in total, resulting in three biological replicates. Data are the mean (± s.d.) and significance was measured by one-way ANOVA (**c**) Voltammetric traces of striatal DA release evoked at 2-min intervals from G2019S, or (**e**) R1441G, and WT controls after 2 h treatment with control vehicle (water), or with 300 μM AdoCbl. (**d**) Summary of DA release sustainability for G2019S mice (n = 9 sites) or (**f**) R1441G (n = 10 sites) compared to WT controls. Data are expressed as the mean (± s.d.) and were analyzed by two-way ANOVA with *Bonferroni's post hoc* analysis. For all figures, * $p \leq 0.01$, ** $p \leq 0.001$, *** $p \leq 0.0001$.

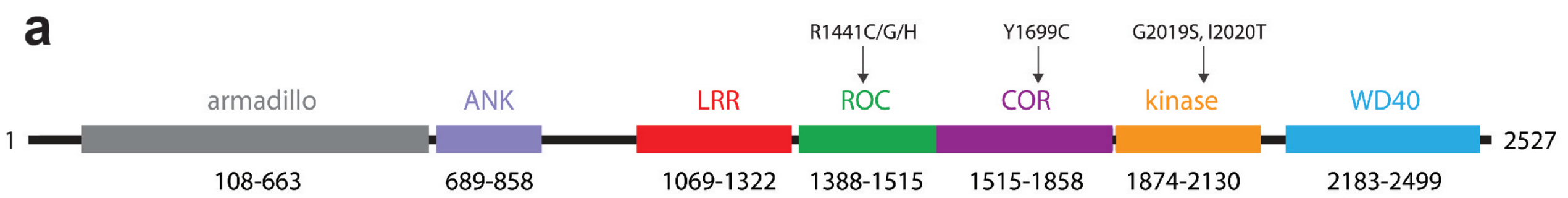
a
R1441C/G/H
Y1699C
G2019S, I2020T
armadillo
ANK
LRR
ROC
COR
kinase
WD40
1
2527
108-663
689-858
1069-1322
1388-1515
1515-1858
1874-2130
2183-2499

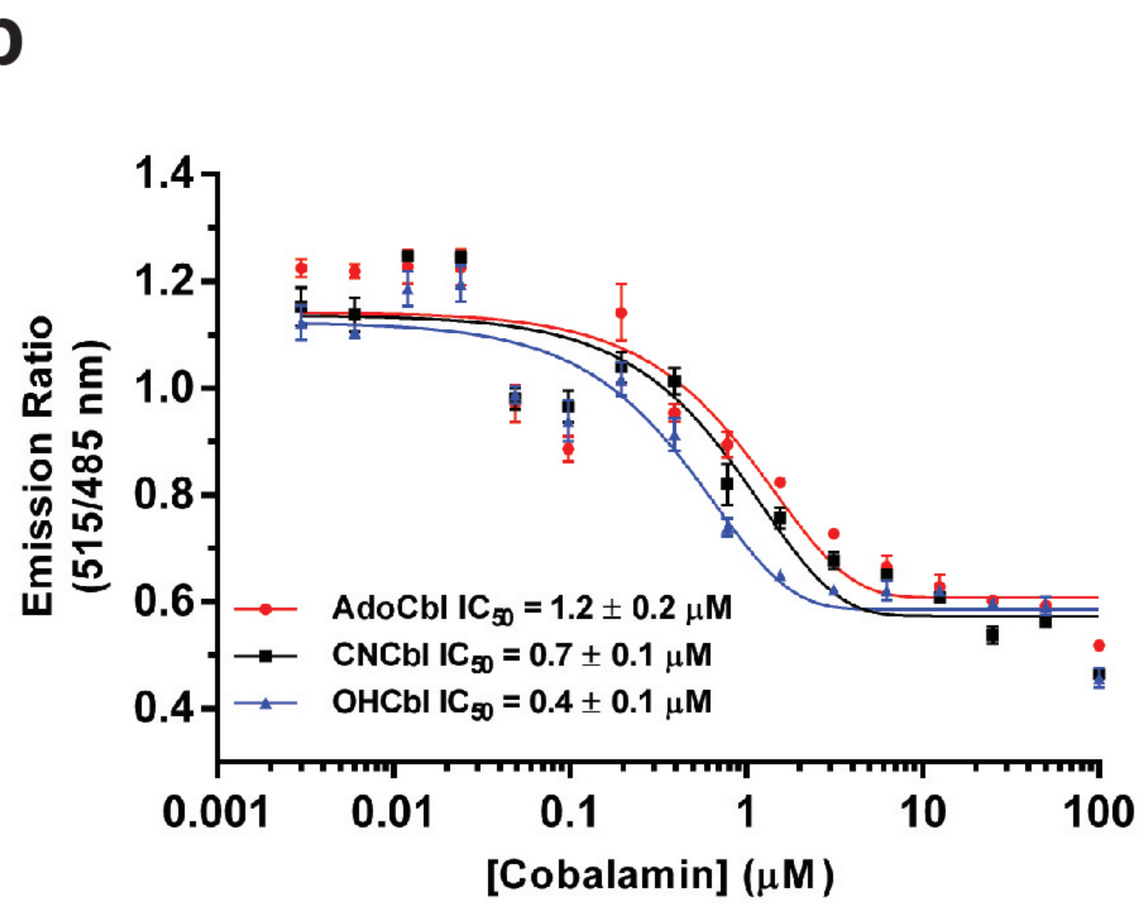
b
Emission Ratio (515/485 nm)
AdoCbl IC50 = 1.2 ± 0.2 μM
CNCbl IC50 = 0.7 ± 0.1 μM
OHCbl IC50 = 0.4 ± 0.1 μM
[Cobalamin] (μM)

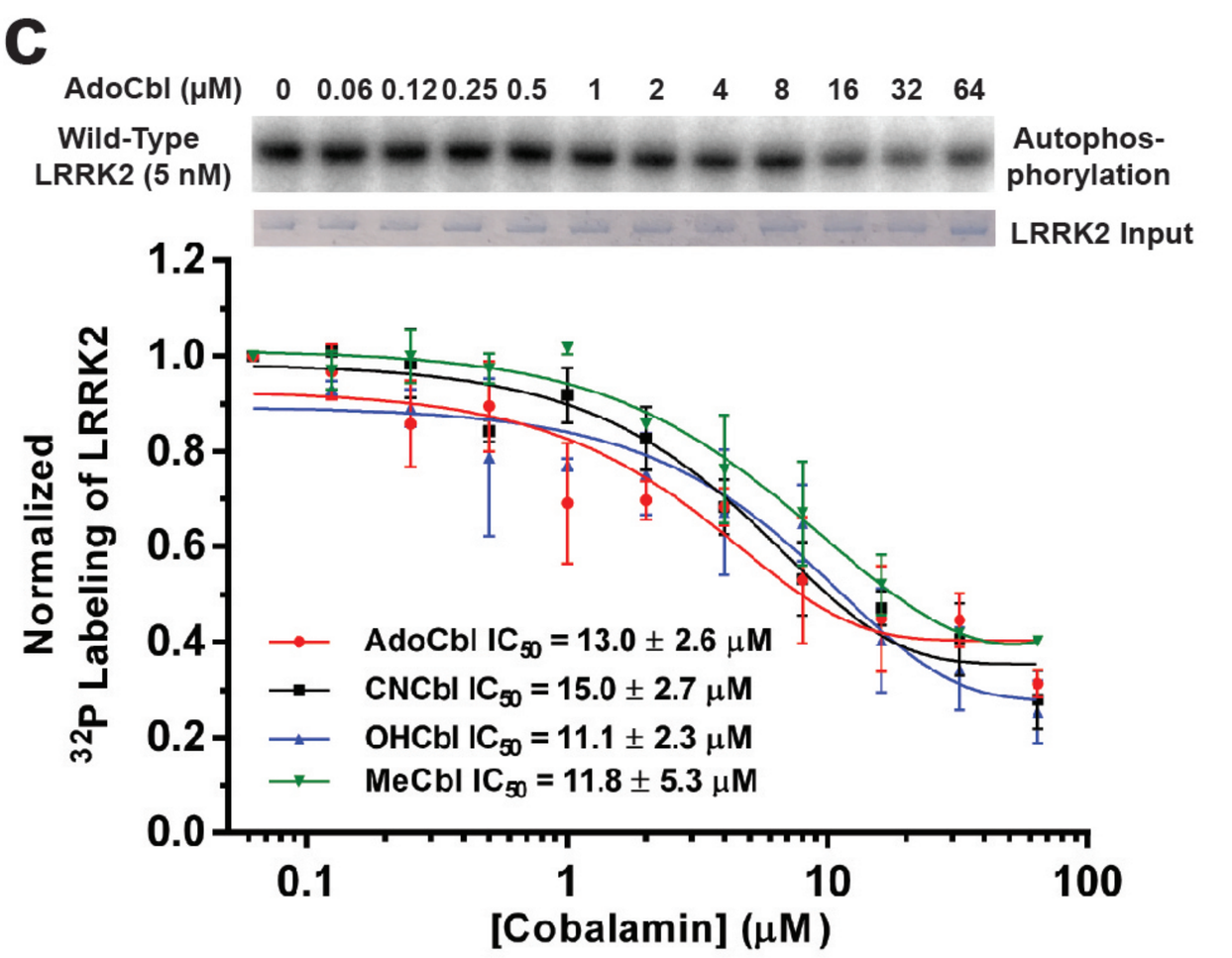
c
AdoCbl (μM) 0 0.06 0.12 0.25 0.5 1 2 4 8 16 32 64
Wild-Type LRRK2 (5 nM)
Autophos-phorylation
LRRK2 Input
Normalized 32P Labeling of LRRK2
AdoCbl IC50 = 13.0 ± 2.6 μM
CNCbl IC50 = 15.0 ± 2.7 μM
OHCbl IC50 = 11.1 ± 2.3 μM
MeCbl IC50 = 11.8 ± 5.3 μM
[Cobalamin] (μM)

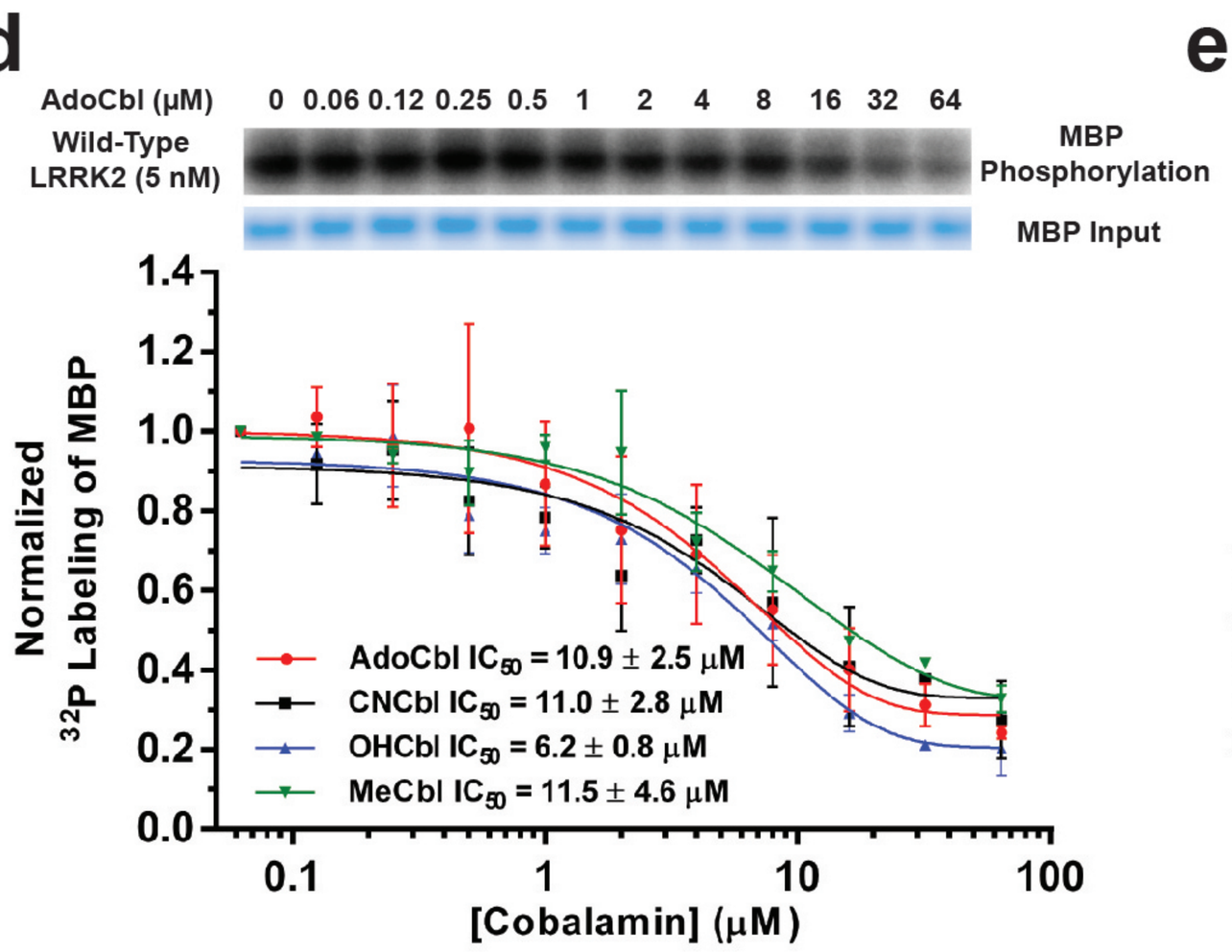
d
AdoCbl (μM) 0 0.06 0.12 0.25 0.5 1 2 4 8 16 32 64
Wild-Type LRRK2 (5 nM)
MBP Phosphorylation
MBP Input
Normalized 32P Labeling of MBP
AdoCbl IC50 = 10.9 ± 2.5 μM
CNCbl IC50 = 11.0 ± 2.8 μM
OHCbl IC50 = 6.2 ± 0.8 μM
MeCbl IC50 = 11.5 ± 4.6 μM
[Cobalamin] (μM)

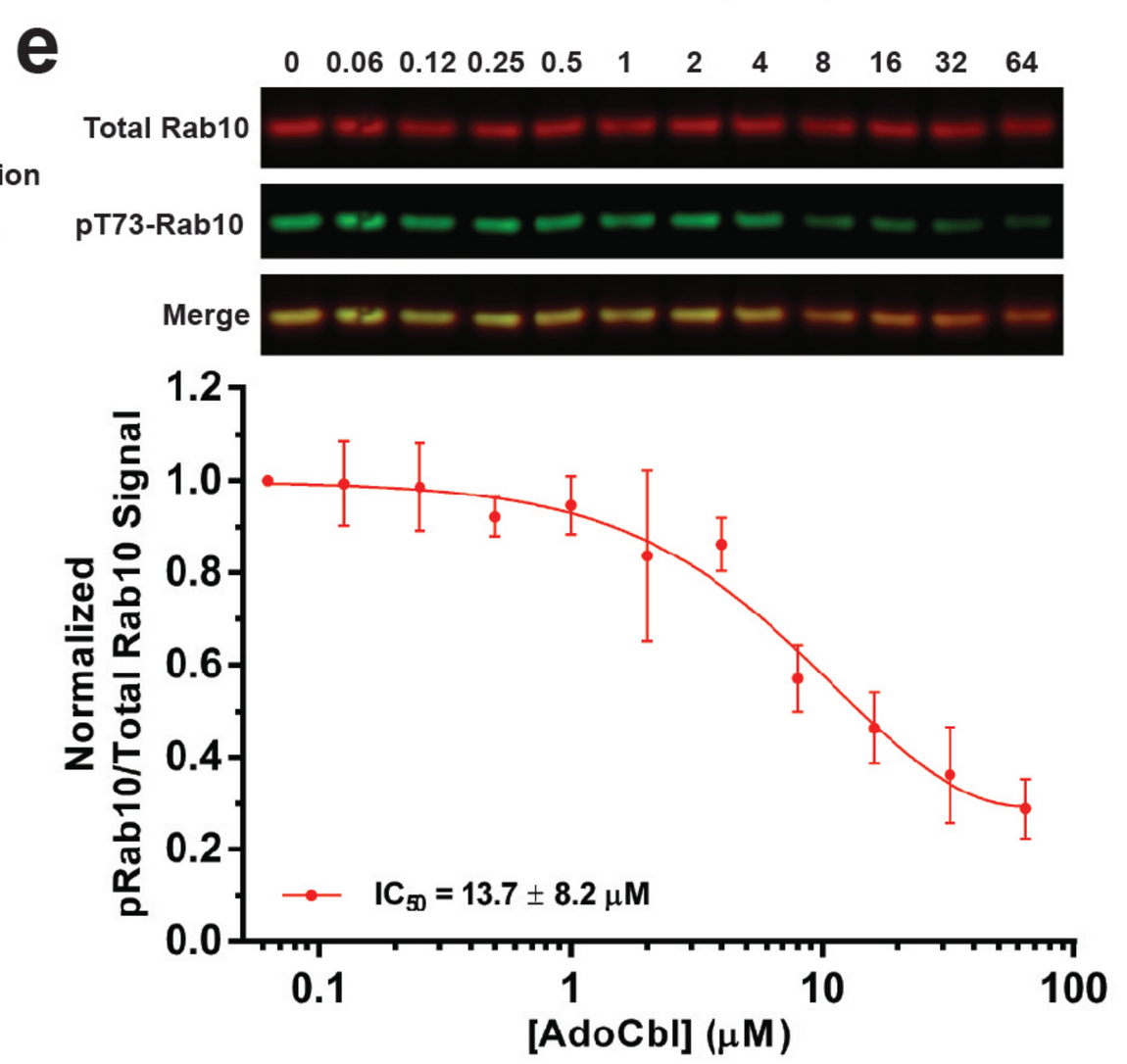
e
0 0.06 0.12 0.25 0.5 1 2 4 8 16 32 64
Total Rab10
pT73-Rab10
Merge
Normalized pRab10/Total Rab10 Signal
IC50 = 13.7 ± 8.2 μM
[AdoCbl] (μM)

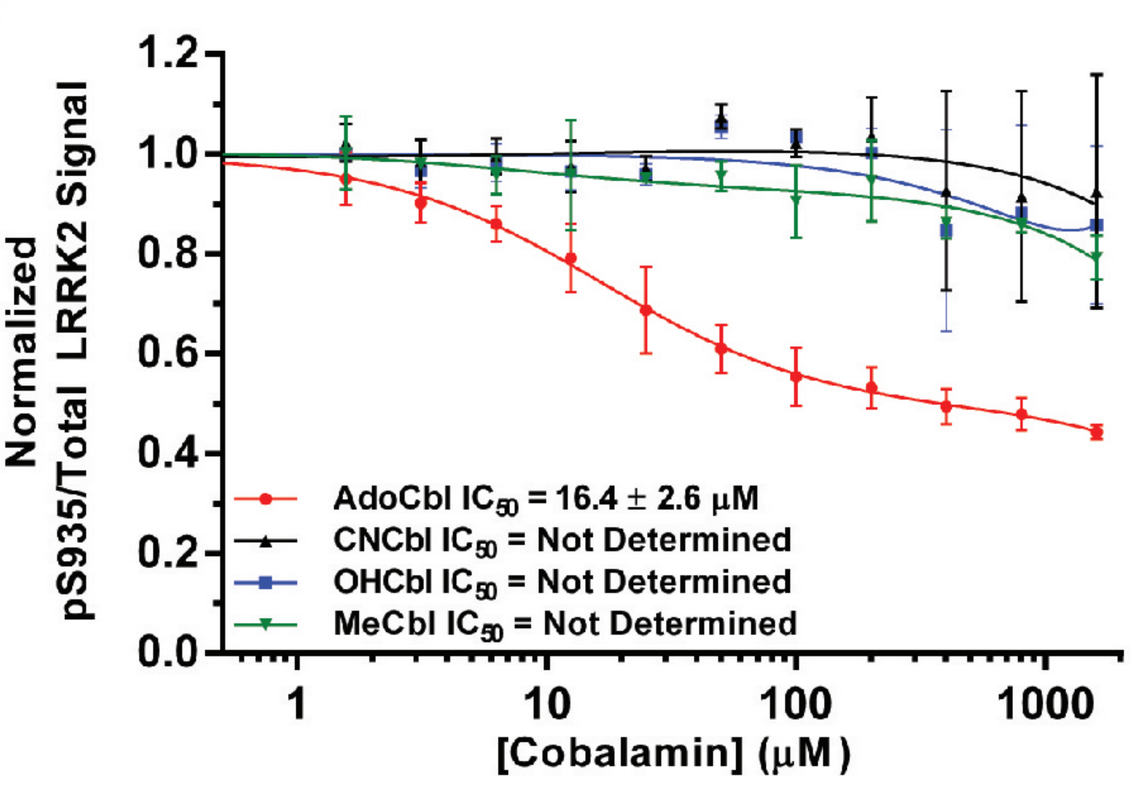
f
Normalized pS935/Total LRRK2 Signal
AdoCbl IC50 = 16.4 ± 2.6 μM
CNCbl IC50 = Not Determined
OHCbl IC50 = Not Determined
MeCbl IC50 = Not Determined
[Cobalamin] (μM)

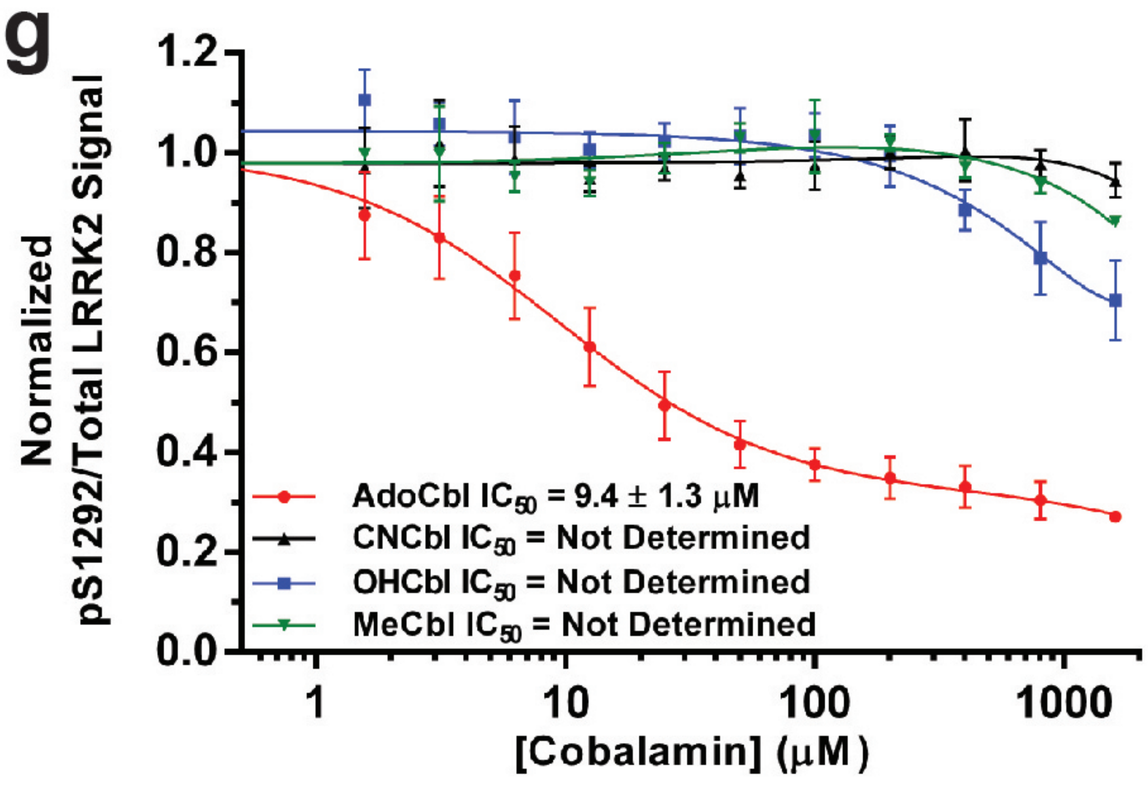
g
Normalized pS1292/Total LRRK2 Signal
AdoCbl IC50 = 9.4 ± 1.3 μM
CNCbl IC50 = Not Determined
OHCbl IC50 = Not Determined
MeCbl IC50 = Not Determined
[Cobalamin] (μM)

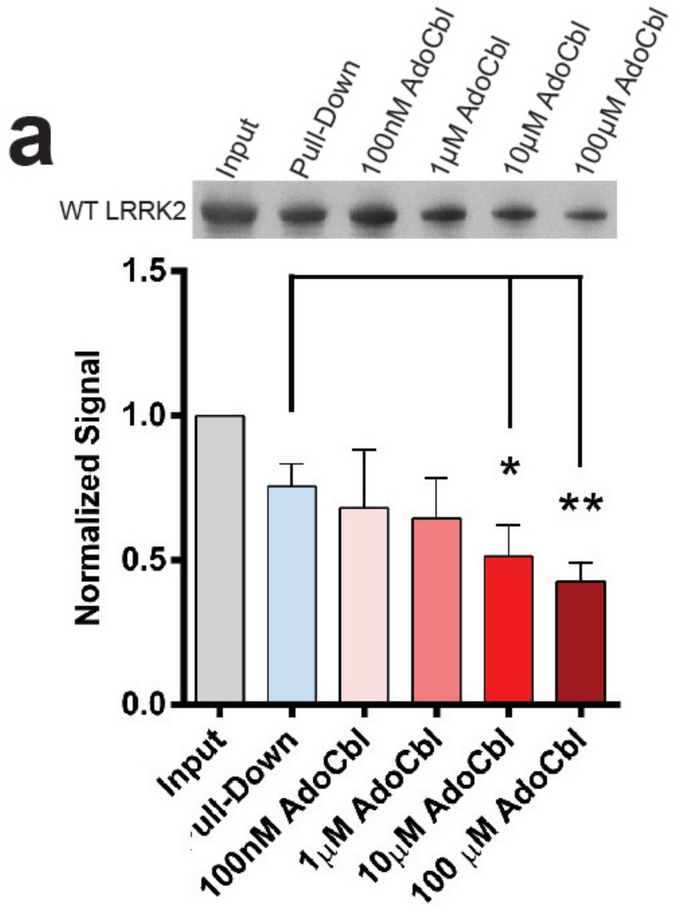
a
Input
Pull-Down
100nM AdoCbl
1μM AdoCbl
10μM AdoCbl
100μM AdoCbl
WT LRRK2
Normalized Signal
1.5
1.0
0.5
0.0
*
**
Input
Pull-Down
100nM AdoCbl
1μM AdoCbl
10μM AdoCbl
100 μM AdoCbl

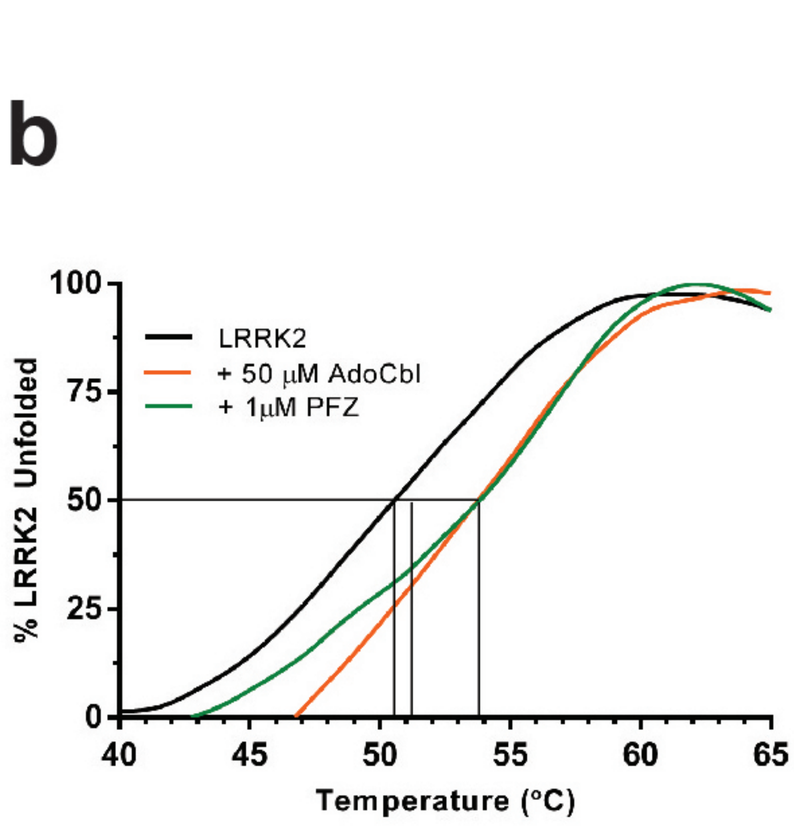
b
100
75
50
25
0
% LRRK2 Unfolded
LRRK2
+ 50 μM AdoCbl
+ 1μM PFZ
40
45
50
55
60
65
Temperature (°C)

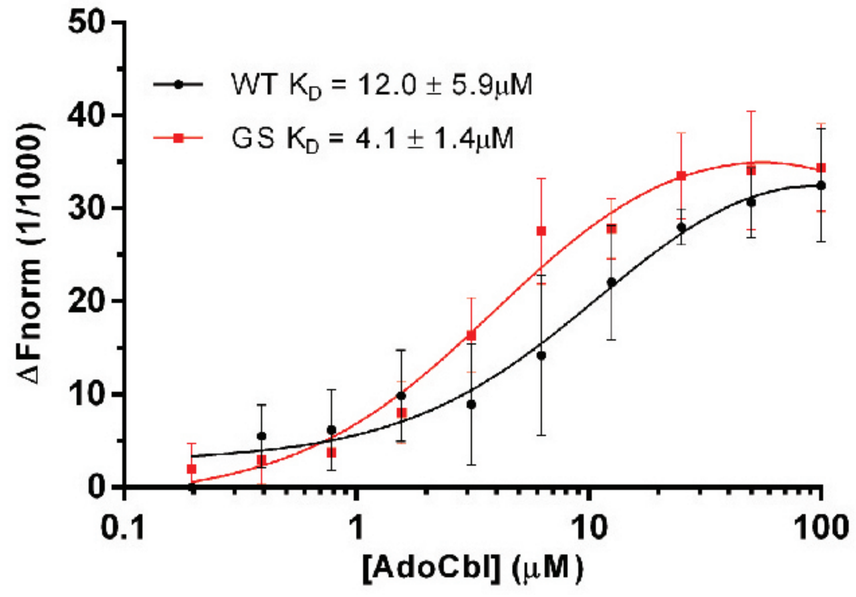
c
50
40
30
20
10
0
ΔFnorm (1/1000)
WT K$_D$ = 12.0 ± 5.9μM
GS K$_D$ = 4.1 ± 1.4μM
0.1
1
10
100
[AdoCbl] (μM)

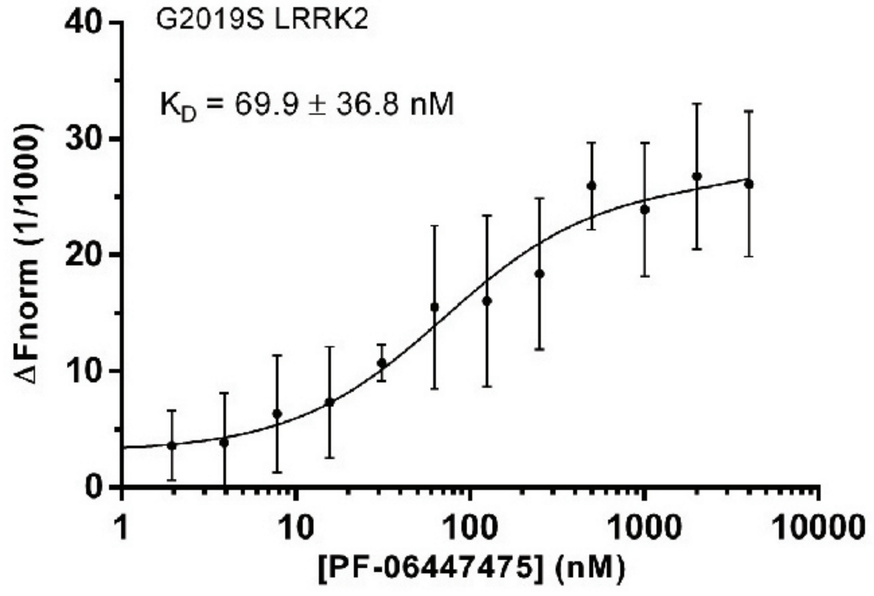
d
G2019S LRRK2
K$_D$ = 69.9 ± 36.8 nM
40
30
20
10
0
ΔFnorm (1/1000)
1
10
100
1000
10000
[PF-06447475] (nM)

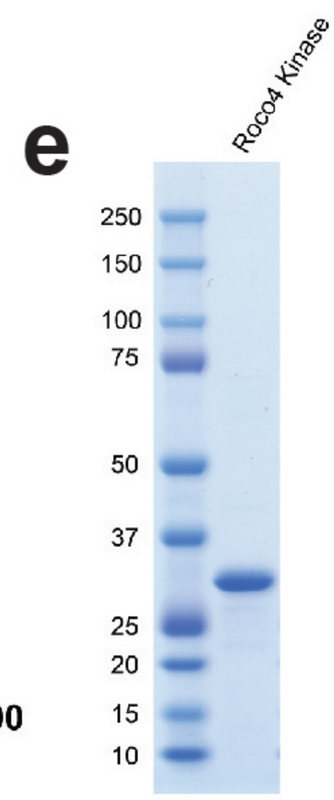
e
Roco4 Kinase
250
150
100
75
50
37
25
20
15
10

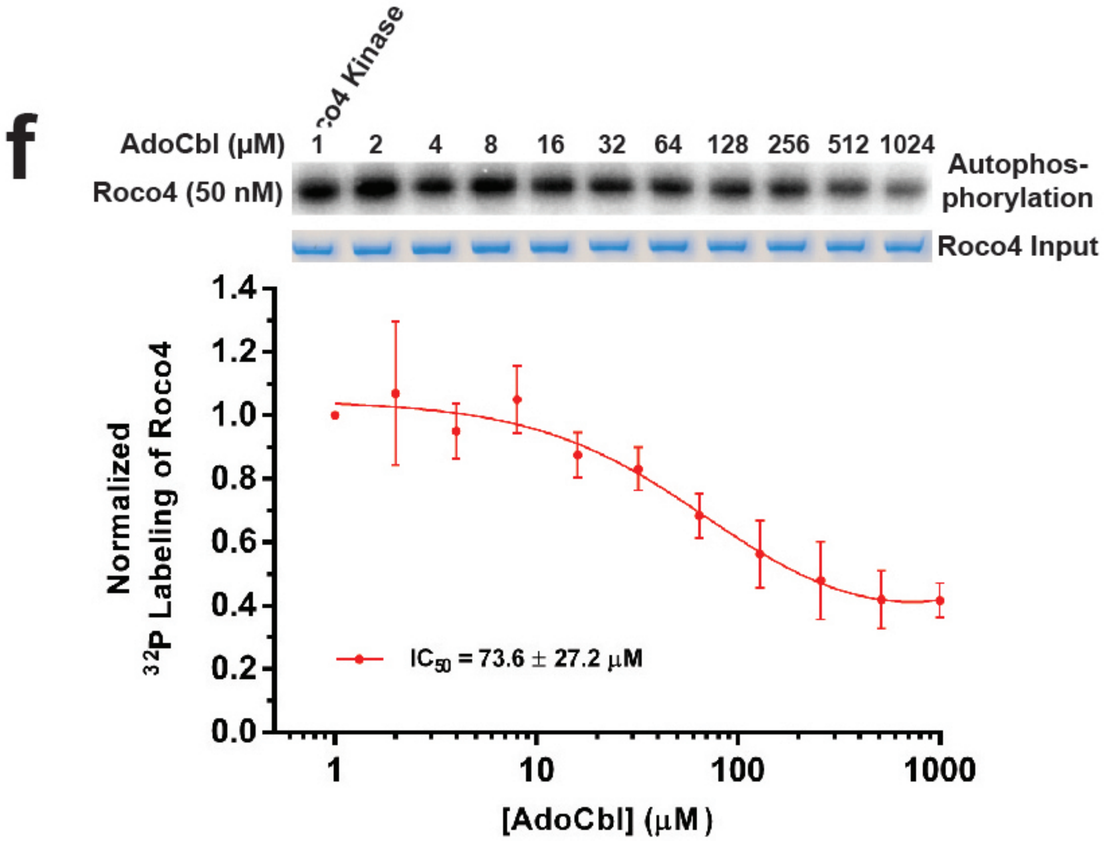
f
Roco4 Kinase
AdoCbl (μM)
1
2
4
8
16
32
64
128
256
512
1024
Roco4 (50 nM)
Autophos-phorylation
Roco4 Input
Normalized ^{32}P Labeling of Roco4
1.4
1.2
1.0
0.8
0.6
0.4
0.2
0.0
IC$_{50}$ = 73.6 ± 27.2 μM
1
10
100
1000
[AdoCbl] (μM)

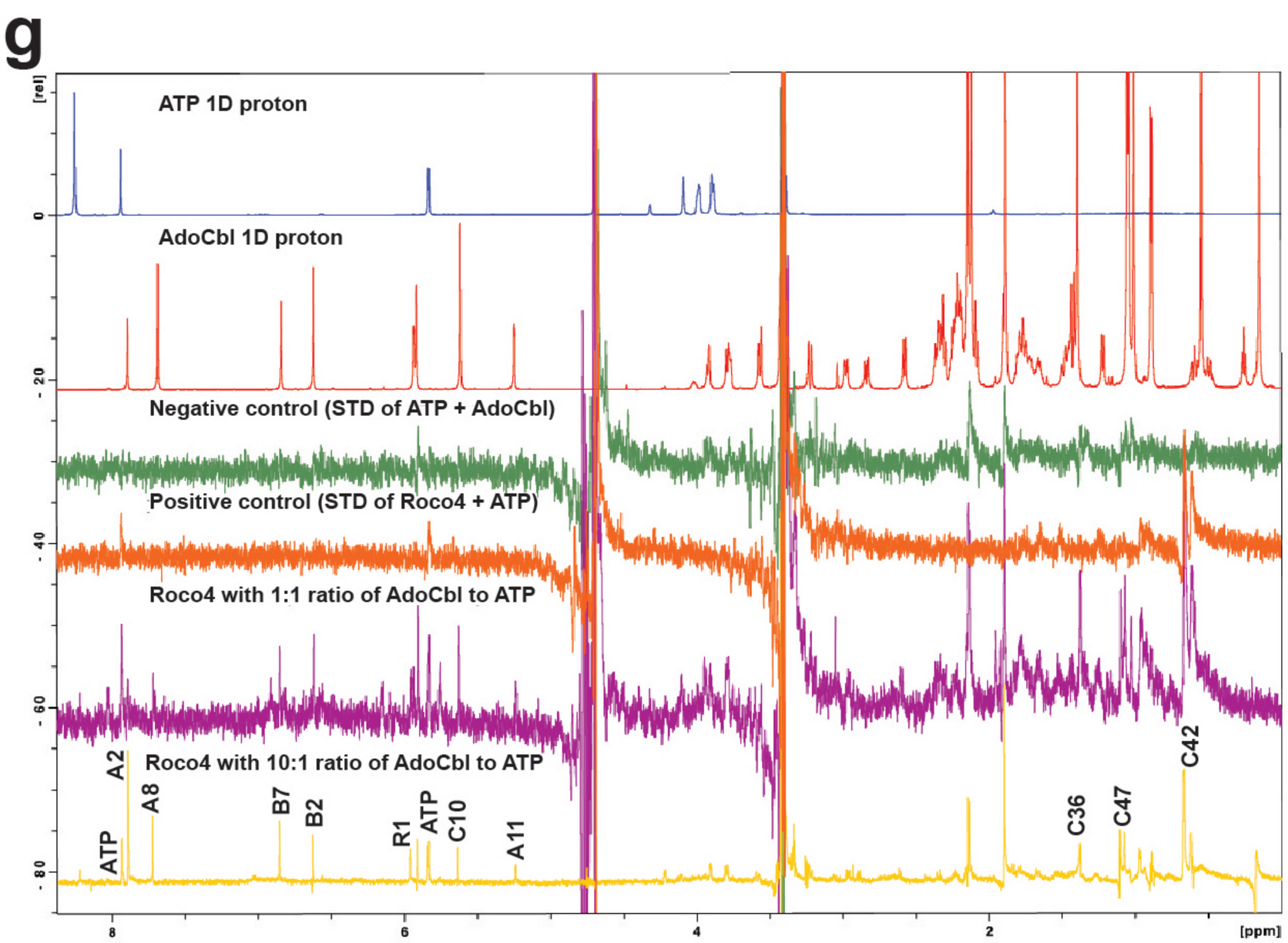
g
[rel]
0
- 20
- 40
- 60
- 80
ATP 1D proton
AdoCbl 1D proton
Negative control (STD of ATP + AdoCbl)
Positive control (STD of Roco4 + ATP)
Roco4 with 1:1 ratio of AdoCbl to ATP
Roco4 with 10:1 ratio of AdoCbl to ATP
ATP
A2
A8
B7
B2
R1
ATP
C10
A11
C36
C47
C42
8
6
4
2
[ppm]

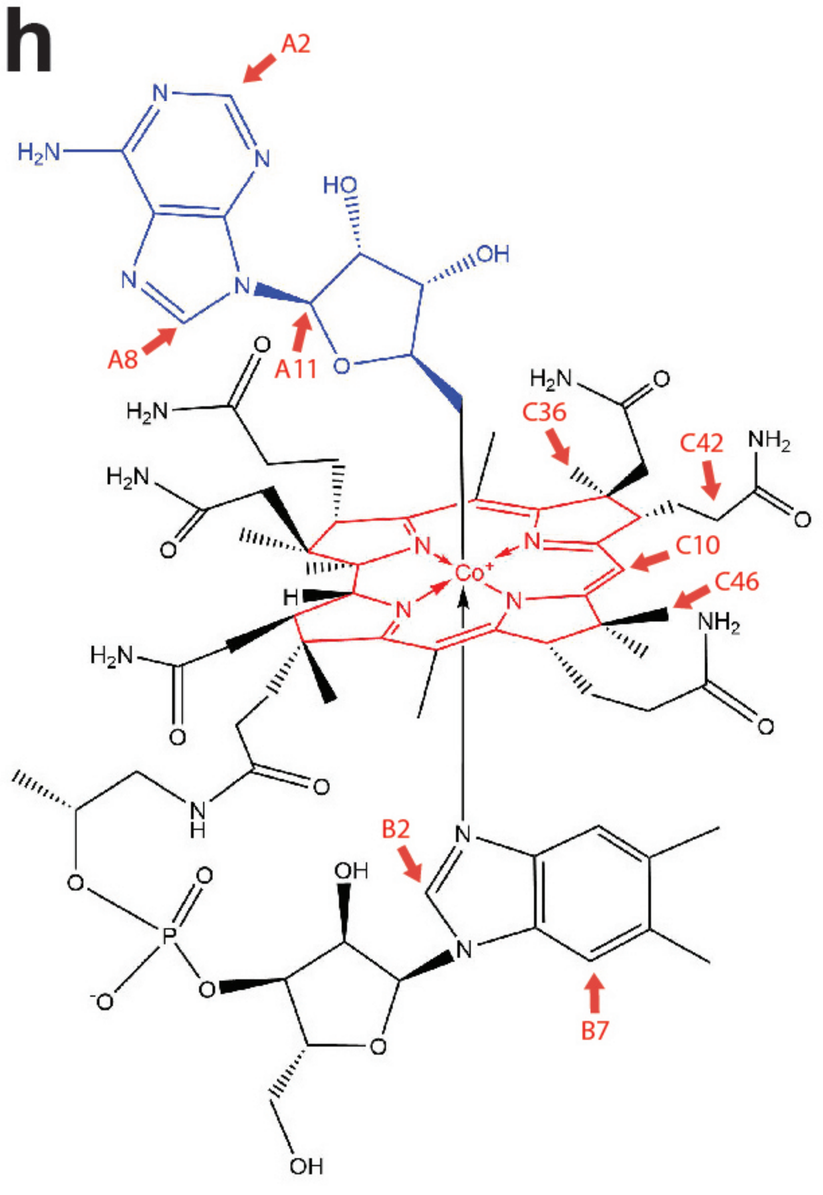
h
A2
A8
A11
B2
B7
C36
C42
C10
C46
Co+

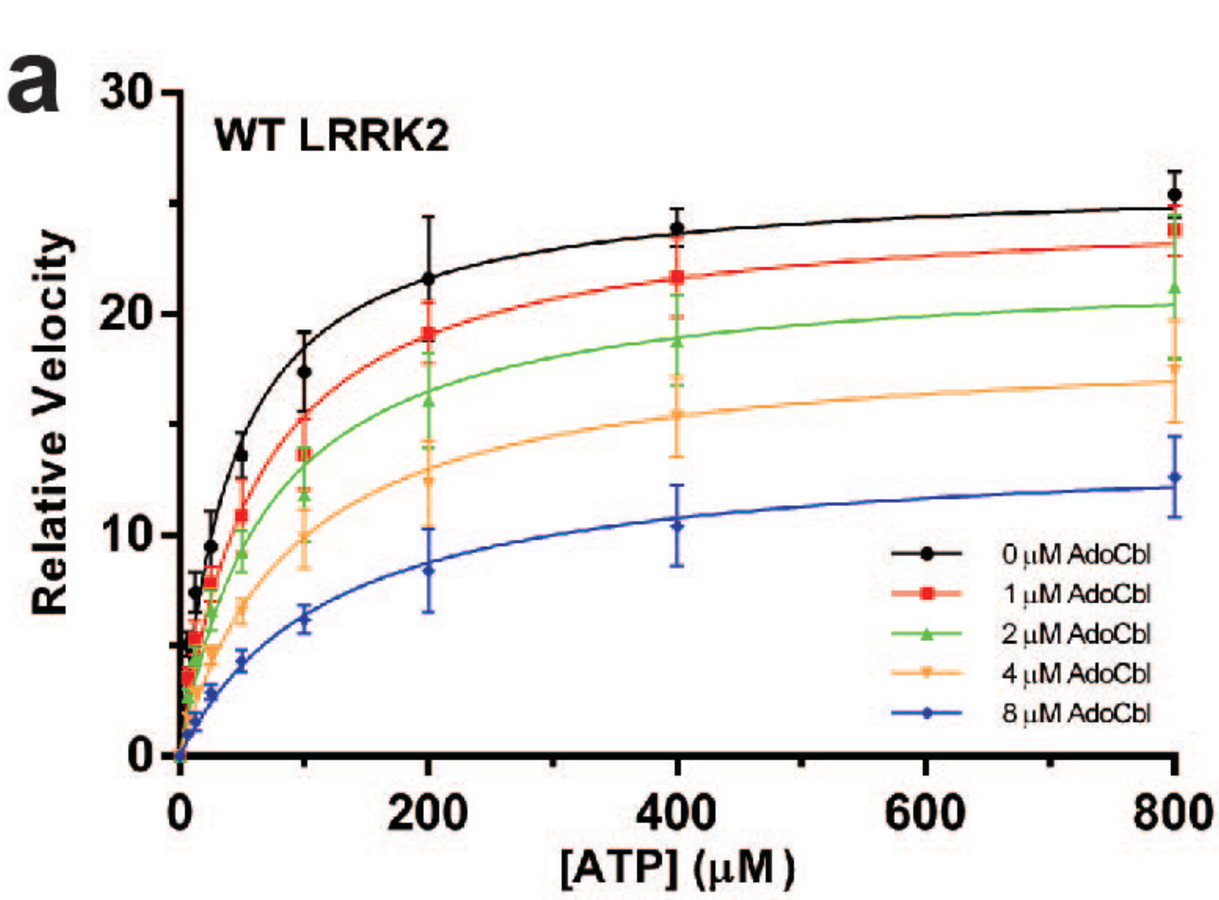
a
WT LRRK2
Relative Velocity
[ATP] (μM)
0 μM AdoCbl
1 μM AdoCbl
2 μM AdoCbl
4 μM AdoCbl
8 μM AdoCbl

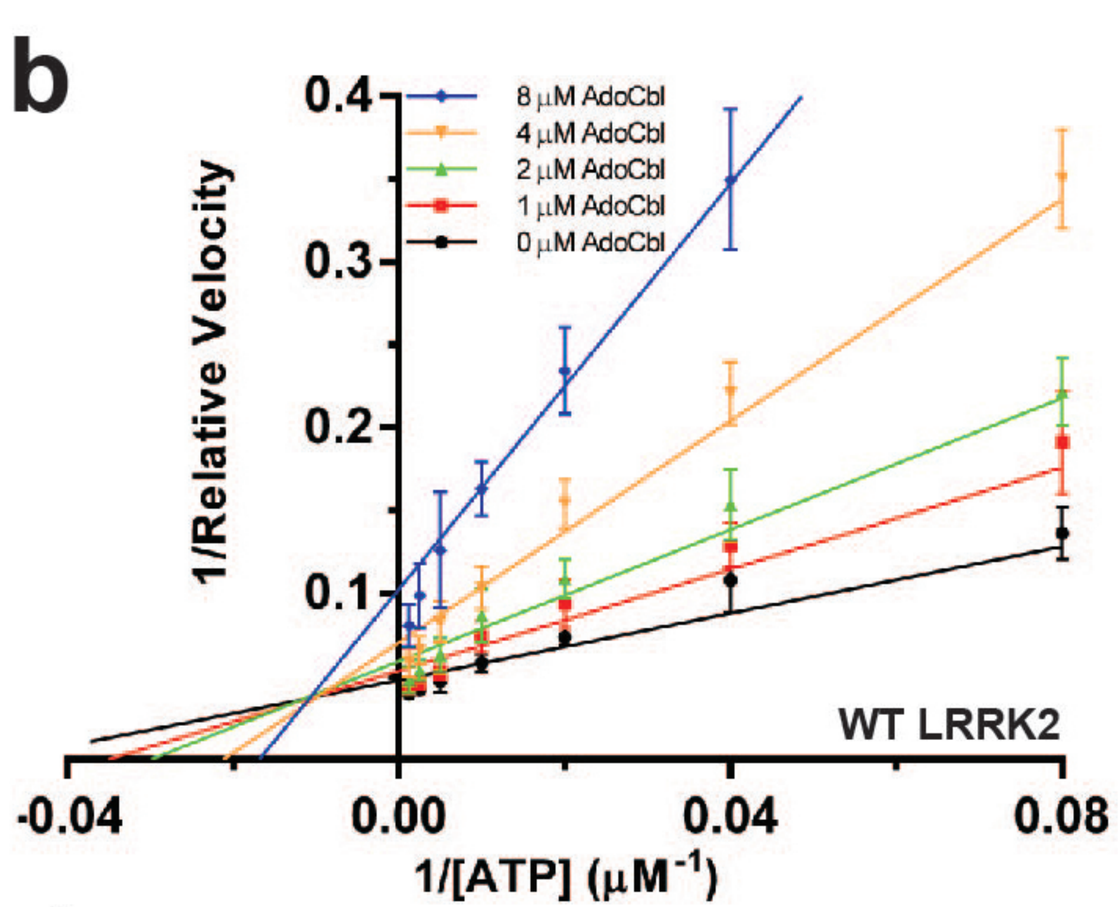
b
WT LRRK2
1/Relative Velocity
1/[ATP] (μM-1)
8 μM AdoCbl
4 μM AdoCbl
2 μM AdoCbl
1 μM AdoCbl
0 μM AdoCbl

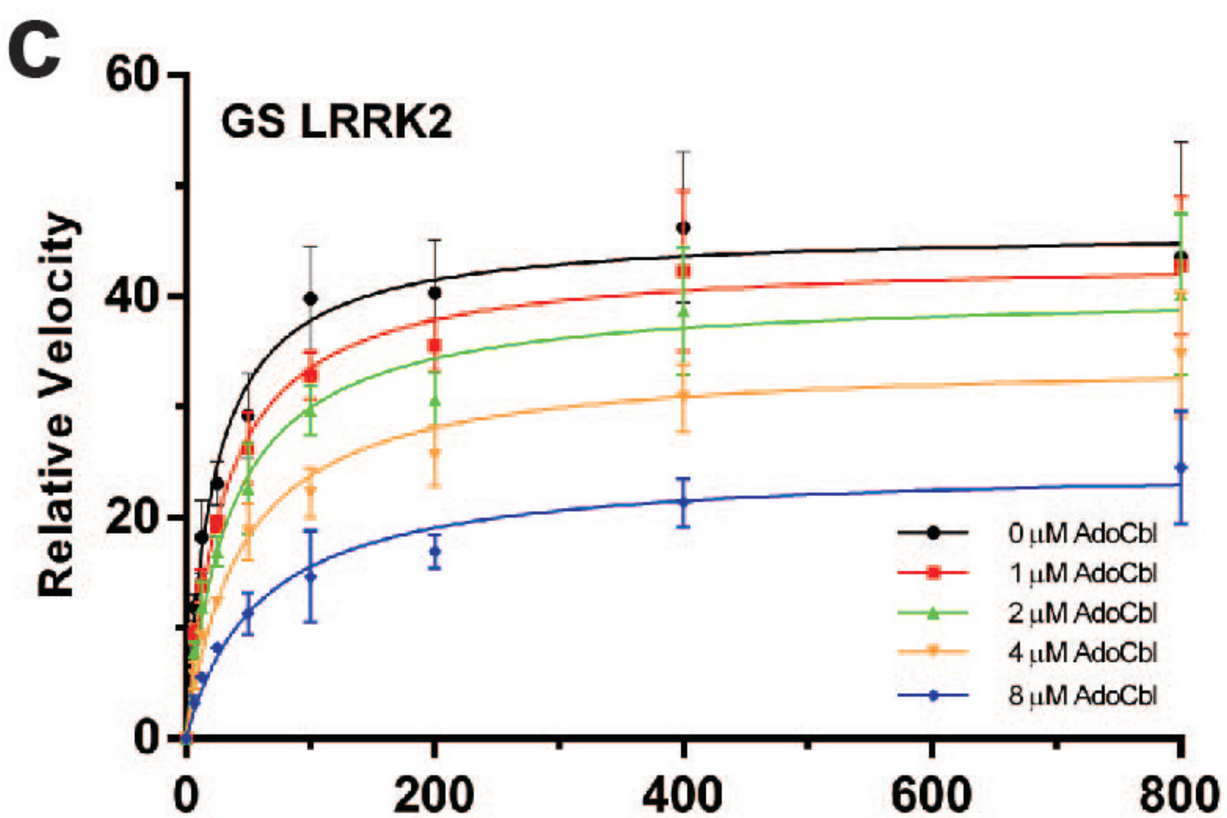
c
GS LRRK2
Relative Velocity
[ATP] (μM)
0 μM AdoCbl
1 μM AdoCbl
2 μM AdoCbl
4 μM AdoCbl
8 μM AdoCbl

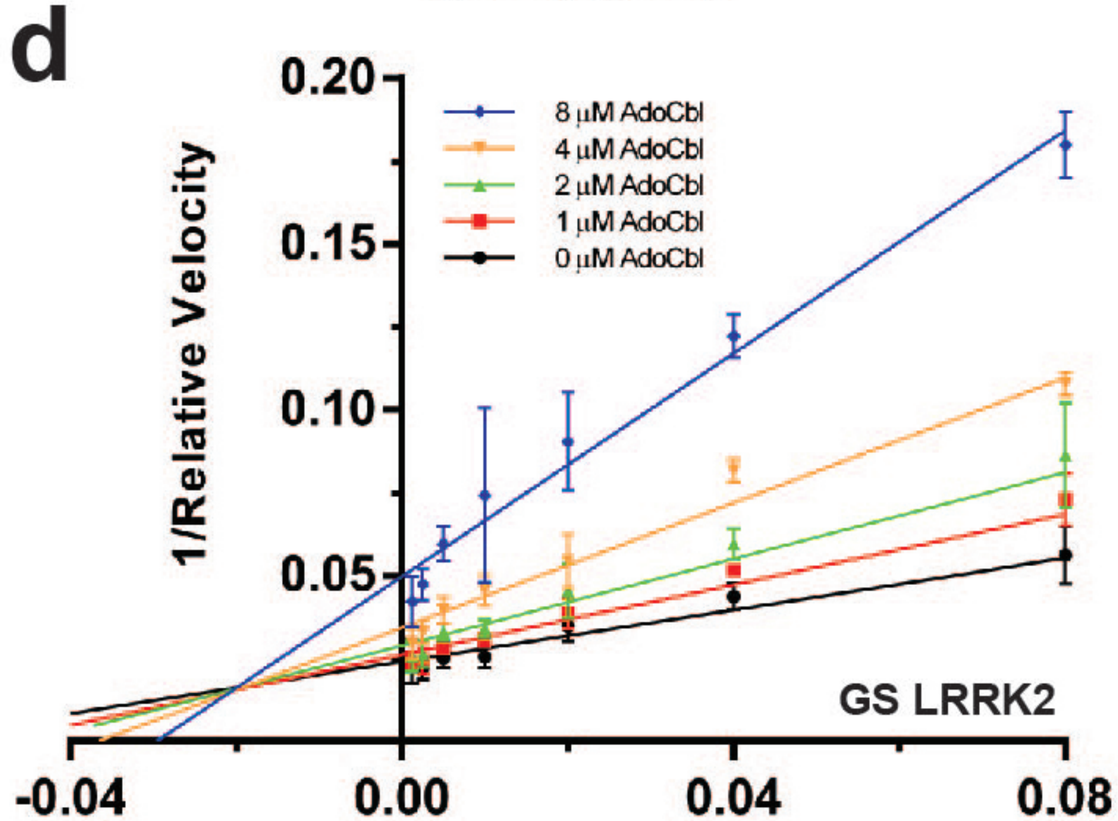
d
GS LRRK2
1/Relative Velocity
1/[ATP] (μM-1)
8 μM AdoCbl
4 μM AdoCbl
2 μM AdoCbl
1 μM AdoCbl
0 μM AdoCbl

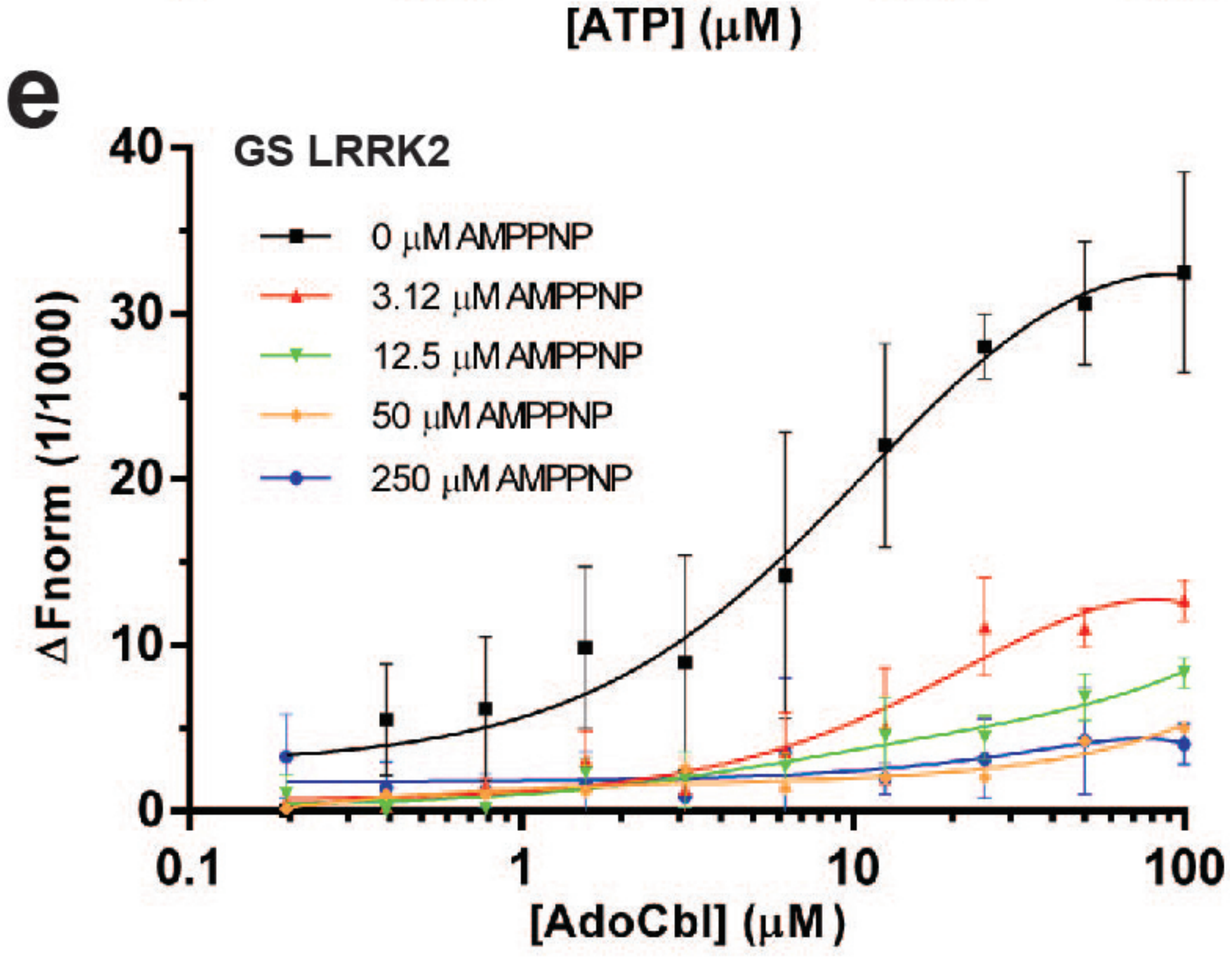
e
GS LRRK2
ΔFnorm (1/1000)
[AdoCbl] (μM)
0 μM AMPPNP
3.12 μM AMPPNP
12.5 μM AMPPNP
50 μM AMPPNP
250 μM AMPPNP

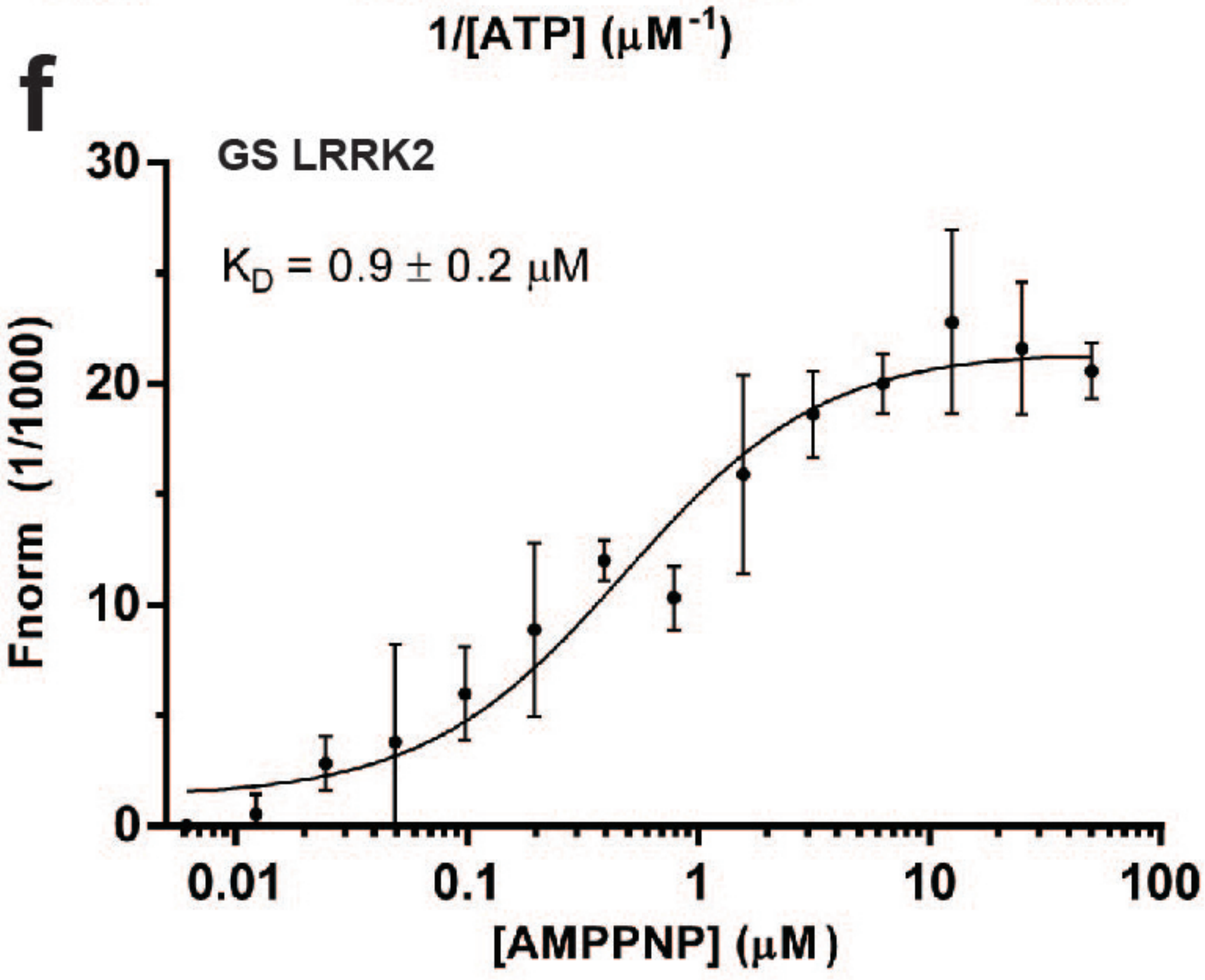
f
GS LRRK2
KD = 0.9 ± 0.2 μM
Fnorm (1/1000)
[AMPPNP] (μM)

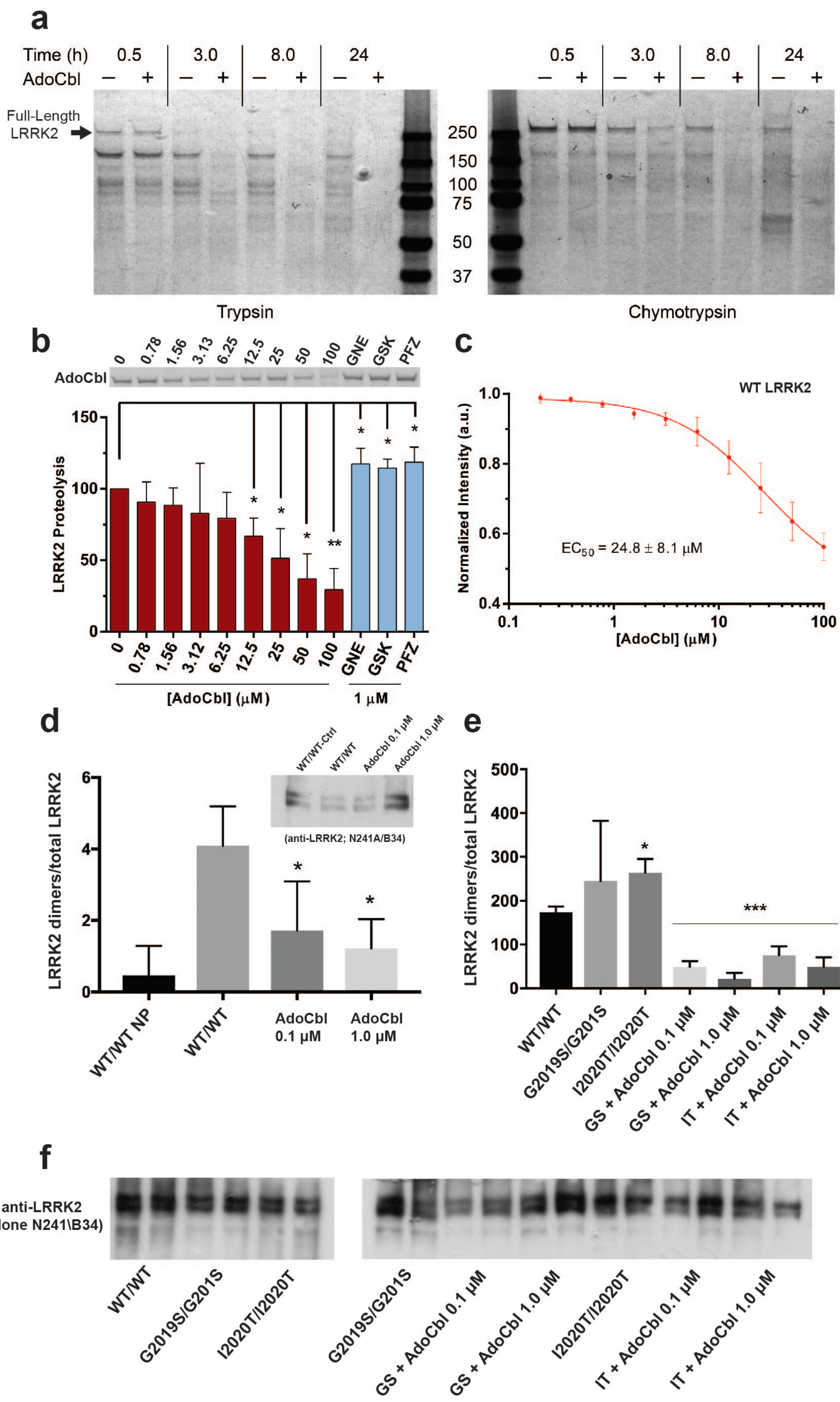
a
Time (h)
0.5
3.0
8.0
24
AdoCbl
Full-Length LRRK2
250
150
100
75
50
37
Trypsin
Chymotrypsin
b
AdoCbl
LRRK2 Proteolysis
[AdoCbl] (μM)
1 μM
0
0.78
1.56
3.13
6.25
12.5
25
50
100
GNE
GSK
PFZ
c
WT LRRK2
Normalized Intensity (a.u.)
EC50 = 24.8 ± 8.1 μM
[AdoCbl] (μM)
d
LRRK2 dimers/total LRRK2
WT/WT-Ctrl
WT/WT
AdoCbl 0.1 μM
AdoCbl 1.0 μM
(anti-LRRK2; N241A/B34)
WT/WT NP
WT/WT
AdoCbl 0.1 μM
AdoCbl 1.0 μM
e
LRRK2 dimers/total LRRK2
WT/WT
G2019S/G201S
I2020T/I2020T
GS + AdoCbl 0.1 μM
GS + AdoCbl 1.0 μM
IT + AdoCbl 0.1 μM
IT + AdoCbl 1.0 μM
f
anti-LRRK2
(clone N241\B34)
WT/WT
G2019S/G201S
I2020T/I2020T
G2019S/G201S
GS + AdoCbl 0.1 μM
GS + AdoCbl 1.0 μM
I2020T/I2020T
IT + AdoCbl 0.1 μM
IT + AdoCbl 1.0 μM

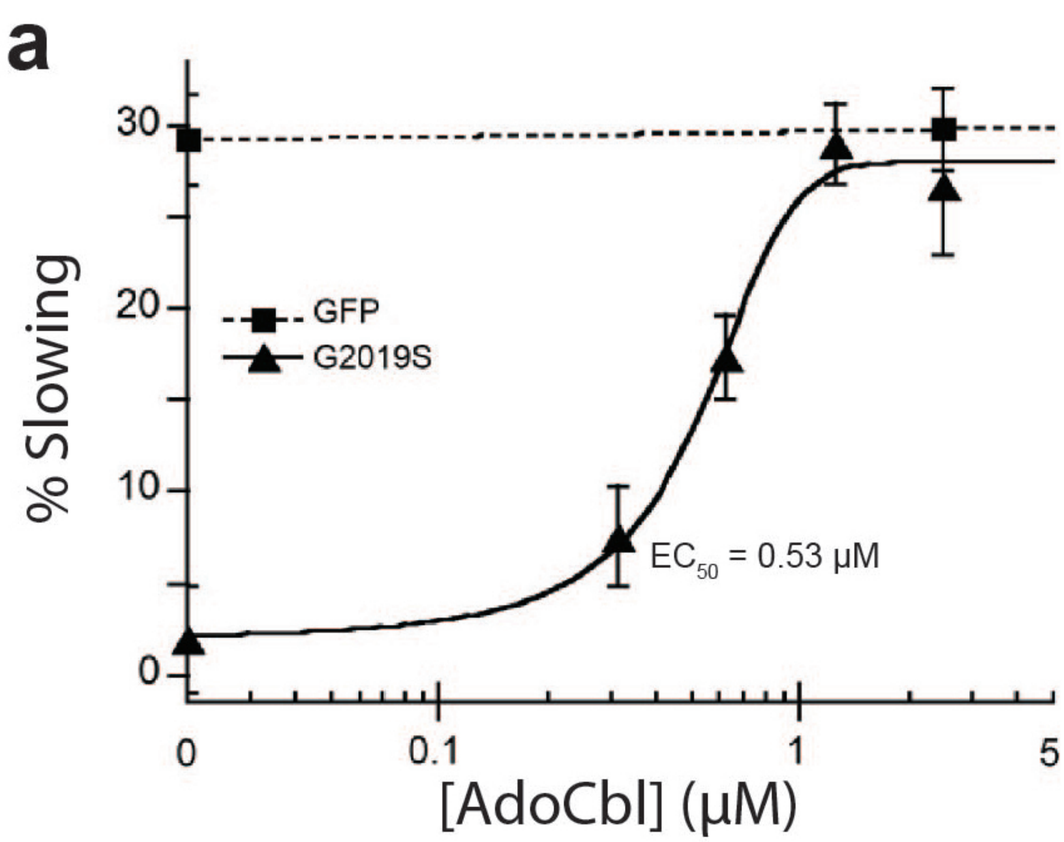
a
30
20
10
0
% Slowing
GFP
G2019S
EC50 = 0.53 μM
0
0.1
1
5
[AdoCbl] (μM)

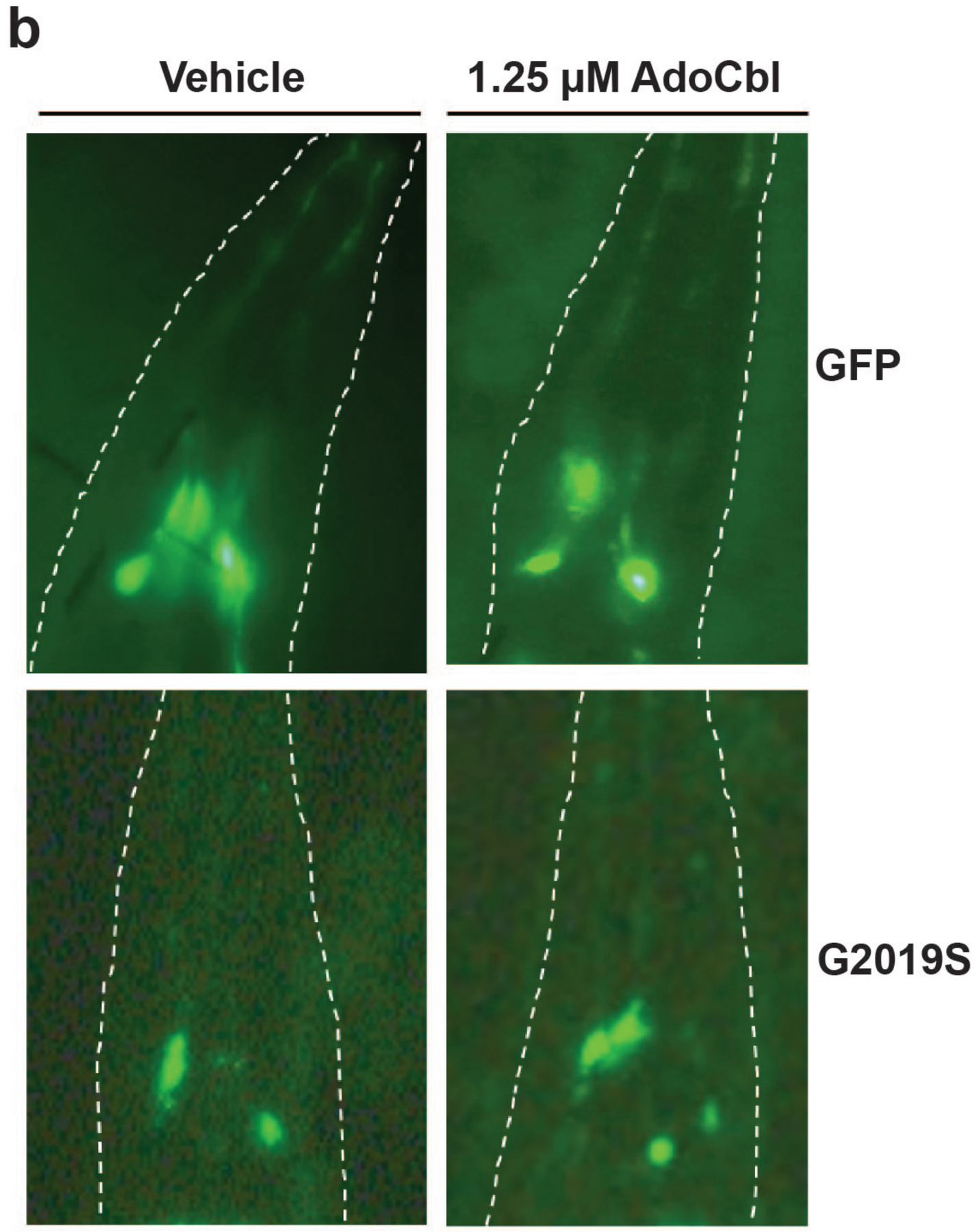
b
Vehicle
1.25 μM AdoCbl
GFP
G2019S

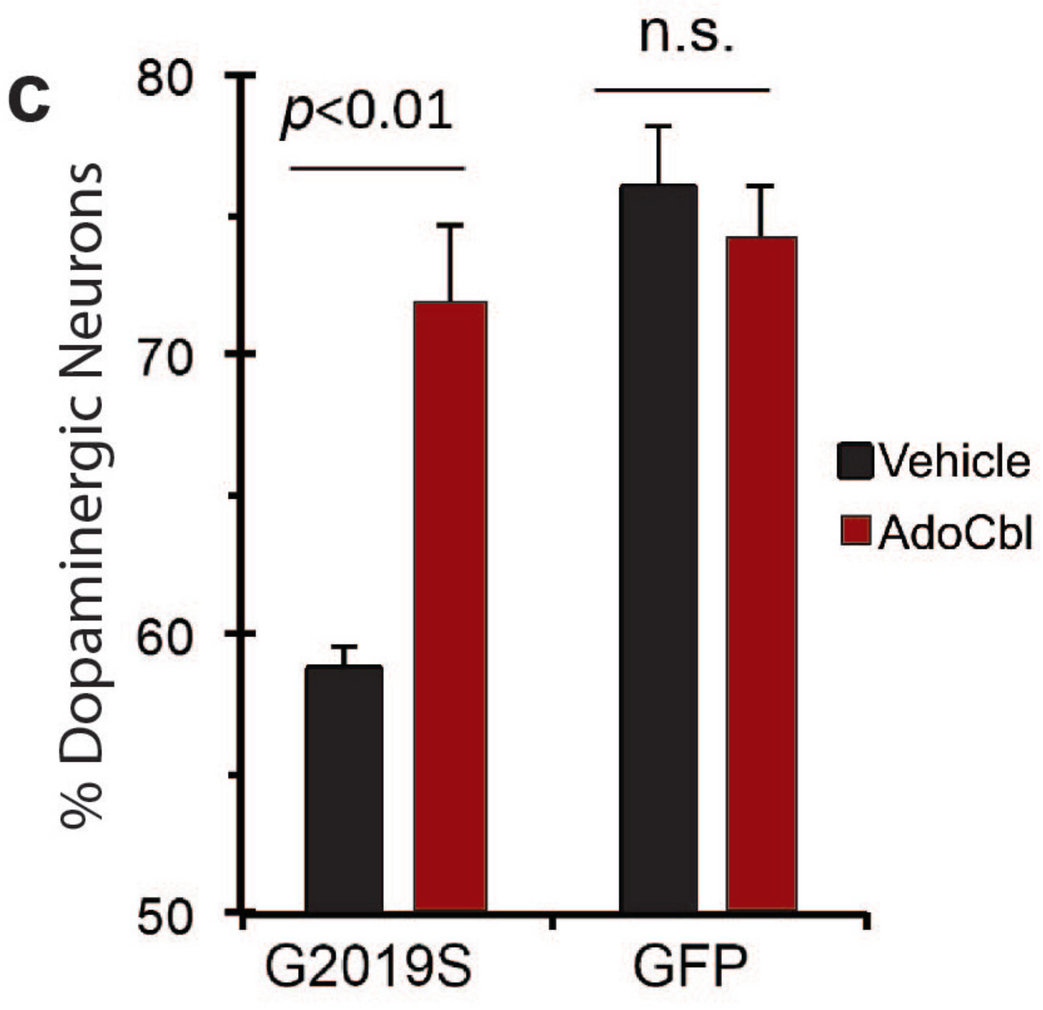
c
n.s.
p<0.01
80
70
60
50
% Dopaminergic Neurons
Vehicle
AdoCbl
G2019S
GFP

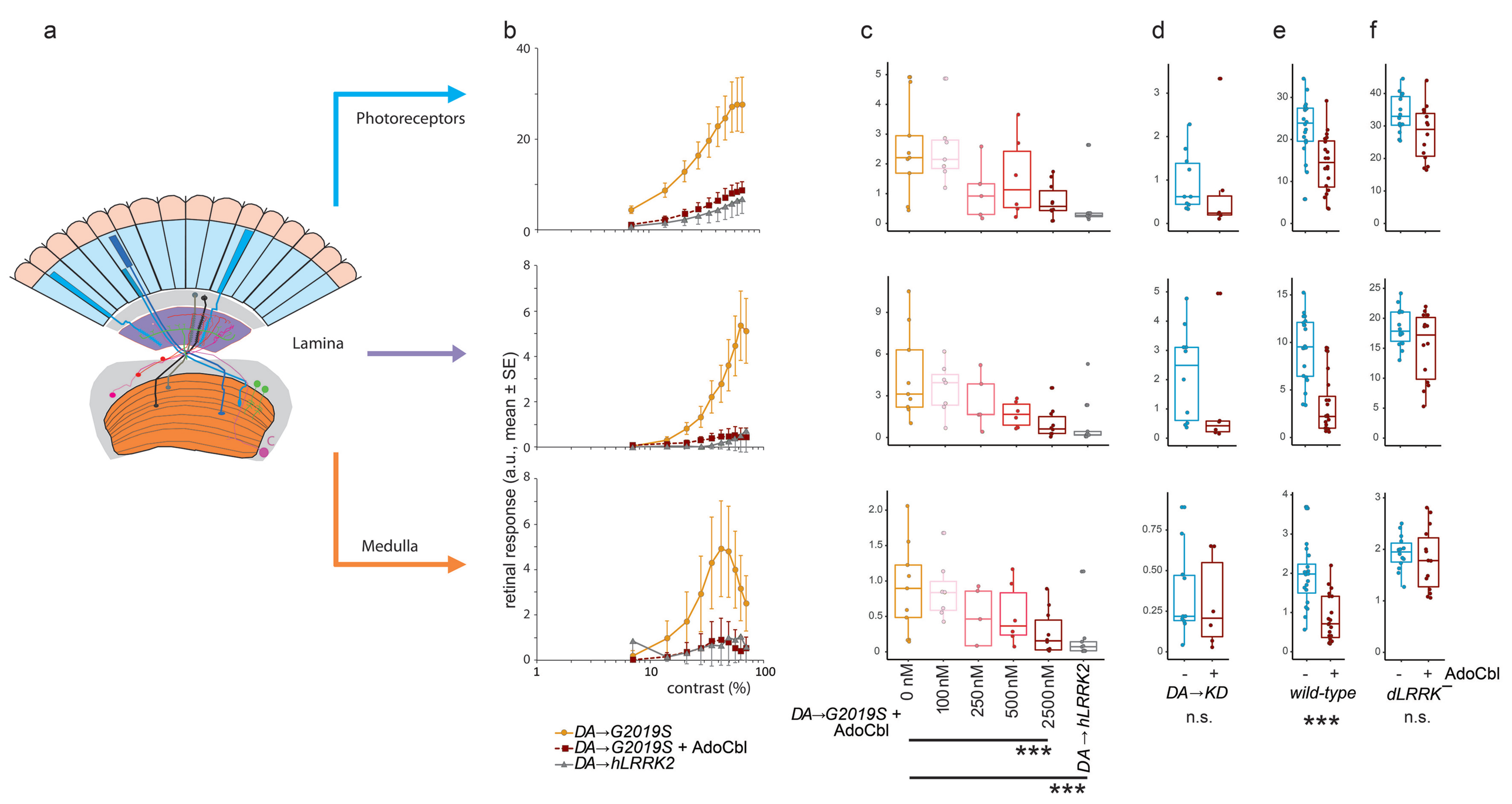
a
Photoreceptors
Lamina
Medulla
b
retinal response (a.u., mean ± SE)
contrast (%)
DA→G2019S
DA→G2019S + AdoCbl
DA→hLRRK2
c
0 nM
100 nM
250 nM
500 nM
2500 nM
DA→G2019S + AdoCbl
DA→hLRRK2
***
***
d
DA→KD
n.s.
e
wild-type
***
f
dLRRK⁻
n.s.
AdoCbl

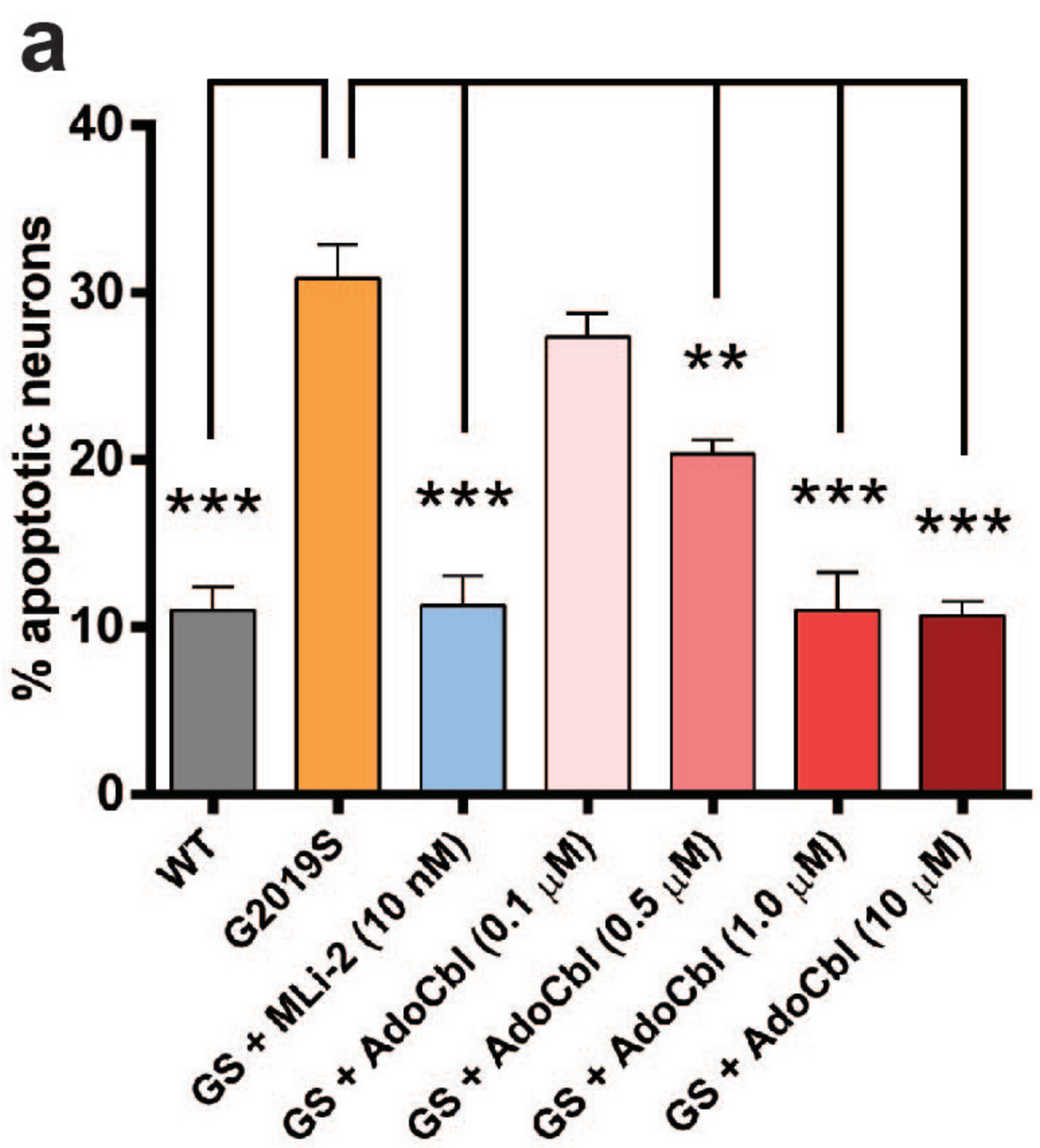
a
% apoptotic neurons
40
30
20
10
0
***
***
**
***
***
WT
G2019S
GS + MLi-2 (10 nM)
GS + AdoCbl (0.1 μM)
GS + AdoCbl (0.5 μM)
GS + AdoCbl (1.0 μM)
GS + AdoCbl (10 μM)

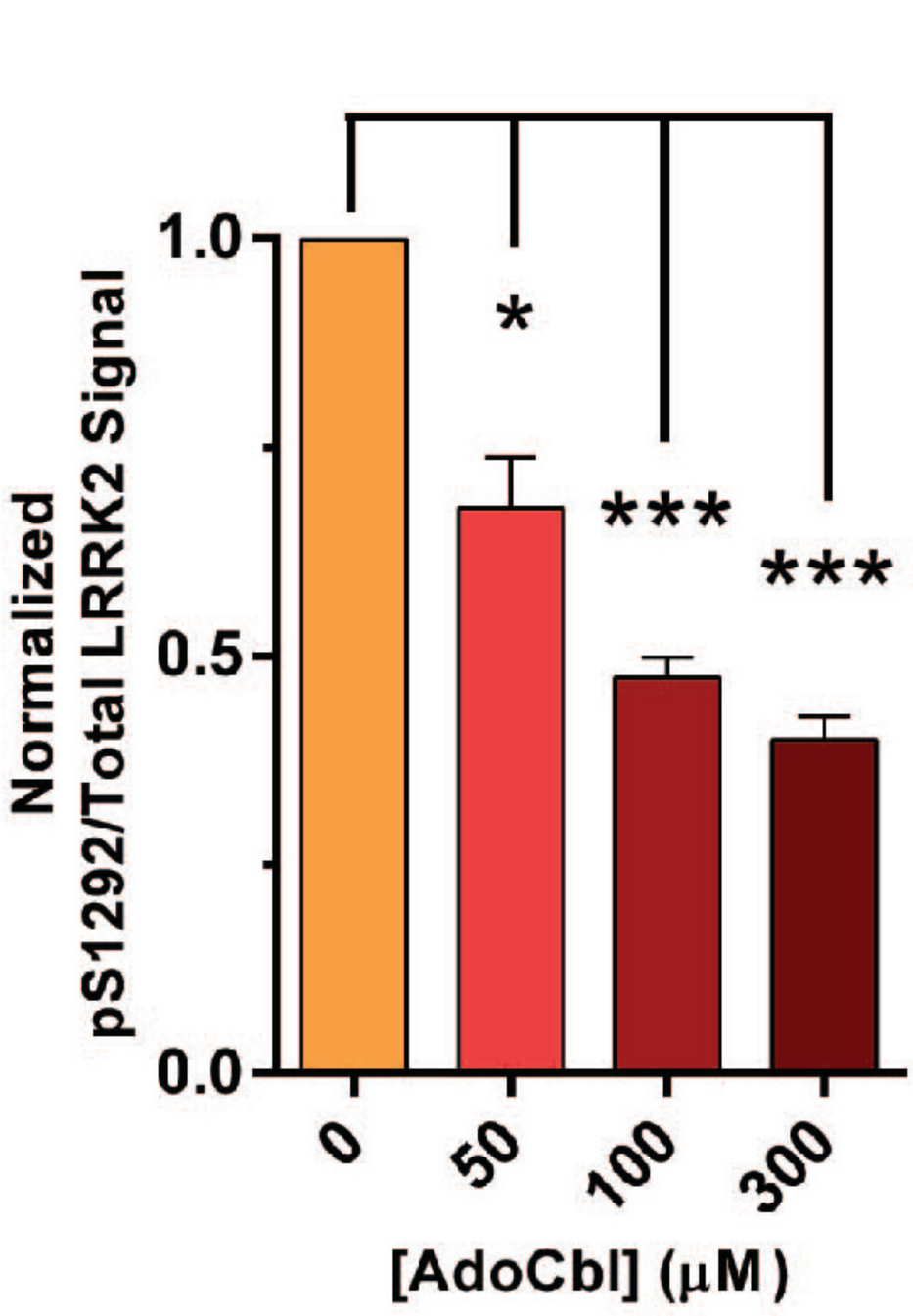
b
Normalized
pS1292/Total LRRK2 Signal
1.0
0.5
0.0
*
***
***
0
50
100
300
[AdoCbl] (μM)

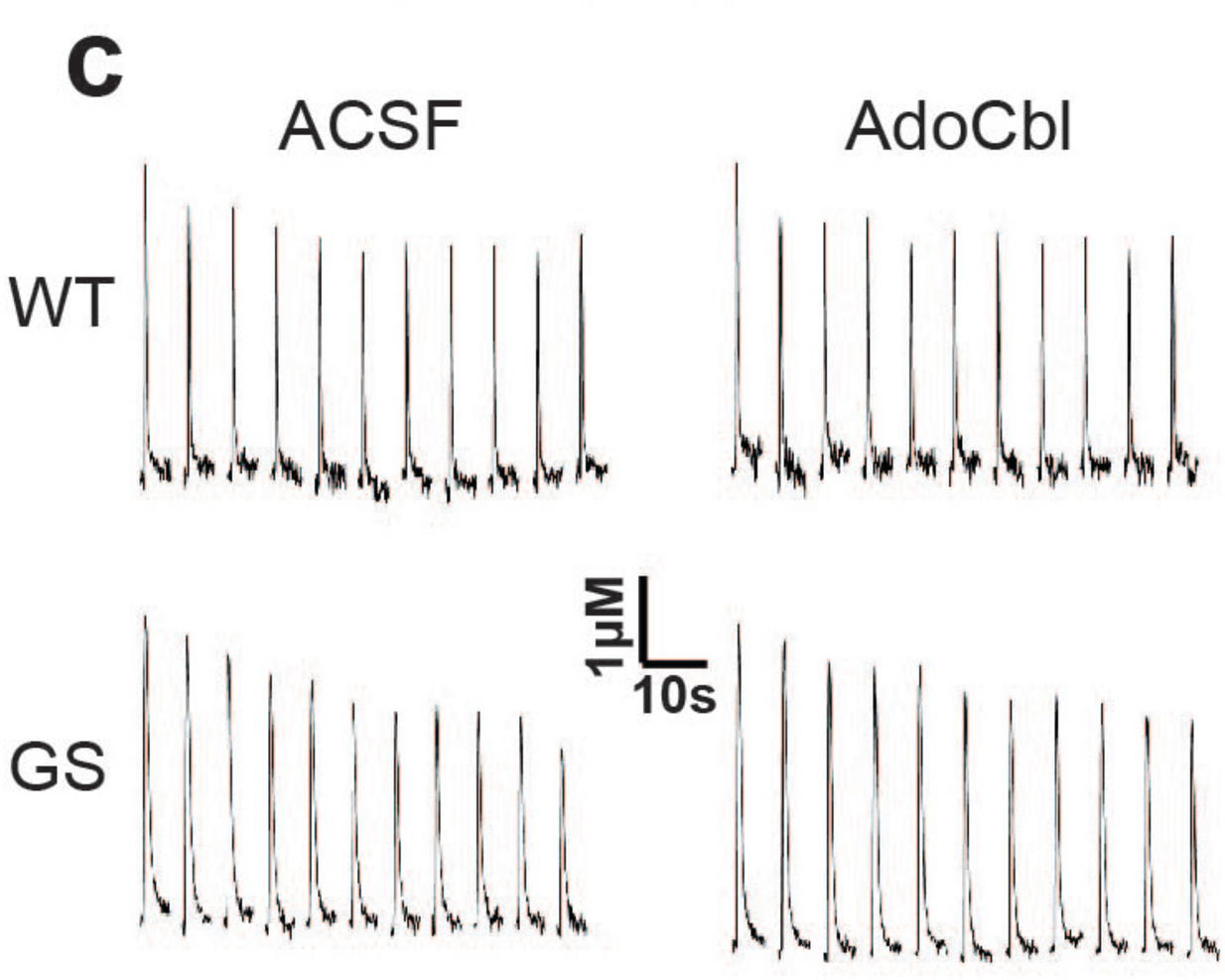
c
ACSF
AdoCbl
WT
GS
1μM
10s

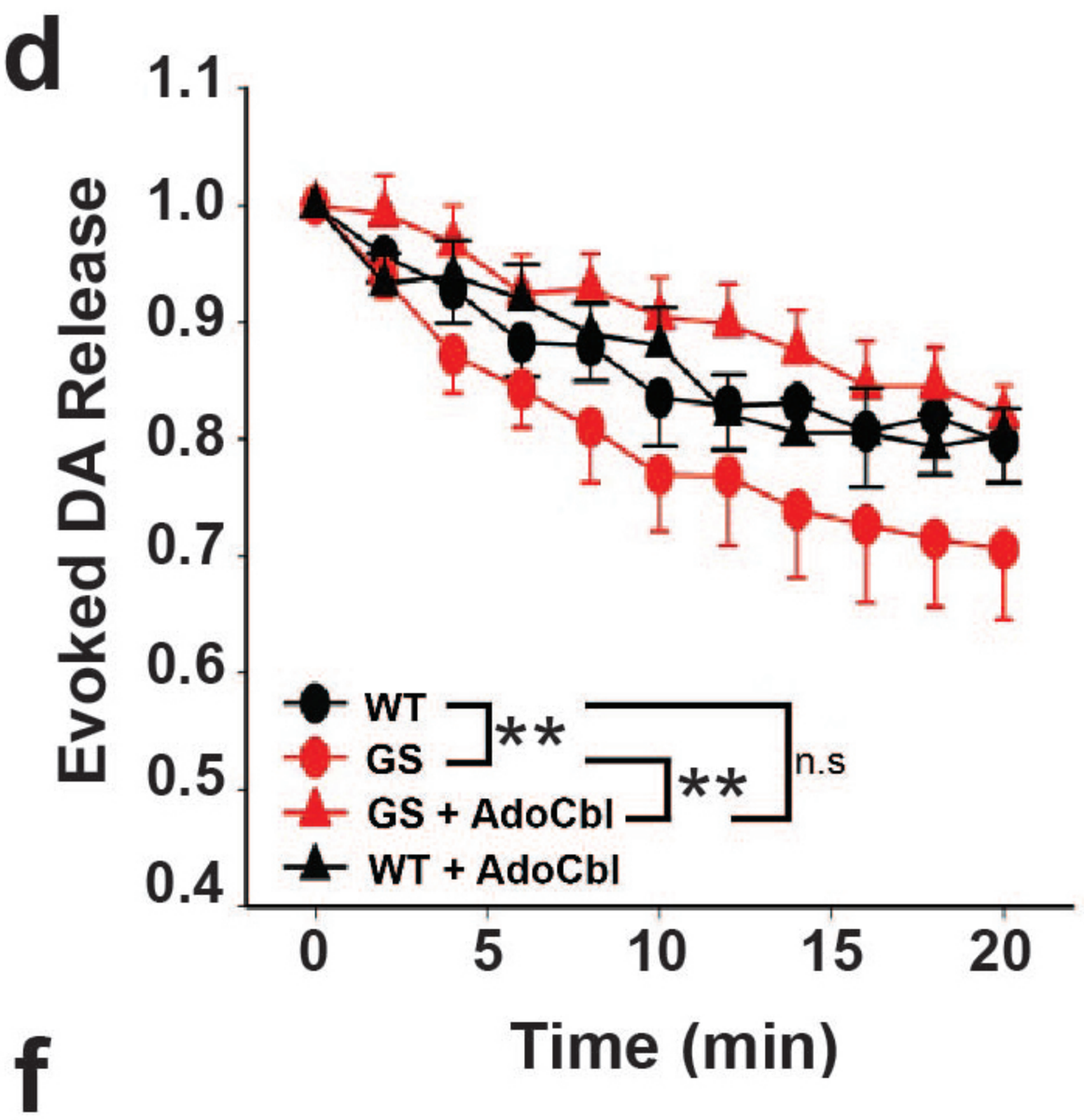
d
Evoked DA Release
1.1
1.0
0.9
0.8
0.7
0.6
0.5
0.4
WT
GS
GS + AdoCbl
WT + AdoCbl
**
**
n.s
0
5
10
15
20
Time (min)

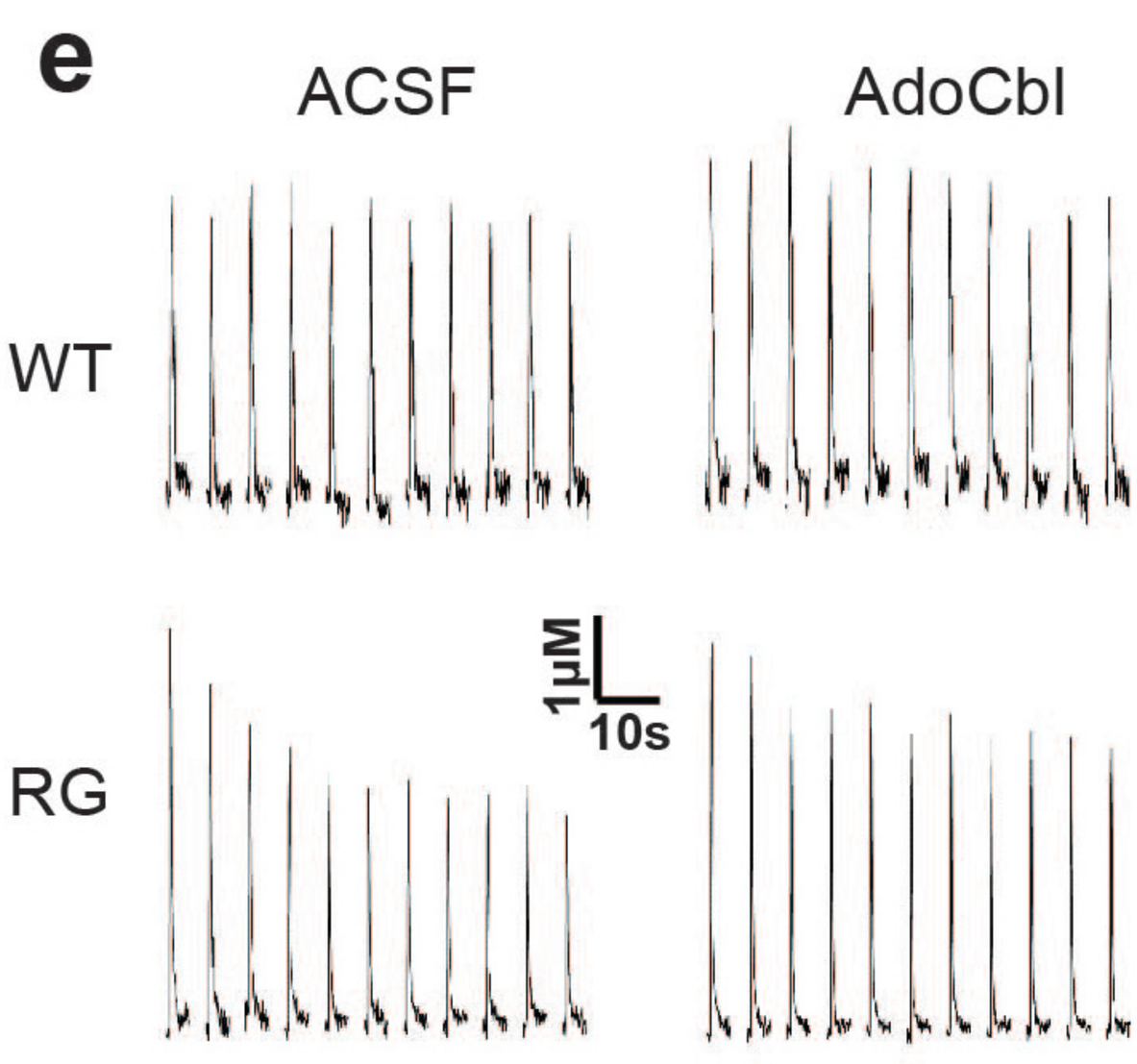
e
ACSF
AdoCbl
WT
RG
1μM
10s

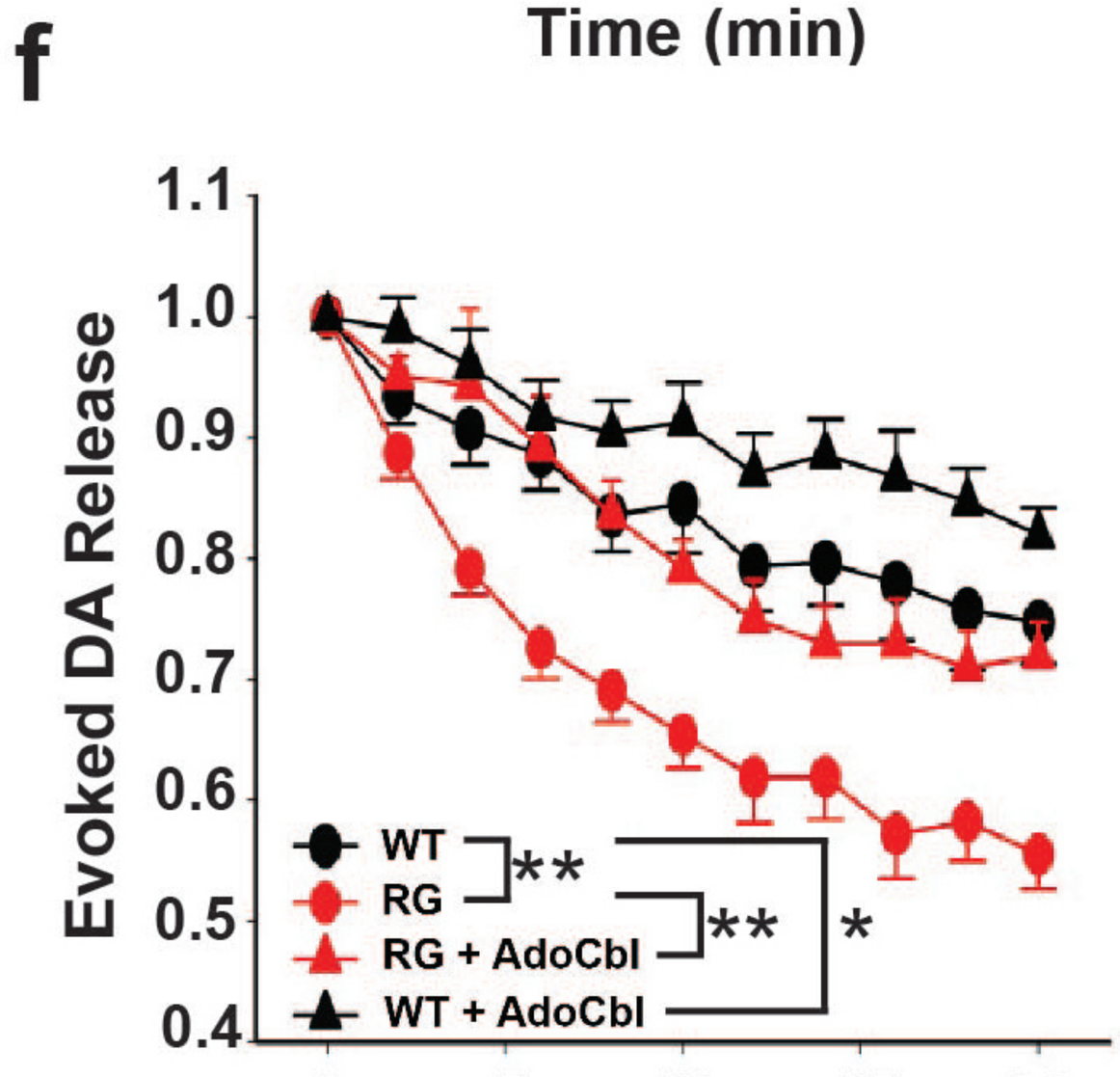
f
Evoked DA Release
1.1
1.0
0.9
0.8
0.7
0.6
0.5
0.4
WT
RG
RG + AdoCbl
WT + AdoCbl
**
**
*
0
5
10
15
20
Time (min)